

TRIMETHYLSILYLATED ALLYL COMPLEXES OF GROUPS I – V:
FORMATION, STRUCTURE, AND CATALYTIC REACTIONS

By

Rosemary Elaine White

Dissertation

Submitted to the Faculty of the
Graduate School of Vanderbilt University
in partial fulfillment of the requirements
for the degree of

DOCTOR OF PHILOSOPHY

in

Chemistry

December, 2006

Nashville, Tennessee

Approved:

Professor Timothy P. Hanusa

Professor Eva Harth

Professor Chuck M. Lukehart

Professor David W. Wright

ACKNOWLEDGEMENTS

I must begin by thanking my chemistry mentors at Duke University, as my interest in chemistry began as an undergraduate. I would especially like to thank Professor James Bonk; his famous no-notes chemistry lectures were always worth waking up for. He also helped me to decide to attend graduate school at Vanderbilt, one of the best decisions of my life. Among others, Professors Michael Montague-Smith and Chris Roy encouraged my interest in chemistry by leading classes that were lively and interesting and by showing a love of chemistry that was infectious.

Numerous mentors made my four years at Vanderbilt educational and exciting in more ways than I ever expected. I especially thank the members of my committee, Professors Tim Hanusa, Eva Harth, Chuck Lukehart, and David Wright. They were all extremely supportive and inquisitive, making committee meetings and presentations extremely helpful and virtually painless. I also thank Professor Adam List, who answered countless email questions from me without batting an eye, and Dr. Jeff Johnston, both of whom were always excited about sharing their love for teaching.

My most important mentor at Vanderbilt has been my advisor Tim Hanusa. He works harder and strives for perfection more than anyone I have ever met. His work ethic has led me to work as hard as I can for him, and to strive to achieve great things throughout the rest of my life. In addition to his hard work, Dr. Hanusa is dedicated to his students (both in his group and in his classes) more than most professors, and he gives new meaning to the term “open-door” policy. No matter what he was doing, Dr. Hanusa was

always there to answer my questions on everything from chemistry research and teaching techniques to life in California and job possibilities.

Another important mentor during graduate school was Dr. Kevin John at the Los Alamos National Lab. His hard work and ability to stay sane despite his strenuous schedule was an inspiration to me. During the two summers I spent with him there, he provided assistance in chemistry research and career decisions and was an invaluable friend and guide throughout my time with him.

Thanks to past and present Hanusa group members for all of their help in lab, and more importantly, for making lab bearable and fun each day. Chrissy, Lacey, Brett, and Keith welcomed me into the lab with helpful advice on classes and research and are responsible for all of my knowledge of experimental air-sensitive techniques. Cameron and Jeff are thanked for making lab feel more like play than work. Lunch with the two of them and the whole eighth floor crew (especially Ryan, Matt, and Mike) was always the most fun part of the day. At LANL, Jackie and Chrissy provided me with assistance with all of my work; without them, summers at LANL would have been far less productive. They were also good friends and spending time with them (as well as Carina, Kim, Tricia, Carl, and Jo) outside of lab made the summers in the desert some of the most fun I have had.

For longer than I can remember, a group of close friends has provided me with limitless love and support throughout my life. They have taught me the value of hard work and perseverance, as well as how to have fun and how to laugh until you cry, without all of which I never would have made it this far. I especially thank my friends Kristen, Laura, Sarah, Marisa, Wylie, Dan, Odette, Julia, Stacey, and Eric, who are a

group of the most wonderfully loyal and special friends one could have. At Vanderbilt, I received equal love and support from friends like Natalie and Ana, and most especially, from Crystal and Sheerin.

Of all of my friends at Vanderbilt, I most especially thank Aren, whose friendship and love throughout the past four years has been immeasurable. I could not have made it through my qualifier, OP, and countless other obstacles without his advice, support, and shoulder to cry on. He is truly a kindred spirit and has touched my life more than I ever could have hoped for. I admire his love for teaching and helping others and can only hope to someday be as passionate about my goals as he is about his.

More than anything, I thank my parents George and Nancy. My dad's hard work and educational goals have inspired me to work as hard and to go as far as I can. My mom's kind nature and love for her husband and children has been an inspiration for the life I strive to have someday. Together they have taught me how to work hard, play hard, love unconditionally, and be myself. Without these values, I would never have made it to where I am, and I would not be who I am today.

TABLE OF CONTENTS

	Page
ACKNOWLEDGEMENTS.....	ii
LIST OF TABLES	vii
LIST OF FIGURES.....	x
INTRODUCTION.....	xii
<i>Chapter</i>	
I. STRUCTURAL AND BONDING MOTIFS IN BULKY ALLYL COMPLEXES OF THE LATE LANTHANIDE METALS.....	1
Introduction.....	1
Experimental.....	3
Results and Discussion.....	8
Conclusion.....	24
II. OBSERVATION OF ELECTRON TRANSFER IN BULKY ALLYL YTTERBIUM COMPLEXES WITH SUBSTITUTED TERPYRIDINE LIGANDS	25
Introduction.....	25
Experimental.....	27
Results and Discussion.....	35
Conclusion.....	50
III. GROUPS I AND II AND LANTHANIDE METAL ALLYL COMPLEXES AS PRE-CATALYSTS IN THE POLYMERIZATION OF METHYL METHACRYLATE.....	51
Introduction.....	51
Experimental.....	53
Results and Discussion.....	58
Conclusion.....	70
IV. SYNTHESIS AND REACTIVITY OF TRIALLYLYTTTRIUM AND DENSITY FUNCTIONAL THEORY CALCULATIONS OF ⁸⁹ Y NMR CHEMICAL SHIFTS FOR ORGANOYTTRIUM COMPLEXES	71
Introduction.....	71

Experimental.....	73
Results and Discussion.....	80
Conclusion.....	102
V. SYNTHETIC, STRUCTURAL, AND COMPUTATIONAL STUDIES OF BULKY ALLYL COMPLEXES OF VANADIUM	104
Introduction.....	104
Experimental.....	105
Results and Discussion.....	108
Conclusion.....	114
<i>Appendix</i>	
A. CRYSTAL DATA, ATOMIC FRACTIONAL COORDINATES, AND ISOTROPIC THERMAL PARAMETERS FOR X-RAY STRUCTURAL DETERMINATIONS	115
B. ATOMIC FRACTIONAL COORDINATES FOR DENSITY FUNCTIONAL THEORY OPTIMIZED STRUCTURES	139
REFERENCES.....	161

LIST OF TABLES

Table	Page
1. Experimental Data for Ln[1,3-(SiMe ₃) ₂ C ₃ H ₃] ₃	5
2. Bond distances for trivalent lanthanide allyl complexes	14
3. Bond distances for divalent lanthanide and alkaline earth allyl complexes	15
4. Selected bond distances for [Ho{1,3-(SiMe ₃) ₂ C ₃ H ₃ }{μ-(1-(SiMe ₃)-3-(SiMe ₂ CH ₂)C ₃ H ₃)}] ₂	17
5. Selected bond distances for Ho ₂ [μ-{1-(SiMe ₃)-3-(SiMe ₂ CH ₂)C ₃ H ₃ }] ₂ [μ-{1,3-(SiMe ₃) ₂ C ₃ H ₂ }](thf) ₂	18
6. Summary of notation for complexes	34
7. Selected bond distances and angles for Yb[1,3-(SiMe ₃) ₂ C ₃ H ₃] ₂ (tpy)	40
8. IR C≡N stretching frequencies	41
9. Selected bond distances for geometry optimized structures of Yb[1-(SiMe ₃)C ₃ H ₄] ₂ (tpy), Yb[1,3-(SiMe ₃) ₂ C ₃ H ₃] ₂ (tpy), and YbCp* ₂ (tpy)	47
10. Elemental analysis data for Sm[1,3-(SiMe ₃) ₂ C ₃ H ₃] ₂ (thf) ₂ , Eu[1,3-(SiMe ₃) ₂ C ₃ H ₃] ₂ (thf) ₂ , Ce[1,3-(SiMe ₃) ₂ C ₃ H ₃] ₃ (thf), and Tb[1,3-(SiMe ₃) ₂ C ₃ H ₃] ₃ (thf)	55
11. Results of MMA polymerization (in ~20 mL toluene at 0 °C) with allyl complexes.	62
12. Results of MMA polymerization (in ~20 mL solvent, 0.5 min) with allyl complexes	69
13. Yttrium complexes and their corresponding ⁸⁹ Y NMR chemical shifts	83
14. Empirical group contributions to ⁸⁹ Y NMR chemical shift for aromatic solvents (benzene or toluene)	85
15. Empirical group contributions to ⁸⁹ Y NMR chemical shift in THF- <i>d</i> ₈	85
16. Shielding constants from various GGA and hybrid functionals	86

17.	Calculated and experimental (X-ray data) Y–X bond distances	88
18.	Predicted shielding constants and chemical shifts in ppm	93
19.	Calculated and experimental (X-ray data) bond distances.....	97
20.	Predicted shielding constants and chemical shifts in ppm for coordination complexes.....	97
21.	Selected bond distances (Å) for $V_2[\mu\text{-}\{1,3\text{-(SiMe}_3\text{)}_2\text{C}_3\text{H}_3\}\}_3\text{Cl}$	111
22.	Bond distances and angles from crystal and calculated structures of $V_2[\mu\text{-}\{1,3\text{-}(X)_2\text{C}_3\text{H}_3\}\}_3\text{Cl}$, where X = H, SiH ₃ , SiMe ₃	115
23.	Crystal data and structure refinement for $Tm[1,3\text{-(SiMe}_3\text{)}_2\text{C}_3\text{H}_3\}_3$	117
24.	Atomic coordinates and equivalent isotropic displacement parameters for $Tm[1,3\text{-(SiMe}_3\text{)}_2\text{C}_3\text{H}_3\}_3$	118
25.	Crystal data and structure refinement for $[Ho\{1,3\text{-(SiMe}_3\text{)}_2\text{C}_3\text{H}_3\}\{\mu\text{-}(1\text{-(SiMe}_3\text{)}\text{-}3\text{-(SiMe}_2\text{CH}_2\text{)C}_3\text{H}_3\})\}_2$	119
26.	Atomic coordinates and equivalent isotropic displacement parameters for $[Ho\{1,3\text{-(SiMe}_3\text{)}_2\text{C}_3\text{H}_3\}\{\mu\text{-}(1\text{-(SiMe}_3\text{)}\text{-}3\text{-(SiMe}_2\text{CH}_2\text{)C}_3\text{H}_3\})\}_2$	120
27.	Crystal data and structure refinement for $Ho_2[\mu\text{-}\{1\text{-(SiMe}_3\text{)}\text{-}3\text{-(SiMe}_2\text{CH}_2\text{)C}_3\text{H}_3\}\}_2[\mu\text{-}\{1,3\text{-(SiMe}_3\text{)}_2\text{C}_3\text{H}_2\}\](thf)_2$	122
28.	Atomic coordinates and equivalent isotropic displacement parameters for $Ho_2[\mu\text{-}\{1\text{-(SiMe}_3\text{)}\text{-}3\text{-(SiMe}_2\text{CH}_2\text{)C}_3\text{H}_3\}\}_2[\mu\text{-}\{1,3\text{-(SiMe}_3\text{)}_2\text{C}_3\text{H}_2\}\](thf)_2$	123
29.	Crystal data and structure refinement for $Yb[1,3\text{-(SiMe}_3\text{)}_2\text{C}_3\text{H}_3\}_2(tpy)$	125
30.	Atomic coordinates and equivalent isotropic displacement parameters for $Yb[1,3\text{-(SiMe}_3\text{)}_2\text{C}_3\text{H}_3\}_2(tpy)$	126
31.	Crystal data and structure refinement for $[K\{1,3\text{-(SiMe}_3\text{)}_2\text{C}_3\text{H}_3\}(dme)]_\infty$	129
32.	Atomic coordinates and equivalent isotropic displacement parameters for $[K\{1,3\text{-(SiMe}_3\text{)}_2\text{C}_3\text{H}_3\}(dme)]_\infty$	130
33.	Crystal data and structure refinement for $Y[1,3\text{-(SiMe}_3\text{)}_2\text{C}_3\text{H}_3\}_3$	132

34.	Atomic coordinates for $Y[1,3-(SiMe_3)_2C_3H_3]_3$	133
35.	Anisotropic displacement parameters for $Y[1,3-(SiMe_3)_2C_3H_3]_3$	135
36.	Crystal data and structure refinement for $V_2[\mu-\{1,3-(SiMe_3)_2C_3H_3\}]_3Cl$	136
37.	Atomic coordinates and equivalent isotropic displacement parameters for $V_2[\mu-\{1,3-(SiMe_3)_2C_3H_3\}]_3Cl$	137
38.	Atomic coordinates for optimized structure of $Yb[1,3-(SiMe_3)_2C_3H_3]_2(tpy)$ (B3PW91/SDD).....	140
39.	Atomic coordinates for optimized structure of $Yb[1-(SiMe_3)C_3H_4]_2(tpy)$ (B3PW91/SDD).....	143
40.	Atomic coordinates for optimized structure of $Yb(C_5Me_5)_2(tpy)$ (B3PW91/SDD).....	145
41.	Atomic coordinates for optimized structure of $Y(C_5H_5)_2(OC_6H_5)$ (C,H,O: B3PW91/6-311G(d,p); Y: B3PW91/DGDZVP).....	147
42.	Atomic coordinates for optimized structure of $Y(C_5H_5)_2(OC_6H_3(t-Bu)_2)$ (C,H,O: B3PW91/6-311G(d,p); Y: B3PW91/DGDZVP).....	148
43.	Atomic coordinates for optimized structure of $Y[N(SiMe_3)_2]_3$ (C,H,N,Si: B3PW91/6-311G(d,p); Y: B3PW91/DGDZVP).....	150
44.	Atomic coordinates for optimized structure of $Y(thd)_3$ (C,H,O: B3PW91/6-311G(d,p); Y: B3PW91/DGDZVP)	152
45.	Atomic coordinates for optimized structure of $V_2[\mu-(C_3H_5)]_3Cl$ (B3PW91/DGDZVP2).....	155
46.	Atomic coordinates for optimized structure of $V_2[\mu-\{1,3-(SiH_3)_2C_3H_3\}]_3Cl$ (B3PW91/DGDZVP2).....	156
47.	Atomic coordinates for optimized structure of $V_2[\mu-\{1,3-(SiMe_3)_2C_3H_3\}]_3Cl$ (B3PW91/DGDZVP2).....	158

LIST OF FIGURES

Figure	Page
1. ORTEP of Tm[1,3-(SiMe ₃) ₂ C ₃ H ₃] ₃	10
2. ORTEP of [Ho{1,3-(SiMe ₃) ₂ C ₃ H ₃ }{μ-(1-(SiMe ₃)-3-(SiMe ₂ CH ₂)C ₃ H ₃)}] ₂	19
3. ORTEP of Ho ₂ [μ-{1-(SiMe ₃)-3-(SiMe ₂ CH ₂)C ₃ H ₃ }] ₂ [μ-{1,3-(SiMe ₃) ₂ C ₃ H ₂ }](thf) ₂	20
4. (a) Delocalized allylidene bonding. (b) Vinylalkylidene bonding scheme. (c) Most stable Lewis structure of the allyl dianion. (d) Geometry optimized [1,3-(SiMe ₃) ₂ C ₃ H ₂] ²⁻ ion	23
5. Terpyridine ligands: 2,2':6',2''-terpyridine, 4'-cyano-2,2':6',2''-terpyridine, and 6,6''-dicyano-2,2':6',2''-terpyridine	37
6. ORTEP of Yb[1,3-(SiMe ₃) ₂ C ₃ H ₃] ₂ (tpy).....	39
7. Possible binding modes for tpy(CN) ₂	42
8. Geometry optimized structure of Yb[1,3-(SiMe ₃) ₂ C ₃ H ₃] ₂ (tpy(CN) ₂) (a) and side-on view of tpy(CN) ₂ ligand in optimized structure (b).....	43
9. Magnetic data plots of for Yb[1,3-(SiMe ₃) ₂ C ₃ H ₃] ₂ (tpy)	45
10. Geometry optimized structures of Yb[1-(SiMe ₃)C ₃ H ₄] ₂ (tpy) (a), Yb[1,3-(SiMe ₃) ₂ C ₃ H ₃] ₂ (tpy) (b), and YbCp* ₂ (tpy) (c).....	46
11. Electron density of LUMO and SOMO of tpy, tpyCN, and tpy(CN) ₂	49
12. ORTEP of K[1,3-(SiMe ₃) ₂ C ₃ H ₃](dme).....	60
13. Geometry optimized structures of organoyttrium complexes and selected bond lengths	89
14. Plot of experimental chemical shifts versus calculated chemical shieldings for geometry optimized organometallic complexes.....	91
15. Crystal (a) and geometry optimized (b) structure of Y(thd) ₃	98

16.	Figure of $Y[1,3-(\text{SiMe}_3)_2\text{C}_3\text{H}_3]_3$ (15), with two disordered parts (bold and non-bold) shown	101
17.	ORTEP of $V_2[\mu-\{1,3-(\text{SiMe}_3)_2\text{C}_3\text{H}_3\}]_3\text{Cl}$, with thermal ellipsoids at the 50% level.....	110
18.	Geometry optimized structures of $V_2[\mu-(\text{C}_3\text{H}_5)]_3\text{Cl}$ (a), $V_2[\mu-\{1,3-(\text{SiH}_3)_2\text{C}_3\text{H}_3\}]_3\text{Cl}$ (b), and $V_2[\mu-\{1,3-(\text{SiMe}_3)_2\text{C}_3\text{H}_3\}]_3\text{Cl}$ (c)	114

INTRODUCTION

In 1961, Wilke and co-workers successfully prepared the first homoleptic π -allyl complex, $\text{Ni}(\text{C}_3\text{H}_5)_2$.¹ Throughout the 1960s, his group synthesized other homoleptic allyl transition metal complexes, including $\text{M}(\text{C}_3\text{H}_5)_2$ ($\text{M} = \text{Ni}, \text{Zn}, \text{Pd}$), $\text{M}(\text{C}_3\text{H}_5)_3$ ($\text{M} = \text{V}, \text{Cr}, \text{Fe}, \text{Co}$), and $\text{M}(\text{C}_3\text{H}_5)_4$ ($\text{M} = \text{Zr}, \text{Nb}$).² Despite Wilke's and subsequent workers' advances in allyl transition metal chemistry, however, homoleptic allyl complexes remain understudied largely due to their thermal instability. For example, triallylcobalt decomposes above $-40\text{ }^\circ\text{C}$ in inert atmosphere, despite its formal electron count of eighteen.³ This instability can be attributed to the fact that the $[\text{C}_3\text{H}_5]^-$ anion is a sterically compact four electron donor, which allows low-energy decomposition pathways to exist.

Since Wilke's initial work in allyl chemistry, the use of sterically bulky allyls has allowed the preparation of more stable homoleptic π -allyl complexes. Even a substituent as small as a methyl group provides substantial stabilization to an allyl complex. Specifically, methylation of the 2-position of the allyl ligand has led to the isolation of thermally stable $\text{Fe}(\text{2-Me-C}_3\text{H}_4)_2(\text{PR}_3)_2$ ($\text{PR}_3 = \text{PMe}_3, \text{PMe}_2\text{Ph}, \text{P}(\text{OMe})_3$) complexes;⁴ the analogous unsubstituted allyl complexes $\text{Fe}(\text{C}_3\text{H}_5)_2(\text{PR}_3)_2$ decompose above $0\text{ }^\circ\text{C}$.⁵ In 1990, a bulkier allyl ligand, bis(1,3-trimethylsilyl)allyl, was synthesized by Fraenkel et al.⁶ Its straightforward and relatively simple preparation has made it a useful ligand in thermally stable complexes with main group,⁶⁻¹⁰ transition,¹¹⁻¹⁷ lanthanide,¹⁸⁻²² and actinide²³ metals.

Using this ligand, the alkaline earth complex $\text{Ca}[1,3-(\text{SiMe}_3)_2\text{C}_3\text{H}_3]_2(\text{thf})_2$ was synthesized and crystallographically characterized in 1999, representing the first structurally authenticated diallylcalcium complex.⁷ Interestingly, its Ca–C bond distances (2.654(5) Å (avg)) are indistinguishable from those for similar cyclopentadienyl calcium complexes (e.g., $\text{Ca}(\text{C}_5\text{Me}_5)_2$, 2.64(2) Å).²⁴ In contrast, however, the Yb–C bond lengths (2.741(9)–2.748(9) Å)¹⁹ in the isomorphous ytterbium allyl complex are notably longer than those in ytterbocene complexes such as $\text{Yb}(\text{C}_5\text{Me}_5)_2$ (2.636(3)–2.690(3) Å).^{19,25} This anomaly has led to an investigation of the bonding of lanthanide allyl complexes. The synthesis and structures of late lanthanide allyl complexes and the effect of varying the reaction precursors is discussed in Chapter I. Differences in the lanthanide chemistry of allyl and cyclopentadienyl complexes are highlighted. Through the course of this work, novel dimethylsilylene and allylidene diholmium complexes were isolated and are also described in Chapter I.

Ytterbium is one of the few redox active lanthanide elements, a property which can lead to complexes with interesting electronic and magnetic behavior. For instance, ytterbocene derivatives have been treated with *N*-heterocyclic ligands to form complexes that display a stable charge-transfer electronic configuration derived from a spontaneous electron transfer from a diamagnetic Yb(II) f^{14} metal center to the lowest unoccupied molecular orbital (LUMO) on the *N*-heterocyclic ligand.^{26,27} Diallylytterbium complexes have been synthesized and treated with substituted terpyridine ligands, resulting in similar charge-transfer species. Chapter II describes the synthesis of these adducts and how various allyl substituents influence the electronics of these complexes.

The samarium complex $\text{Sm}[1,3\text{-(SiMe}_3)_2\text{C}_3\text{H}_3]_2(\text{thf})_2$ is isomorphous with the aforementioned calcium and ytterbium complexes.¹⁹ It has been explored as an initiator for the polymerization of methyl methacrylate (MMA), but exhibited limited activity.²⁸ In contrast, the mixed metal complex $[\{\text{K}(\text{thf})_2\}\{\text{Sm}[1,3\text{-(SiMe}_3)_2\text{C}_3\text{H}_3]_3\}]_2$ is shown to have exceptionally high activity compared to $\text{Sm}[1,3\text{-(SiMe}_3)_2\text{C}_3\text{H}_3]_2(\text{thf})_2$.²⁸ Similarly, lanthanate complexes of the type $\{\text{Li}(\text{thf})_4\}\{\text{Ln}[1,3\text{-(SiMe}_3)_2\text{C}_3\text{H}_3]_3\text{I}\}$ are more efficient catalysts for MMA polymerization than their neutral counterparts, indicating that the counterion may be responsible for the heightened activity in mixed metal allyl complexes.¹⁹ To explore this hypothesis, the catalytic activity of $\text{K}[1,3\text{-(SiMe}_3)_2\text{C}_3\text{H}_3]$ and $\text{Li}[1,3\text{-(SiMe}_3)_2\text{C}_3\text{H}_3]$ has been investigated and is described in Chapter III. For comparison, the catalytic behavior of $\text{Cs}[1,3\text{-(SiMe}_3)_2\text{C}_3\text{H}_3]$, $\text{Ca}[1,3\text{-(SiMe}_3)_2\text{C}_3\text{H}_3]_2(\text{thf})_2$, $\text{Sr}[1,3\text{-(SiMe}_3)_2\text{C}_3\text{H}_3]_2(\text{thf})_2$, and various lanthanide allyl complexes is also discussed.

Solution NMR spectroscopy is not commonly used in the characterization of lanthanide organometallic complexes, as most lanthanide metals are paramagnetic, producing unpredictable chemical shifts and broadening of NMR peaks. Fortunately, structural similarities between complexes with late lanthanide metals and the diamagnetic yttrium(III) center make yttrium complexes ideal models for lanthanide structures.¹⁹ ^{89}Y NMR spectroscopy is a particularly advantageous characterization tool, as yttrium-89 is a monoisotopic species with $I = -1/2$ and a wide chemical shift range (ca. 1300 ppm).²⁹ It has been used to identify the structure of a bis(1,3-trimethylsilyl)allyl yttrium complex; its experimental ^{89}Y NMR chemical shift was compared to its shift predicted with

density functional theory calculations. This work, as well as similar calculations on a wide variety of organometallic yttrium complexes, is presented in Chapter IV.

While the bulky bis(1,3-trimethylsilyl)allyl ligand has been used to stabilize complexes with metals throughout the periodic table, compounds with the early transition metals still remain rare due to the low electron count of such species.¹⁶ Chapter V describes attempts to synthesize divalent and trivalent vanadium allyl complexes and the subsequent synthesis of a unique divanadium compound. Computational studies are used to understand the role the trimethylsilyl groups play in the bonding of this complex.

The use of bulky allyl ligands has led to expansion of the organometallic chemistry of early transition metals and lanthanides. This extension helps in understanding bonding and structural trends of Groups I and II and lanthanide organometallic species. Furthermore, potential applications of allyl complexes make them desirable in materials and engineering fields. Bis(1,3-trimethylsilyl)allyl metal complexes are efficient catalysts in the polymerization of MMA, so may have benefits in additional catalytic processes. Moreover, observation of charge transfer in terpyridine adducts of diallylterbium complexes may lead to further exploration of the electronic and magnetic behavior of similar species. The true impact of the trimethylsilylated allyl ligand has only begun to be realized, and subsequent work will likely reveal even more applications.

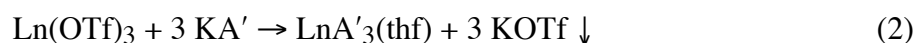
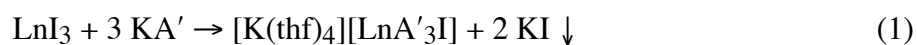
CHAPTER I

STRUCTURAL AND BONDING MOTIFS IN BULKY ALLYL COMPLEXES OF THE LATE LANTHANIDE METALS

Introduction

The lanthanide series of elements is a unique section of the periodic table, because unlike transition metals, all the lanthanides have the same common oxidation state (3+) and display closely spaced radius sizes (La(III), $4f^0$ to Lu(III), $4f^{14}$: 1.03-0.861 Å for CN = 6).³⁰ These features allow for direct comparisons between the structures of lanthanide compounds. The influence of size on geometry is easily noticeable in the crystal structures of the lanthanide trihalides. For example, lanthanides lighter than terbium have the UCl_3 -type structure, those heavier than terbium exist in the YCl_3 -type structure, and $TbCl_3$ (and a second form of $DyCl_3$) has a different geometry from either of these.³¹⁻³⁴ Similar themes are seen in lanthanide organometallic chemistry. Most $LnCp_3$ ($Cp = C_5H_5$) complexes exist as polymeric chains, where the structure of the chain varies with metal size. For the smallest lanthanide, lutetium, σ -bound cyclopentadienyl ligands bridge $LuCp_2$ units forming a $[LuCp_2(\mu-\eta^1:\eta^1-Cp)]_\infty$ chain. Despite the small difference in radius size between lutetium and ytterbium ($Yb(III) = 0.985$ Å; $Lu(III) = 0.977$ Å for CN = 8),³⁰ the ytterbium complex exists as a monomer. The structure of metals with radii only slightly larger ($Y(III)$, $Tm(III)$, $Er(III) = 1.004$ – 1.052 Å for CN = 8)³⁰ consists of three η^5 -Cp ligands around the metal atom in which the monomer units form a chain via van der Waals interactions.³⁵

We have recently synthesized bis(1,3-trimethylsilyl)allyl lanthanide complexes as pre-catalysts for the polymerization of methyl methacrylate and observed variety in the structures of these complexes. It is reported that when three equivalents of KA' (where A' = [1,3-(SiMe₃)₂C₃H₃]) are treated with LnI₃ in THF, lanthanate complexes of the type [K(thf)₄][LnA'₃I] (Ln = Ce, Pr, Nd, Gd, Tb, Dy, and Er) are isolated (eq 1).¹⁸ However, when two equivalents of the same potassium allyl precursor is treated with NdI₃(thf)_{3,5}, a mixture of two neutral species, NdA'I₂(thf)_{1.25} and NdA'₂I(thf)₂, is isolated.^{20,36} Replacement of the iodide starting material with the analogous lanthanide triflate and treatment in a 1:3 ratio with KA' yields neutral triallyl species with a coordinated thf molecule (eq 2).^{18,19} These types of complexes have been synthesized with cerium, neodymium, and terbium.



Regardless of the reaction stoichiometry, when either two or three equivalents of KA' are treated with YCl₃, the unsolvated triallylyttrium product is isolated (see Chapter IV). This is the first example of a homoleptic unsolvated lanthanide complex with this allyl ligand. Surprisingly, LaA'₂Cl(thf) is isolated when LaCl₃ is treated with two or three equivalents of the potassium allyl starting material, a result that is counterintuitive based on radius size (La(III) = 1.03 Å; Y(III) = 0.90 Å for CN = 6)³⁰, as lanthanum should be more readily able to accommodate three allyl ligands.²¹

To explore further the influence of radius size and reaction precursors on the structures of trimethylsilyl-substituted allyl complexes containing late lanthanide metals, triallyl complexes were synthesized with dysprosium, holmium, erbium, thulium, and lutetium. In all these compounds (as well as analogous complexes with metals throughout the periodic table), the trimethylsilylated ligands function as bulky η^3 -bonded units that provide enhanced solubility and kinetic stability, but are not involved in more complex metal–ligand interactions. However, the trimethylsilyl groups are shown to be potential sites of reactivity in holmium allyl complexes. The resultant generation of dimethylsilylene and allylidene ligands represents previously unobserved transformations in f-element chemistry.

Experimental

General Considerations. All manipulations were performed with the rigorous exclusion of air and moisture using high vacuum, Schlenk, or drybox techniques. ^1H NMR spectra were collected on a Bruker NMR spectrometer at 300 MHz. Solution magnetic susceptibility data were obtained in toluene- d_8 on a Bruker DRX300 spectrometer using the Evans' NMR method.³⁷⁻⁴⁰ Elemental analyses (for C and H) were performed by Desert Analytics, Tucson, AZ. Complexometric methods were used for elemental analysis of lanthanide metals.⁴¹ Thermogravimetric analysis (TGA) was performed on a TA Instruments high-resolution TGA model 2950. Samples were heated in a N_2 atmosphere at 10 $^\circ\text{C}/\text{min}$ from room temperature to 900 $^\circ\text{C}$.

Materials. Nominally anhydrous lanthanide triflates (Aldrich) were dried under vacuum (10^{-2} Torr) for 12 h at 100–120 $^\circ\text{C}$ prior to use. Anhydrous HoCl_3 (Strem), HoI_3

(Aldrich), DyI₃ (Strem), and ErCl₃ (Strem) were used as received. Holmium triflate (Ho(OTf)₃•xH₂O) was purchased from Alfa Aesar and dried for one week under vacuum (10⁻² Torr) at 125 °C. Even after drying, TGA measurements on Ho(OTf)₃•xH₂O indicate a 2.8% mass decrease at ca. 134 °C, consistent with the loss of coordinated H₂O (boiling point of triflic acid = 162 °C at atmospheric pressure). LiA' and KA' were prepared according to literature procedure.^{6,19} Hexanes and toluene were distilled under nitrogen from potassium benzophenone ketyl.⁴² Anhydrous tetrahydrofuran (THF) was purchased from Aldrich and used as received. Toluene-*d*₈ was vacuum distilled from Na/K (22/78) alloy and stored over Type 4A molecular sieves.

Synthesis of LuA'3. A 125 mL Schlenk flask was charged with Lu(OTf)₃ (0.221 g, 0.355 mmol), THF (50 mL), and a stirring bar. An addition funnel was prepared with KA' (0.239 g, 1.065 mmol) in THF (40 mL). After assembly in the glovebox, the apparatus was placed on a Schlenk line. After cooling the Lu(OTf)₃ solution to -78 °C, the KA' solution was added dropwise with stirring over 30 min. After warming to room temperature overnight, the orange reaction mixture was evaporated to dryness, then extracted with hexanes. The extract was filtered through a medium porosity frit, and the removal of hexanes under vacuum yielded an orange oil with small crystals along the side of the flask. Dissolution of the product in a small amount of toluene and cooling to -30 °C allowed for the growth of X-ray quality orange crystals (0.20 g, 77%). Anal. Calc. C₂₇H₆₃Si₆Lu: Lu, 23.93. Found: Lu, 23.84. ¹H NMR (25 °C, 300 MHz, tol-*d*₈): δ 0.20 (s, 72H, SiMe₃), 3.73 (d, *J* = 16.2 Hz, 6H, CHCHCH), 7.49 (t, *J* = 16.2 Hz, 3H, CHCHCH).

Synthesis of LnA'₃, where Ln = Dy, Ho, Er, Tm. The procedure follows that of the synthesis of LuA'₃. All reactions yielded orange products that crystallized upon cooling to -30 °C. The yield, metal analysis, and solution magnetic moments for each complex are listed in Table 1.

Using the same procedure, HoA'₃ (identified with elemental analysis) was also obtained with vacuum dried Ho(OTf)₃•xH₂O if the solvent is removed no later than 4 h after addition of the KA' solution.

Table 1. Experimental data for LnA'₃, where A' = [1,3-(SiMe₃)₂C₃H₃], Ln = Dy, Ho, Er, Tm, Lu.

Complex	Precursor	Yield (%)	Calc. Anal. (Ln%)	Exp. Anal. (Ln%)	Calc. μ _{eff} (BM)	Exp. μ _{eff} (BM)
DyA' ₃	Dy(OTf) ₃	75.7	22.61	22.85	10.65	10.64
DyA' ₃	DyI ₃	74.3	22.61	22.03	10.65	10.52
HoA' ₃	Ho(OTf) ₃	86.0	22.87	22.60	10.60	10.00
HoA' ₃	HoI ₃	91.1	22.87	22.50	10.60	10.25
HoA' ₃	HoCl ₃	80.0	22.87	22.18	10.60	9.95
ErA' ₃	Er(OTf) ₃	87.8	23.12	22.89	9.58	8.94
ErA' ₃	ErCl ₃	76.7	23.12	23.24	9.58	9.23
TmA' ₃	Tm(OTf) ₃	76.7	23.29	23.48	7.56	7.13
LuA' ₃	Lu(OTf) ₃	77.0	23.93	23.84	0	0

Synthesis of [Li(thf)₄][HoA'₃I]. A 125 mL Schlenk flask was charged with HoI₃ (0.279 g, 0.511 mmol), THF (50 mL), and a stirring bar. An addition funnel was prepared

with LiA' (0.299 g, 1.555 mmol) in THF (40 mL). After assembly in the glovebox, the apparatus was placed on a Schlenk line. After cooling the HoI₃ solution to -78 °C, the LiA' solution was added dropwise with stirring over 30 min. After warming to room temperature overnight, the orange reaction mixture was evaporated to dryness, then extracted with hexanes. The extract was filtered through a medium porosity frit, and the removal of hexanes under vacuum yielded an orange oil with small crystals along the side of the flask. Dissolution of the product in a small amount of toluene and cooling to -30 °C allowed for the growth of small orange crystals (0.52 g, 88.9%). X-ray crystallography was not possible presumably due to loss of solvent during shipping. Anal. Calc. C₄₃H₉₅O₄Si₆HoILi: Ho, 14.42. Found: Ho, 14.36. Solution magnetic moment (μ_{eff}); Calculated: 10.60 BM. Experimental: 10.37 BM.

Attempted synthesis of HoA'3. Synthesis of [Ho{1,3-(SiMe₃)₂C₃H₃}{ μ -(1-(SiMe₃)-3-(SiMe₂CH₂)C₃H₃)}]2 (1). A 125 mL Schlenk flask was charged with vacuum dried Ho(OTf)₃•xH₂O (0.258 g, 0.380 mmol), THF (50 mL), and a stirring bar. An addition funnel was prepared with KA' (0.260 g, 1.16 mmol) in THF (40 mL). After assembly in the glovebox, the apparatus was placed on a Schlenk line. When the Ho(OTf)₃ solution had been cooled to -78 °C, the KA' solution was added dropwise with stirring over 30 min. After warming to room temperature (6.5–15 h), the orange reaction mixture was evaporated to dryness, then extracted with hexanes. The extract was filtered, and removal of hexanes under vacuum yielded an orange oil with small crystals along the side of the flask, 0.15 g (74%). Dissolution of the product in a small amount of hexanes and cooling to -30 °C allowed for the growth of X-ray quality yellow-orange crystals.

Anal. Calc. C₃₆H₈₂Ho₂Si₈: C, 40.43; H, 7.73. Found: C, 40.34; H, 8.21. Solution magnetic moment (μ_{eff}); Calculated: 10.6 BM (single center). Experimental: 11.7 BM.

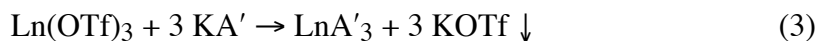
Synthesis of Ho₂[μ -{1-(SiMe₃)-3-(SiMe₂CH₂)C₃H₃}]₂[μ -{1,3-(SiMe₃)₂C₃H₂}](thf)₂ (2). A 125 mL Schlenk flask was charged with vacuum dried Ho(OTf)₃·xH₂O (0.252 g, 0.371 mmol), THF (50 mL), and a stirring bar. An addition funnel was prepared with KA' (0.258 g, 1.15 mmol) in THF (40 mL). After assembly in the glovebox, the apparatus was placed on a Schlenk line. When the Ho(OTf)₃ solution had been cooled to -78 °C, the KA' solution was added dropwise with stirring over 30 min. After warming to room temperature overnight (~20 h), the orange reaction mixture was evaporated to dryness, then extracted with hexanes. The extract was filtered, and the removal of hexanes under vacuum yielded an orange oil with small crystals along the side of the flask (0.15 g, 79%). Dissolution of the product in a small amount of hexanes and cooling to -30 °C allowed for the growth of X-ray quality yellow-orange crystals. Anal. Calc. C₃₅H₇₆Ho₂O₂Si₆: C, 40.92; H, 7.46. Found: C, 40.05; H, 7.46. Solution magnetic moment (μ_{eff}); Calculated: 10.6 BM (single center). Experimental: 12.4 BM.

General Procedures for X-ray Crystallography. Data collection and structure solution were conducted at the X-Ray Crystallographic Laboratory at the University of Minnesota. All calculations were performed using the current SHELXTL⁴³ suite of programs. A suitable crystal was located and attached to the tip of a glass capillary and mounted on a Siemens SMART Platform CCD diffractometer for data collection at 173(2) K.⁴⁴ A preliminary set of cell constants was calculated from reflections harvested from three sets of 20 frames. These initial sets of frames were oriented such that orthogonal wedges of reciprocal space were surveyed. Data collection of a randomly

oriented region of reciprocal space was carried out using Mo K α radiation (graphite monochromator). The intensity data were corrected for absorption with SADABS.⁴⁵ Final cell constants were calculated from strong reflections from the actual data collection after integration (SAINT).⁴⁶ Relevant crystal and collection data parameters for TmA'₃, **1**, and **2** can be found in Tables 23–28.

Results and Discussion

Synthesis of Triallyllanthanide Complexes. Unsolvated triallyllanthanide complexes were prepared by treating anhydrous Ln(OTf)₃ (Ln = Dy, Ho, Er, Tm, Lu) with three equivalents of KA' in THF at –78 °C (eq 3). After overnight stirring, THF was removed under reduced pressure from the orange reaction mixtures, the residues were extracted with hexanes, and the solutions were filtered to remove KOTf.



Removal of hexanes under reduced pressure, dissolution in toluene, and cooling to –30 °C overnight allowed for the growth of X-ray quality orange crystals of each product in good yield (75–81%). Each product is indefinitely stable at room temperature under inert atmosphere and tolerates brief (< 5 min) exposure to air without visible decomposition. Solving the crystal structures of these complexes proved difficult, as several conformations of the allyl ligands around the metal center are favorable leading to disorder in the crystal structure (a phenomenon also observed with yttrium, see Chapter IV). Although the thulium complex, TmA'₃, was the only structure that could be solved,

crystallographic information for the other complexes indicates that an analogous unsolvated triallyllanthanide product was isolated for the other metals. Elemental analysis and solution magnetic susceptibility (or ^1H NMR, for LuA'_3) of each compound further confirmed this.

Three allyl ligands are η^3 -bound to the metal center in TmA'_3 , with $\text{Tm}-\text{C}$ bond distances ranging from 2.326(2) to 2.606(2) Å (Figure 1). The ligands are arranged around the metal center such that one allyl ligand is oriented anti-parallel to the other two. The trimethylsilyl groups are in a *syn, syn* configuration, as is true with other trimethylsilyl-substituted allyl lanthanide complexes.^{18-20,36}

The isolation of unsolvated triallyl complexes is not surprising, as the radii of the five lanthanide metals ($\text{Dy(III)}-\text{Lu(III)} = 0.912-0.861$ Å for CN 6) are smaller than those of the previously synthesized solvated complexes ($\text{Ce(III)}-\text{Tb(III)} = 1.01-0.923$ Å for CN 6).³⁰ The smaller radii of the late lanthanide metals inhibits the binding of a thf molecule. The unsolvated triallylyttrium complex described in Chapter IV follows this trend as well, as its radius is in the range of that of the metals in the unsolvated complexes ($\text{Y(III)} = 0.90$ Å for CN 6).³⁰

In separate experiments, HoCl_3 and ErCl_3 were each treated with two or three equivalents of KA' under the reaction conditions previously described (eq 4). All four reactions produced an orange oil from which X-ray quality crystals were grown. The crystallized products of the reactions were the unsolvated LnA'_3 species. They possess the same unit cell as the disordered complex TmA'_3 . These results are analogous to reaction of KA' and YCl_3 ; YA'_3 was isolated when either two or three equivalents of KA' were used (see Chapter IV).

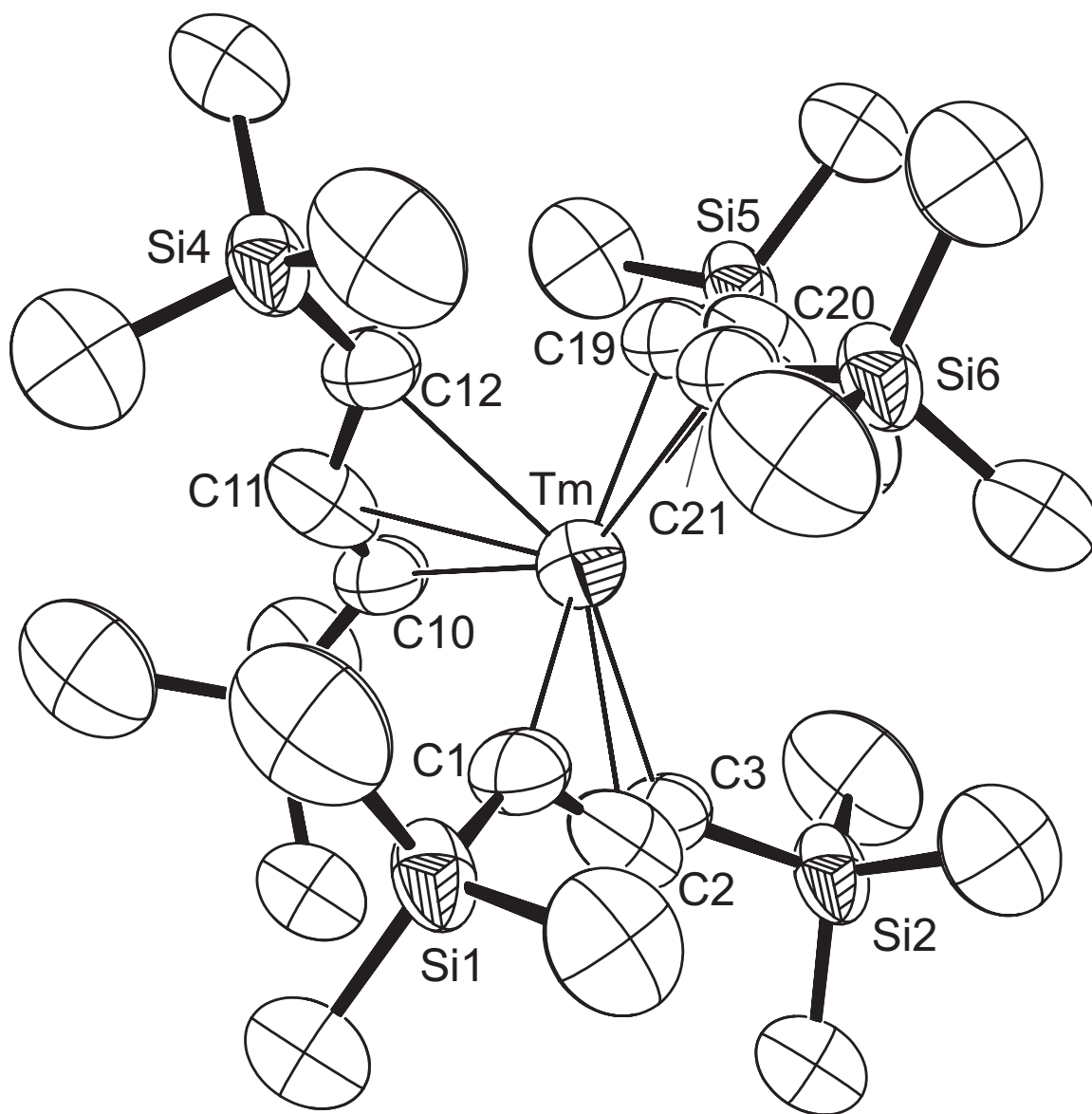
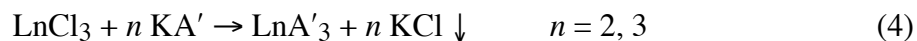


Figure 1. ORTEP of TmA'3, with thermal ellipsoids at the 50% level. Hydrogen atoms have been omitted for clarity.



Under the same reaction conditions, three equivalents of KA' were treated with HoI₃ (eq 5), and a concentrated toluene solution crystallized overnight yielding X-ray quality crystals. The crystal structure was afflicted with the same disorder seen in all of these complexes, but enough information was available to indicate that the product was the unsolvated complex HoA'₃. When HoI₃ was treated with two equivalents of KA', HoA'₃ was again isolated, despite the mismatch in stoichiometry.



The isolation of the triallylholmium complex from the iodide starting material was unexpected, since it has been reported that the use of iodide salts of holmium's neighboring metals (dysprosium and erbium) in the same reaction scheme produced lanthanate products [K(thf)₄][LnA'₃I] (eq 1).¹⁸ The crystal structure of the erbium complex was reported, but the dysprosium complex was not fully characterized. Therefore, in this work, the reaction was repeated and the dysprosium product was fully characterized (see Table 1). Single crystal X-ray diffraction indicates that the unit cell is isomorphous with the previously described unsolvated complexes, rather than a lanthanate complex. Isolation of DyA'₃ is further supported by elemental analysis and solution magnetic susceptibility measurements.

The synthesis of DyA'₃ and HoA'₃ from the LnI₃ starting material is puzzling, since lanthanate products are formed with neighboring metals (Tb and Er, eq 1). To investigate

this anomaly, the crystal structures of $[\text{K}(\text{thf})_4][\text{LnA}'_3\text{I}]$ ($\text{Ln} = \text{Ce}, \text{Tb}, \text{Er}$) were reevaluated. It seems that lithium, not potassium, is the majority cation in each complex. The coordination of four THF molecules is typical for Li^+ , while higher coordination is observed with K^+ (cf., $[\text{K}(\text{thf})_6][\text{Pr}\{\text{N}(\text{SiMe}_3)_2\}_4]$;⁴⁷ $[\text{K}(\text{thf})_6][\text{Si}(\text{NEt})_2\text{C}_6\text{H}_4]_4$;⁴⁸ no references for complexes containing $[\text{K}(\text{thf})_4]^+$ were found upon searching the Cambridge Structural Database System (November 2005)). Also, the Li–O bond lengths (1.86(5)–1.94(5) Å) in each lanthanate structure are typical for other $[\text{Li}(\text{thf})_4]^+$ species (cf., 1.889(5)–1.922(5) Å in $[\text{Li}(\text{thf})_4][\text{Ga}\{\text{Si}[\text{Si}(t\text{-Bu})_2\text{Me}]_2\}_2]$ ⁴⁹ and 1.86(2)–1.97(2) Å in $[\text{Li}(\text{thf})_4][\text{Th}\{1,3\text{-}[2,6\text{-}(i\text{-Pr})_2\text{-C}_6\text{H}_3\text{N}]_2(\text{CH}_2)_3\}_2\text{Cl}]$;⁵⁰ whereas K–O(thf) bond lengths tend to be longer ($\sim 2.62\text{--}2.76$ Å).^{47,48,51}

Incomplete transmetalation of LiA' with potassium *t*-butoxide in the synthesis of KA' would lead to the presence of Li^+ in the reaction mixture. Furthermore, LiI is slightly soluble in THF (unlike KI), which could cause incomplete metathesis and isolation of the lanthanate products $[\text{Li}(\text{thf})_4][\text{LnA}'_3\text{I}]$. Therefore, the difference in allyl starting material would account for the variation in products when lanthanide iodide salts are used. To further support this idea, HoI_3 was treated with three equivalents of LiA' , under the previously described reaction conditions. Solution magnetic susceptibility and elemental analysis indicate the isolation of $[\text{Li}(\text{thf})_4][\text{HoA}'_3\text{I}]$; an aqueous AgNO_3 test further supports the synthesis of the lanthanate product (i.e., yellow AgI precipitated). While HoA'_3 is formed upon treatment of HoI_3 with KA' , the use of LiA' leads to the isolation of $[\text{Li}(\text{thf})_4][\text{HoA}'_3\text{I}]$.

With the bis(1,3-trimethylsilyl)allyl ligand, it seems that although variations in lanthanide starting materials do not change the product of late lanthanide allyl complexes, the metal cation of the allyl precursor has a profound effect on the isolated product. This differs from observations in cyclopentadienyl lanthanide chemistry, where varying the metal of the cyclopentadienyl starting material does not influence the outcome of the reaction.³⁵

Analysis of Bonding in Lanthanide Allyl Complexes. The degree of covalency in organometallic lanthanide complexes is a topic that has been investigated through comparison of metal–ligand bond lengths in X-ray crystal structures of such compounds.⁵²⁻⁵⁴ One approach is to examine the ability of the sum of the cation and anion radii to reproduce observed metal–ligand distances. With non-spherical ligands, however, the ligand radius is difficult to define; therefore, the difference between the metal–carbon distance of the ligand and the metal radius has been used to define a ligand’s “radius” (R_{M-C}). While previous surveys have focused on cyclopentadienyl and cyclooctatetraenyl lanthanide compounds, compounds with allyl ligands have not been included. A variety of lanthanide complexes with the bis(1,3-trimethylsilyl)allyl ligand have been synthesized and crystallographically characterized, enabling a similar study to be performed on bulky allyl lanthanide complexes. Bond distances for the structurally authenticated trivalent bis(1,3-trimethylsilyl)allyllanthanide complexes and their corresponding radii are listed in Table 2. The unit cell of $NdA'_2I(thf)_2$ contains two essentially identical molecules; bond distances for both molecules are listed.²⁰

As evidenced by the cerium and terbium compounds, the charge on the complex seems to have little influence on the radius of the allyl ligand. The R_{M-C} radius in each

anionic complex is only slightly longer ($\Delta = 0.02 \text{ \AA}$) than that of the corresponding neutral complex. With the exception of TmA'_3 , the range in $R_{\text{M-C}}$ radii is very narrow (1.675 to 1.70 \AA), indicative of ionic bonding in these complexes. This is similar to the trend observed with cyclopentadienyl lanthanide complexes, where complexes with the same charge display a small range of bond lengths.⁵² Although the ligand radius in TmA'_3 is slightly smaller (1.65 \AA), this difference is likely to be merely an artifact of the aforementioned disorder in the crystal structure.

Table 2. Bond distances for trivalent lanthanide allyl complexes, where $R_{\text{M-C}} = (\text{M-C}(\text{avg})) - (\text{radius})$. All distances and radii are in \AA . $\text{A}' = [1,3-(\text{SiMe}_3)_2\text{C}_3\text{H}_3]$.

Complex	Radius ³⁰	M-C	M-C(avg)	$R_{\text{M-C}}$
$\text{CeA}'_3(\text{thf})$ ¹⁹	1.07 (CN 7)	2.658(8)–2.805(6)	2.75(2)	1.68
$[\text{CeA}'_3\text{I}]^-$ ¹⁸	1.07 (CN 7)	2.677(9)–2.859(10)	2.77(3)	1.70
$\text{NdA}'_3(\text{thf})$ ¹⁸	1.03 (CN 7)	2.634(8)–2.786(7)	2.73(2)	1.70
$\text{NdA}'_2\text{I}(\text{thf})_2$ ²⁰	1.03 (CN 7)	2.671(6)–2.781(6) 2.678(6)–2.757(5)	2.73(1) 2.72(1)	1.70 1.69
$\text{TbA}'_3(\text{thf})$ ¹⁹	0.98 (CN 7)	2.556(9)–2.765(9)	2.66(2)	1.68
$[\text{TbA}'_3\text{I}]^-$ ¹⁸	0.98 (CN 7)	2.56(2)–2.835(19)	2.68(3)	1.70
$[\text{ErA}'_3\text{I}]^-$ ¹⁸	0.945 (CN 7)	2.462(19)–2.88(2)	2.62(2)	1.675
TmA'_3	0.88 (CN 6)	2.326(2)–2.606(2)	2.53(1)	1.65

In general, the $R_{\text{M-C}}$ radii for divalent lanthanide bis(1,3-trimethylsilyl)allyl complexes (Table 3) are smaller than those of the trivalent compounds; this charge dependence is also observed in cyclopentadienyl lanthanide complexes.⁵² The

diallyllanthanide complexes $\text{LnA}'_2(\text{thf})_2$ ($\text{Ln} = \text{Eu}, \text{Sm}, \text{Yb}$) are isomorphous with calcium⁷ and strontium⁸ allyl complexes, the bond distances of which are also listed in Table 3. The $R_{\text{M-C}}$ radii for the europium, samarium, and strontium complexes are almost identical (1.60–1.621 Å), but the analogous value for the calcium complex (1.654 Å) is slightly higher, and that of $\text{YbA}'_2(\text{thf})_2$ is even larger (1.72 Å). These two compounds contradict the typical structural similarities observed in divalent lanthanide and alkaline earth complexes.⁵²

Table 3. Bond distances for divalent lanthanide and alkaline earth allyl complexes, where $R_{\text{M-C}} = (\text{M-C}(\text{avg})) - (\text{radius})$. All bond distances and radii are in Å. $\text{A}' = [1,3\text{-}(\text{SiMe}_3)_2\text{C}_3\text{H}_3]$.

Metal	Radius ³⁰	M–C	M–C(avg)	$R_{\text{M-C}}$
$\text{SrA}'_2(\text{thf})_2$ ⁸	1.18 (CN 6)	2.797(3)–2.805(3)	2.801(5)	1.621
$\text{EuA}'_2(\text{thf})_2$ ¹⁹	1.17 (CN 6)	2.762(14)–2.789(14)	2.77(2)	1.60
$\text{SmA}'_2(\text{thf})_2$ ¹⁹	1.17 (CN 6)	2.765(6)–2.796(6)	2.78(1)	1.61
$[\text{SmA}'_3]^-$ ³⁶	1.17 (CN 6)	2.743(5)–2.895(5)	2.84(1)	1.67
$\text{YbA}'_2(\text{thf})_2$ ¹⁹	1.02 (CN 6)	2.729(9)–2.754(9)	2.74(1)	1.72
$\text{CaA}'_2(\text{thf})_2$ ⁷	1.00 (CN 6)	2.648(3)–2.662(3)	2.654(5)	1.654

The dissimilarity in the calcium and ytterbium complexes' $R_{\text{M-C}}$ radii and M–C bond distances is also surprising. Since the ionic radii of calcium and ytterbium differ only slightly (Ca(II), 1.00 Å; Yb(II), 1.02 Å for CN 6),³⁰ bond distances and angles of the ligands in their respective complexes are almost always similar.²⁸ It is unusual, therefore,

to find that this is not the case with these $\text{MA}'_2(\text{thf})_2$ complexes (Table 3). The general expansion of the ytterbium compound is also reflected in the unit cell constants and resulting volumes of the two compounds: 3613 \AA^3 for $\text{CaA}'_2(\text{thf})_2$ and 3991 \AA^3 for $\text{YbA}'_2(\text{thf})_2$, a 10.5% increase.

The original report of the $\text{CaA}'_2(\text{thf})_2$ complex notes that the average Ca–C distance of $2.654(5) \text{ \AA}$ in $\text{CaA}'_2(\text{thf})_2$ is indistinguishable from that for cyclopentadienyl rings in complexes with formally six-coordinate Ca(II) centers (e.g., $2.64(1) \text{ \AA}$ in $\text{Ca}[\text{C}_5(i\text{-Pr})_4\text{H}]_2$ ⁵⁵ or $2.677(4) \text{ \AA}$ in $\text{Ca}[\text{C}_5(t\text{-Bu})_3\text{H}_2]\text{I}(\text{thf})_2$).⁵⁶ In contrast, the Yb–C range of $2.741(9)\text{--}2.748(9) \text{ \AA}$ in $\text{YbA}'_2(\text{thf})_2$ is noticeably longer than that for cyclopentadienyl rings in complexes with six-coordinate Yb(II) centers (e.g., $2.636(3)\text{--}2.690(3) \text{ \AA}$ in $\text{Yb}(\text{C}_5\text{Me}_5)_2$ ²⁵ and $2.63(2)\text{--}2.670(13) \text{ \AA}$ in $\text{Yb}(\text{C}_5\text{Me}_5)\text{Si}(\text{SiMe}_3)_3(\text{thf})_2$).⁵⁷ Harder has recently proposed that Yb–L bonds may be weaker than analogous Ca–L bonds, even when of similar lengths, owing to repulsion from the filled f^{14} shell of Yb(II).²⁸ If so, $\text{YbA}'_2(\text{thf})_2$ may represent a case in which the weakness is reflected in longer bonds.

The only crystallographically authenticated divalent lanthanide bis(1,3-trimethylsilyl)allyl complex that does not have the $\text{MA}'_2(\text{thf})_2$ formula is the dimer $[\{\text{K}(\text{thf})_2\}\{\text{SmA}'_3\}]_2$ (shown as $[\text{SmA}'_3]^-$ in Table 3);³⁶ it has a larger $R_{\text{M-C}}$ radius than the other divalent complexes. Although it is a formally six-coordinate complex, its cyclic structure and the coordination of the allyl ligands to potassium atoms are likely to affect the M–C bond lengths, so its radius deviates from the trend of the monomeric complexes.

Synthesis of Diholmium Complexes. In an attempt to isolate HoA'_3 , holmium triflate that contains ca. 3% water (see Experimental Section) was treated with three

equivalents of KA' in THF at $-78\text{ }^{\circ}\text{C}$. Removal of THF from the orange solution after no more than 4 hours yields HoA'3; however, if the reaction time is extended up to 15 hours, a different hydrocarbon-soluble yellow-orange complex (**1**) is isolated in good (74%) yield. It is indefinitely stable at room temperature under inert atmosphere and tolerates brief ($< 10\text{ min}$) exposure to air without visible decomposition. Crystals of **1** grown from a concentrated hexanes solution contain the dimeric species illustrated in Figure 2. There are two independent but virtually identical molecules in the asymmetric unit, each containing a crystallographic inversion center. One η^3 -coordinated allyl ligand is bound to each metal, but hydrogen abstraction from a trimethylsilyl group has occurred on a second allyl ligand associated with each metal center, forming dimethylsilylene units that bridge the holmium atoms. The bridging carbons are nearly symmetrically positioned between the holmium centers at 2.478(4) and 2.512(4) Å (Table 4). These distances are slightly shorter than the 2.563(18) Å separation observed for the bridging methyl groups in $[\text{Li}(\text{tmed})]_3[\text{Ho}(\mu\text{-Me})_6]$,⁵⁸ perhaps reflecting the dinegative charge of the ligands in **1**.

Table 4. Selected bond distances (Å) for **1**.

Atoms	Distance	Atoms	Distance
Ho1–C4	2.603(4)	Ho1–C15	2.575(4)
Ho1–C5	2.617(4)	Ho1–C18	2.478(4)
Ho1–C6	2.510(4)	Ho1'–C18	2.512(4)
Ho1–C13	2.528(4)	Ho1···Ho1'	3.5243(8)
Ho1–C14	2.595(4)		

When the reaction that produced **1** was allowed to continue for 20 hours before workup, a different yellow-orange dinuclear product (**2**) was isolated. The X-ray structure of crystals grown from hexanes reveals that in addition to two dimethylsilylene bridges, the metal centers are joined with a μ - η^1, η^3 -allylidene ligand (Figure 3). A thf ligand completes the coordination sphere of each metal. In **2**, the methylene carbons of the dimethylsilylene bridges are at longer distances and are more asymmetrically bonded than in **1**, with distances from C16 and C25 ranging from 2.517(5) Å to 2.629(5) Å (Table 5). The bridging allylidene has Ho–C6 distances of 2.422(5) and 2.500(5) Å. As a consequence of being bridged by three dianionic ligands, the Ho···Ho distance in **2** has contracted from the 3.5243(8) Å separation observed in **1** to 3.1874(4) Å. The latter is the shortest yet observed in an organoholmium compound.⁵⁹

Table 5. Selected bond distances (Å) for **2**.

Atoms	Distance	Atoms	Distance
Ho1–C4	2.564(5)	Ho2–C16	2.517(5)
Ho1–C5	2.645(5)	Ho2–C22	2.681(5)
Ho1–C6	2.500(5)	Ho2–C23	2.683(5)
Ho2–C6	2.422(5)	Ho2–C24	2.571(5)
Ho1–C16	2.570(5)	Ho1–C25	2.629(5)
Ho1–O1	2.383(4)	Ho2–C25	2.519(5)
Ho1–C13	2.683(5)	Ho2–O2	2.367(4)
Ho1–C14	2.663(5)	Ho1···Ho2	3.1874(4)
Ho1–C15	2.584(5)		

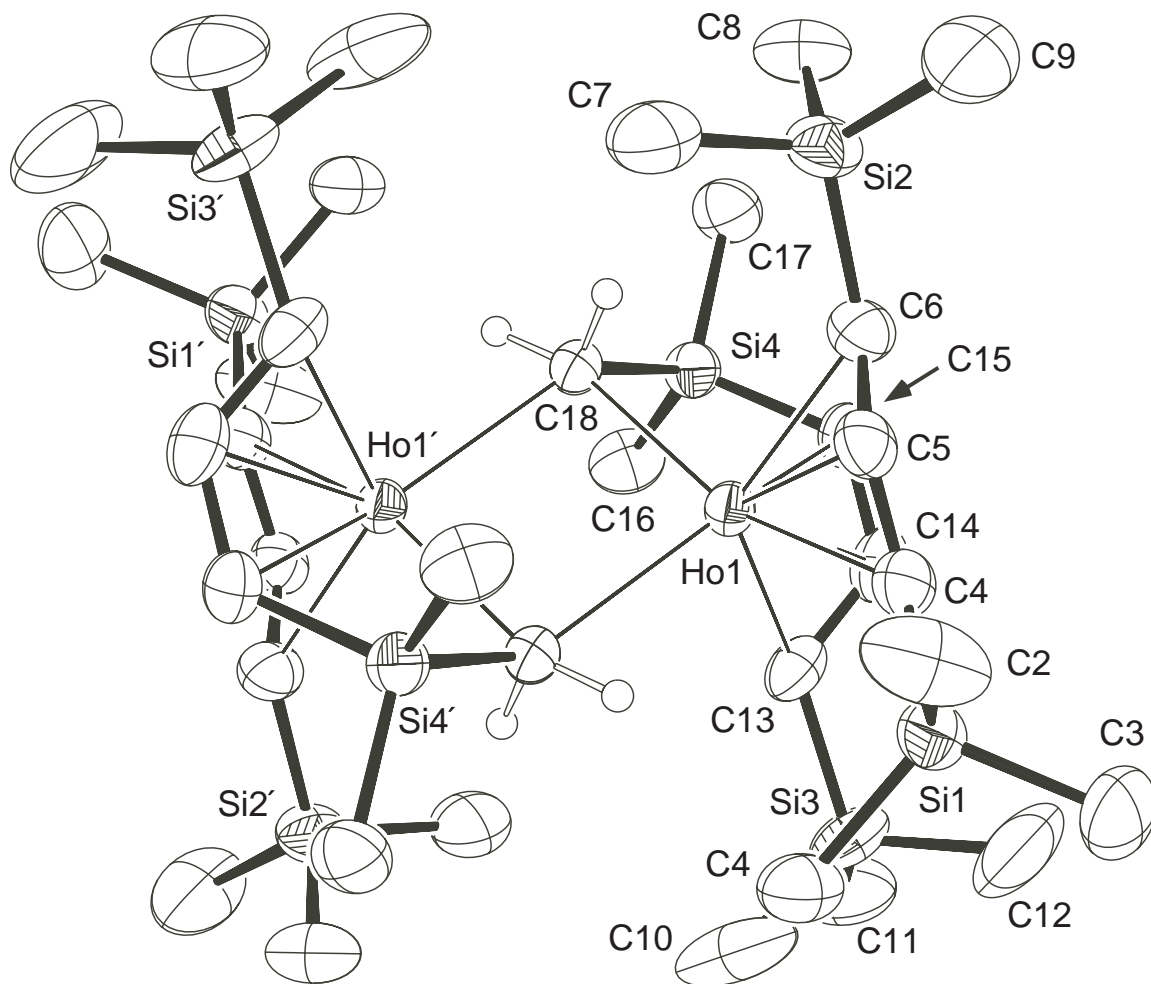


Figure 2. ORTEP of **1**, with thermal ellipsoids at the 50% level. Hydrogen atoms not involved in the dimethylsilylene bridges have been omitted for clarity.

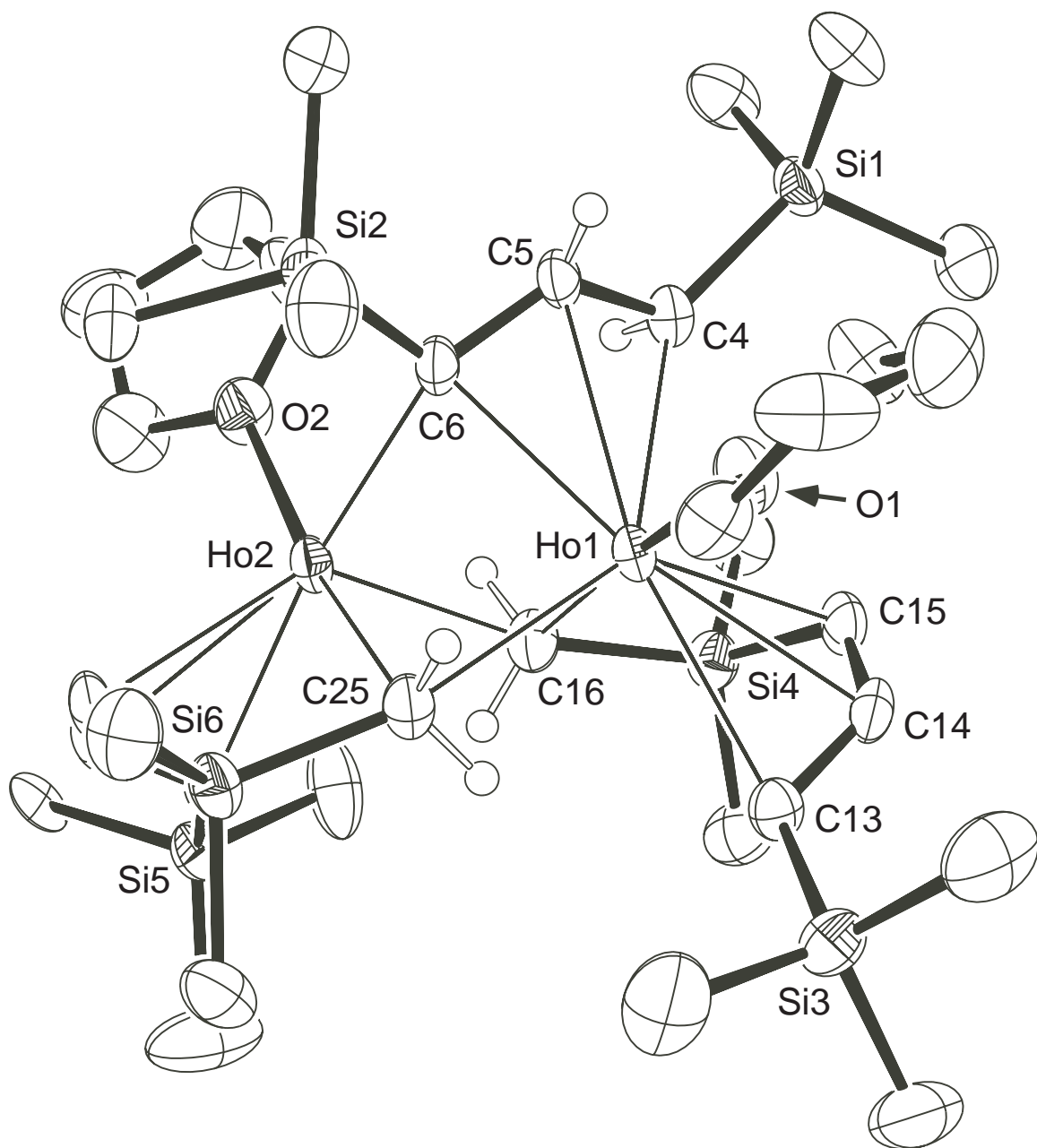
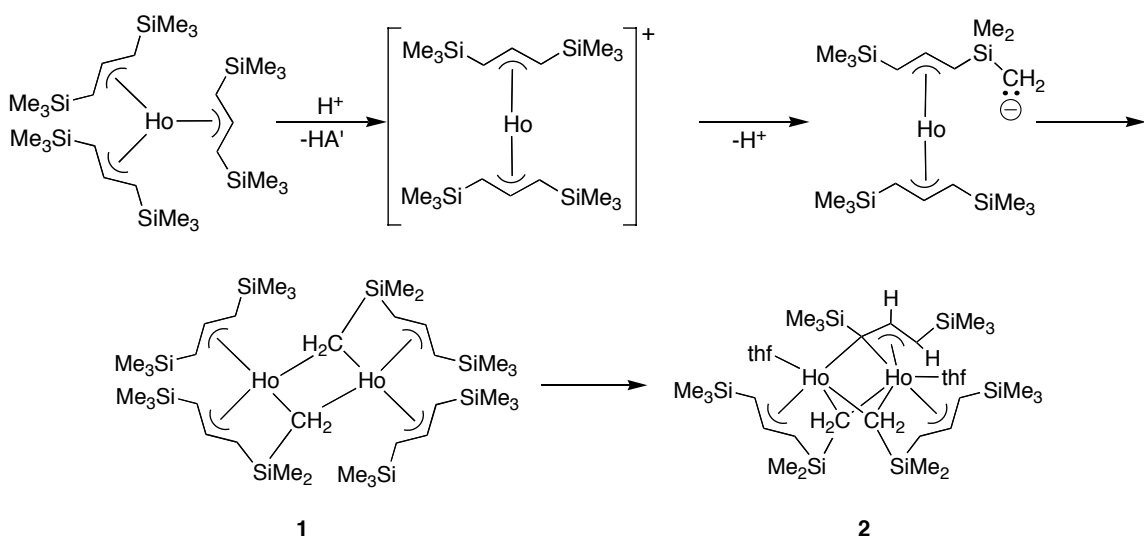


Figure 3. ORTEP of **2**, with thermal ellipsoids at the 50% level. Hydrogen atoms not involved in the dimethylsilylene or allylidene bridges have been omitted for clarity.

The mechanism of formation of **1** and **2** is of interest, particularly as lanthanide triflates are widely used as Lewis acids in organic transformations.⁶⁰ Although not previously observed in allyl complexes, C–H activation of trimethylsilyl groups is known in cyclopentadienyl compounds of the early transition metals. For example, when $\text{Ti}^{\text{IV}}(\text{C}_5\text{Me}_4\text{SiMe}_3)_2\text{Cl}_2$ is treated with magnesium metal, the paramagnetic species $\text{Ti}^{\text{III}}(\eta^5:\eta^1\text{-C}_5\text{Me}_4\text{SiMe}_2\text{CH}_2)(\eta^5\text{-C}_5\text{Me}_4\text{SiMe}_3)$ is one of the products.⁶¹ Similar C–H activation has been extensively investigated in zirconium metallocenes.⁶² Analogous reductive elimination is not available for the generation of **1**, as holmium is not known in oxidation states other than zero and three (the $\text{Ho}(\text{III})/\text{Ho}(\text{II})$ reduction potential is estimated at -2.9 V;⁶³ no $\text{Ho}(\text{II})$ compounds exist).⁶⁴ Abstraction of a proton from a SiMe_3 group can also be initiated with a Lewis acid such as $\text{B}(\text{C}_6\text{F}_5)_3$, with no formal change of oxidation state required. In these cases, the Lewis acid serves to abstract an alkyl group from the metal to form a cationic intermediate, followed by the cyclometalation of the SiMe_3 group.^{65,66} Such a situation does not exist with the present compounds.

Residual water in the holmium triflate is probably responsible for the formation of **1** and **2**. A possible reaction sequence involves the initial, rapid formation of the neutral HoA'_3 complex (eq 3), but slow protonation of a single allyl ligand would produce an equivalent of the HA' propene and the monocation $[\text{HoA}'_2]^+$. The latter could undergo self-abstraction of a hydrogen from a trimethylsilyl group, followed by dimerization to form **1** ($[\text{Ho}(\text{A}')(\text{A}'\text{-SiMe}_2\text{CH}_2)]_2$) (Scheme 1). A second protonation and removal of an allyl ligand in **1** would generate the cationic $[\text{Ho}_2(\text{A}'\text{-SiMe}_2\text{CH}_2)_2(\text{A}')]^+$ complex, which on loss of a C–H proton would yield the allyl dianion in complex **2**. This ligand

transformation is reminiscent of the ability of air-deactivated (presumably hydrated) silica gel to convert the allyl complex $\text{Ru}(\text{CO})(\eta^3\text{-C}_3\text{H}_5)\text{Cp}$ to the allylidene species $\text{Ru}_2(\text{CO})(\mu\text{-CO})(\mu\text{-}\eta^1, \eta^3\text{-CHCHCH}_2)\text{Cp}_2$.⁶⁷



Scheme 1. Possible route to the synthesis of **1** and **2**.

Analysis of Bonding in 1 and 2. In **1**, the average M–C bond distance for the η^3 -bound allyl ligands is 2.57(1) Å (Table 4), and the $R_{\text{M-C}}$ radius is 1.669 Å. In **2**, the average Ho1–C bond distance for the dimethylsilylene bridged allyl ligand (excluding the bridging carbon atom) is 2.64(1) Å (Table 5), and the $R_{\text{M-C}}$ radius is 1.695 Å. Both of these values fall into the range of $R_{\text{M-C}}$ values for the aforementioned trivalent lanthanide allyl complexes (Table 2). However, in **2**, the analogous Ho2–C bond distance is 2.64(1) Å (Table 5), and the $R_{\text{M-C}}$ radius is 1.739 Å. This radius is significantly larger than that of any of the trivalent complexes; presumably, the discrepancy between the

bonding for Ho2 and the monomeric complexes is due to steric restraints evoked by dimerization.

It is also interesting to consider the bonding in the allylidene ligand of **2**. The similar carbon–carbon distances within the allylidene ligand ($C4-C5 = 1.425(7) \text{ \AA}$, $C5-C6 = 1.410(7) \text{ \AA}$; $C4-C5-C6 = 126.2(5)^\circ$) are an indication that a delocalized description of the bonding (Figure 4(a)) is more appropriate than a localized vinylalkylidene scheme (Figure 4(b)). The delocalization appears to be a feature of the allyl dianion itself. Although several Lewis structures can be written for the ion, the most stable suggests that it should have distinctly different C–C bonds (Figure 4(c)). Nevertheless, a DFT geometry optimization of the (gas-phase) $[H_2CC(H)CH]^{2-}$ ion converges to bond lengths of 1.403 and 1.402 \AA ($C-C-C = 127.3^\circ$).⁶⁸ When the model includes trimethylsilyl groups (i.e., $[(Me_3Si)HCC(H)C(SiMe_3)]^{2-}$), the C–C bond lengths differ by only 0.06 \AA (Figure 4(d)).⁶⁸ Consistent with the largely ionic bonding expected in organolanthanide complexes,⁶⁹ the holmium framework appears to have preserved the major structural features of the isolated anion.

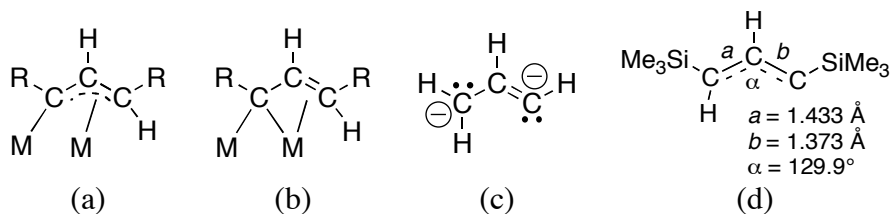


Figure 4. (a) Delocalized allylidene bonding (R = SiMe₃ in **2**). (b) Vinylalkylidene bonding scheme. (c) Most stable Lewis structure of the allyl dianion. (d) Geometry optimized $[1,3-(SiMe_3)_2C_3H_2]^{2-}$ ion.

Conclusion

Lanthanide complexes with bis(1,3-trimethylsilyl)allyl ligands can form products that do not match the stoichiometry of the reactants, a property that is seldom seen in cyclopentadienyl chemistry of the f-elements. Also, in contrast to cyclopentadienyl chemistry, variations in the metal cation of the allyl starting material effect the product isolated. In other cases, however, substituted allyl and cyclopentadienyl ligands share similar characteristics. Among these is the ionic bonding character of the M–C bond in both types of complexes. Another feature of lanthanide allyl complexes that has parallels in cyclopentadienyl chemistry is the reactivity of trimethylsilyl groups on the allyl ligands. This reactivity has led to the first example of binuclear dimethylsilylene and allylidene lanthanide compounds obtained from the conversion of a sterically bulky allyl anion in the presence of partially hydrated holmium triflate.

CHAPTER II

OBSERVATION OF ELECTRON TRANSFER IN BULKY ALLYL YTTERBIUM COMPLEXES WITH SUBSTITUTED TERPYRIDINE LIGANDS

Introduction

The use of trimethylsilyl-substituted allyl ligands has become a common way to synthesize thermally stable allyl complexes with metals throughout the periodic table. In particular, the symmetrically substituted allyl, $[1,3-(\text{SiMe}_3)_2\text{C}_3\text{H}_3]^-$, has been incorporated into complexes with early main group metals,^{7-9,19} transition metals,^{12,14,15} lanthanides,^{18,19,21,22,36} and actinides.²³ Use of the less bulky asymmetric allyl ligand, $[1-(\text{SiMe}_3)\text{C}_3\text{H}_4]^-$, has been less common, but can lead to different products than with the symmetrically substituted allyl. For example, the product of two equivalents of $\text{K}[1-(\text{SiMe}_3)\text{C}_3\text{H}_4]$ and CrCl_2 is a dimer,¹⁵ analogous to the parent allyl compound.⁷⁰ However, the same reaction with $\text{K}[1,3-(\text{SiMe}_3)_2\text{C}_3\text{H}_3]$ yields a thermally stable monomeric diallylchromium product.¹⁵

The structures and catalytic activity of a series of lanthanide complexes with trimethylsilyl-substituted allyl ligands have been reported. Among these is the divalent complex $\text{Yb}[1,3-(\text{SiMe}_3)_2\text{C}_3\text{H}_3]_2(\text{thf})_2$, which displays low activity as a catalyst for methyl methacrylate polymerization ($\text{TOF} = 100 \text{ h}^{-1}$).¹⁹ Although its catalytic properties are unpromising, the diallyl ytterbium complex could have other noteworthy characteristics, as it resembles the ether adduct of ytterbocene, a complex that has been treated with a range of *N*-heterocyclic ligands revealing interesting electronic and magnetic properties.

Adducts of ytterbocene with *N*-heterocyclic ligands (e.g., $\text{YbCp}^*_2(\text{L})$, where $\text{Cp}^* = \text{C}_5\text{Me}_5$; $\text{L} = 2,2'$ -bipyridine (bpy),²⁶ 10-phenanthroline (phen),²⁶ 2,2':6',2''-terpyridine (tpy),²⁷ or 4'-cyano-2,2':6',2''-terpyridine (tpyCN))²⁷ display a stable charge-transfer electronic configuration derived from a spontaneous electron transfer from a diamagnetic Yb(II) f^{14} metal center to the lowest unoccupied molecular orbital (LUMO) on the *N*-heterocyclic ligand, ($f^{14}-\pi^{*0} \rightarrow f^{13}-\pi^{*1}$). This spontaneous electron transfer has been extensively examined with electrochemical and spectroscopic methods.^{27,71,72} These adducts exhibit temperature-dependent magnetic susceptibilities and room-temperature magnetic moments (μ_{eff}) that are lower than what is predicted for a Yb(III) f^{13} metal center with a π^{*1} ligand. This feature has been explained by a thermally induced valence tautomeric (VT) equilibrium between the diamagnetic ($4f^{14}-\pi^{*0}$) and paramagnetic ($4f^{13}-\pi^{*1}$) forms of the complexes, in which the paramagnetic species is dominant at room temperature and the diamagnetic form dominates at low temperature.²⁷

The resemblance of substituted diallylytterbium complexes to ytterbocene has led to an exploration of the electronics of bulky allyl ytterbium complexes with terpyridyl ligands. A variety of diallylytterbium complexes with the aforementioned allyl ligands ($[\text{1}-(\text{SiMe}_3)\text{C}_3\text{H}_4]^-$ and $[\text{1,3}-(\text{SiMe}_3)_2\text{C}_3\text{H}_3]^-$), as well as a new asymmetric allyl ligand ($[\text{1}-(\text{SiPh}_3)\text{-3}-(\text{SiMe}_3)\text{C}_3\text{H}_3]^-$), have been synthesized. Terpyridine adducts of these diallylytterbium complexes have been studied to determine the difference in the magnetic behavior between Cp^* and bulky allyl terpyridyl-ytterbium complexes and to tune the electronic and magnetic behavior of these complexes through allyl substitution.

Experimental

General Considerations. All manipulations were performed with the rigorous exclusion of air and moisture using Schlenk or glovebox techniques. Proton NMR spectra were obtained on a Bruker DPX-300 MHz or Avance 400 MHz spectrometer. Infrared Spectra were recorded on a Thermo-Nicolet FT-IR module instrument Magna 760 spectrometer at 4 cm⁻¹ resolution as mineral oil mulls. Elemental analysis (C, H) was performed by Desert Analytics (Tucson, AZ); complexometric methods were used for analysis of ytterbium.⁴¹

Materials. Yb[1,3-(SiMe₃)₂C₃H₃]₂(thf)₂ (**1**) and Yb(OTf)₂(thf)₃ were prepared as previously described.¹⁹ K[1-(SiMe₃)C₃H₄] was prepared as a lithium salt according to the literature procedure⁶ and transmetalated with KO*t*-Bu. Allyltrimethylsilane was purchased from Gelest and degassed prior to use. Chlorotriphenylsilane (Gelest), *n*-butyllithium (2.5 M in hexane, Acros), potassium *t*-butoxide (Strem), anhydrous YbI₂ (Aldrich), and 2,2':6',2''-terpyridine (tpy, Aldrich) were used as received. The 4'-cyano-2,2':6',2''-terpyridine (tpyCN) and 6,6''-dicyano-2,2':6',2''-terpyridine (tpy(CN)₂) were prepared according to literature procedures.⁷³ Potassium 6,6''-dicyano-2,2':6',2''-terpyridine (K⁺[tpy(CN)₂]⁻) was prepared by adding one equivalent of freshly cut potassium metal to one equivalent of 6,6''-dicyano-2,2':6',2''-terpyridine in THF and stirring overnight at room temperature. HPLC-grade solvents, stored under argon in stainless steel cylinders, were purified by passing them under argon pressure through a stainless steel system consisting of either two 4.5 in. × 24 in. (1 gal) columns of activated A2 alumina (THF) or one column of activated A2 alumina and one column of activated BASF R3-11 catalyst (toluene and hexanes). Deuterated solvents (C₆D₆, THF-*d*₈,

toluene-*d*₈) were sparged with argon and stirred over Na/K (1:2) alloy, from which they were transferred under vacuum and stored over Type 4A molecular sieves; CDCl₃ (Acros) was used as received. Notation used throughout this chapter is listed in Table 6.

Preparation of 1-(SiPh₃)-3-(SiMe₃)C₃H₄. Allyltrimethylsilane (3.55 g, 31.07 mmol) and hexanes (100 mL) were added to a 250 mL Schlenk flask equipped with a stirring bar. After cooling the solution to 0 °C, *n*-BuLi (12.4 mL, 31.10 mmol) was added dropwise over 20 min. After allowing the solution to warm to room temperature overnight, it was brought into the glovebox. Chlorotriphenylsilane (9.16 g, 31.07 mmol) was added slowly over 10 min. The chlorotriphenylsilane was not soluble in the reaction mixture; therefore THF (40 mL) was added to the solution, which immediately turned light orange and cloudy. The reaction was allowed to stir for 8 h. The solution was extracted with ~ 25 mL deionized water and ~10 mL diethyl ether three times each. The organic layers were combined, dried with magnesium sulfate, and filtered. Solvent was removed under vacuum, yielding 7.58 g of a white powder (65%). ¹H NMR (25 °C, 300 MHz, CDCl₃): δ -0.08 (s, 9H, SiMe₃), 2.48 (d, *J* = 7.7 Hz, 2H, CHCHCH₂), 5.48 (d, *J* = 18.5 Hz, 1H, CHCHCH₂), 6.07 (dt, *J*₁ = 18.5 Hz, *J*₂ = 7.7 Hz, 1H, CHCHCH₂), 7.38 (m, 9H, SiPh₃), 7.51 (m, 6H, SiPh₃). MS, *m/e*: 372 (M⁺), 259 (SiPh₃⁺), 105 (SiPh⁺).

Preparation of K[1-(SiPh₃)-3-(SiMe₃)C₃H₃]. Hexanes (75 mL) was added to a 125 mL Schlenk flask containing vacuum-dried 1-(SiPh₃)-3-(SiMe₃)C₃H₄ (5.00 g, 13.41 mmol) and a stirring bar. After cooling the solution to 0 °C, *n*-BuLi (5.4 mL, 13.50 mmol) was added dropwise over 10 min. After the solution was stirred overnight while warming to room temperature, KO^{*t*}-Bu (1.52 g, 13.51 mmol) was added slowly. The solution became sticky and dark orange, and THF (25 mL) was added to increase the

solubility of the product. The solution was stirred for 10 h. The THF was removed under vacuum, and additional hexanes was added. The reaction mixture was filtered over a medium-porosity glass frit. The solid was washed with hexanes and dried under vacuum, yielding 2.08 g of yellow powder (46%). ^1H NMR (25 °C, 300 MHz, C_6D_6): δ 0.15 (s, 9H, SiMe_3), 3.17 (d, $J = 16.1$ Hz, 1H, CHCHCH), 3.39 (d, $J = 16.1$ Hz, 1H, CHCHCH), 6.90 (t, $J = 16.1$ Hz, 1H, CHCHCH), 7.20 (m, 9H, SiPh_3), 7.66 (m, 6H, SiPh_3).

Preparation of $\text{Yb}[1-(\text{SiMe}_3)\text{C}_3\text{H}_4]_2(\text{thf})_2$ (2). In a scintillation vial, $\text{Yb}(\text{OTf})_2(\text{thf})_3$ (0.55 g, 0.80 mmol) was suspended in 10 mL of THF and cooled to -30 °C. In a separate vial, $\text{K}[1-(\text{SiMe}_3)\text{C}_3\text{H}_4]$ (0.27 g, 1.77 mmol) in 5 mL of THF was also cooled to -30 °C. The latter solution was added to the stirring $\text{Yb}(\text{OTf})_2(\text{thf})_3$ suspension dropwise over 10 min. The resulting solution turned red-brown immediately and was allowed to stir overnight while warming to room temperature. The solvent was removed under vacuum, hexanes (30 mL) was added, and the resulting solution was filtered through a fine-porosity glass frit. The filtrate was dried under vacuum, yielding 0.35 g of a red-brown solid powder (76%). ^1H NMR (25 °C, 300 MHz, *tol- d_8*): δ 0.25 (s, SiMe_3). Other allylic peaks were either not observed or were obscured by solvent peaks. Anal. Calcd for $\text{C}_{20}\text{H}_{42}\text{O}_2\text{Si}_2\text{Yb}$: Yb, 31.82. Found: Yb, 31.79.

Preparation of $\text{Yb}[1-(\text{SiPh}_3)-3-(\text{SiMe}_3)\text{C}_3\text{H}_3]_2(\text{thf})$ (3). In a scintillation vial, $\text{Yb}(\text{OTf})_2(\text{thf})_3$ (0.21 g, 0.31 mmol) was suspended in 10 mL of THF and cooled to -30 °C. In a separate vial, $\text{K}[1-(\text{SiPh}_3)-3-(\text{SiMe}_3)\text{C}_3\text{H}_3]$ (0.26 g, 0.63 mmol) in 5 mL of THF was cooled to -30 °C. The latter solution was added to the stirring $\text{Yb}(\text{OTf})_2(\text{thf})_3$ suspension dropwise over 10 min. The resulting solution turned red-brown immediately and was allowed to stir overnight while warming to room temperature. The solvent was

removed under vacuum, hexanes (30 mL) was added, and the resulting solution was filtered through a fine-porosity glass frit. The filtrate was dried under vacuum, yielding 0.24 g of a red-brown solid powder (75%). Dissolution of the product in a small amount of hexanes and cooling to $-30\text{ }^{\circ}\text{C}$ allowed for the growth of X-ray quality crystals. ^1H NMR evidence and elemental analysis both indicate coordination of two thf molecules in **3**, while crystallographic data of **3** indicates the presence of one thf molecule. This disagreement may result from differences in solution and solid-state environments. ^1H NMR (25 $^{\circ}\text{C}$, 300 MHz, THF- d_8): δ 0.15 (s, 18H, SiMe₃), 0.15 (s, 18H, SiMe₃), 2.4 (br s, 8H, thf), 3.50 (d, $J = 14.6$ Hz, 2H, SiPh₃CHCHCHSiMe₃), 3.56 (d, $J = 14.6$ Hz, 2H, SiPh₃CHCHCHSiMe₃), 4.00 (br s, 8H, thf), 7.28 (m, 22H, SiPh₃ and CHCHCH), 7.61 (m, 10H, SiPh₃). Anal. Calcd for C₅₆H₇₀O₂Si₄Yb: Yb, 16.32. Found: Yb, 16.87.

Preparation of Yb[1,3-(SiMe₃)₂C₃H₃]₂(tpy) (1•tpy). In a scintillation vial, **1** (0.10 g, 0.15 mmol) was suspended in 15 mL of toluene. This solution was added dropwise to a second vial containing tpy (0.04 g, 0.19 mmol). The reaction mixture immediately turned dark green and was allowed to stir overnight (16 h). The solvent was then removed under vacuum, approx. 15 mL of hexanes was added to the dark green residue, and the solution was filtered through Celite and glass microfiber filter paper. The solvent was removed under vacuum, resulting in a dark green powder (0.09 g, 75%). X-ray quality crystals were grown from a concentrated solution of hexanes. ^1H NMR (25 $^{\circ}\text{C}$, 400 MHz, THF- d_8): δ -0.13 (s, SiMe₃). ^1H NMR spectra at room temperature and $-20\text{ }^{\circ}\text{C}$ were identical; terpyridyl and C₃ allyl resonances were not observed. Anal. Calcd for C₃₃H₅₂N₃Si₄Yb: Yb, 22.27. Found: Yb, 21.97. λ_{max} (nm): 404, 610, 951.

Preparation of Yb[1,3-(SiMe₃)₂C₃H₃]₂(tpyCN) (1•tpyCN). Complex **1•tpyCN** was prepared using the same method as that for **1•tpy**, using 0.09 g (0.14 mmol) of **1** and 0.05 g (0.18 mmol) of tpyCN. The reaction mixture turned dark blue upon addition of **1** in solution, and the isolated product was a dark blue powder (0.09 g, 80%). ¹H NMR (25 °C, 400 MHz, THF-*d*₈): δ -0.02 (br s, SiMe₃), 0.01 (br s, SiMe₃). Terpyridyl and C₃ allyl resonances were not observed. Anal. Calcd for C₃₄H₅₂N₄Si₄Yb: Yb, 21.57. Found: Yb, 21.16. IR (mineral oil): 2130 cm⁻¹, ν_{C≡N}. λ_{max} (nm): 356, 573, 923.

Preparation of Yb[1,3-(SiMe₃)₂C₃H₃]₂(tpy(CN)₂) (1•tpy(CN)₂). Complex **1•tpy(CN)₂** was prepared using the same method as that for **1•tpy**, using 0.10 g (0.15 mmol) of **1** and 0.06 g (0.20 mmol) of tpy(CN)₂. The reaction mixture turned dark red-brown upon addition of **1** in solution, and a dark red-brown powder (0.11 g) was isolated in 86% yield. ¹H NMR (25 °C, 400 MHz, THF-*d*₈): δ -0.04 (br s, SiMe₃), -0.02 (br s, SiMe₃). Terpyridyl and C₃ allyl resonances were not observed. IR (mineral oil): 2125 cm⁻¹, ν_{C≡N}. λ_{max} (nm): 411, 577.

Preparation of Yb[1-(SiMe₃)C₃H₄]₂(tpyCN) (2•tpyCN). Complex **2•tpyCN** was prepared using the same method as that for **1•tpy**, using 0.88 g (1.62 mmol) of **2** and 0.42 g (1.64 mmol) of tpyCN. The reaction mixture turned dark blue upon addition of **2** in solution, and a dark blue powder (0.86 g) was isolated in 80% yield. ¹H NMR (25 °C, 400 MHz, THF-*d*₈): δ -0.02 (br s, SiMe₃). Terpyridyl and C₃ allyl resonances were not observed. Anal. Calcd for C₂₈H₃₆N₄Si₂Yb: Yb, 26.30. Found: Yb, 26.40. IR (mineral oil): 2171 cm⁻¹, ν_{C≡N}.

Preparation of Yb[1-(SiPh₃)-3-(SiMe₃)C₃H₃]₂(tpyCN) (3•tpyCN). Complex 3•tpyCN was prepared using the same method as that for 1•tpy, using 0.26 g (0.24 mmol) of 3 and 0.06 g (0.24 mmol) of tpyCN. The reaction mixture turned dark blue upon addition of 3 in solution, and a dark blue powder (0.23 g) was isolated in 81% yield. Terpyridyl and C₃ allyl resonances were not observed in the ¹H NMR spectrum. Anal. Calcd for C₆₄H₆₄N₄Si₄Yb: Yb, 14.73. Found: Yb, 14.59. IR (mineral oil): 2164 cm⁻¹, ν_{C≡N}.

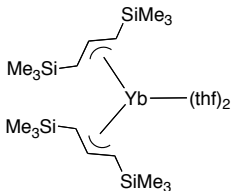
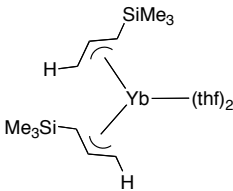
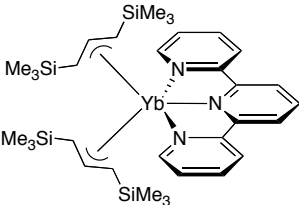
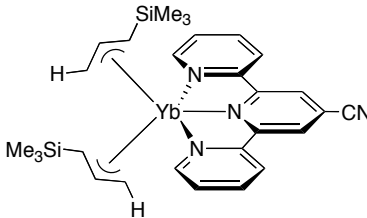
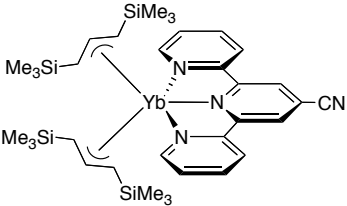
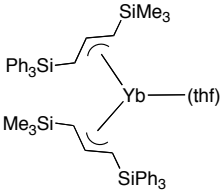
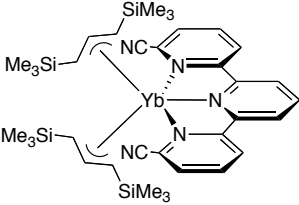
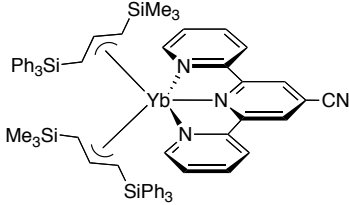
Magnetic Measurements. Magnetic measurements over the temperature range 2 to 350 K were made using a Quantum Design Superconducting Quantum Interference Device (SQUID) magnetometer. The microcrystalline samples were sealed in borosilicate NMR tubes along with a small amount of quartz wool, which held the sample near the tube center. Contributions to the magnetization from quartz wool and tube were measured independently and subtracted from the total measured signal. The magnetic susceptibility, defined as the sample magnetization *M* divided by the applied magnetic field *H*, was measured for 1•tpy as a function of temperature at an applied field of 0.1 T. Diamagnetic corrections were made using Pascal's constants.

General Procedures for X-ray Crystallography. Single-crystal X-ray diffraction experiments were performed on a Bruker P4/CCD/PC diffractometer at Los Alamos National Laboratory. Diffraction data were refined using SHELXTL PC.⁷⁴ Crystals were coated in mineral oil and mounted on a glass fiber at 203 K. Data collection and initial indexing and cell refinement was performed using SMART⁷⁵ software. Frame integration and final cell parameter calculation were carried out using SAINT⁷⁶ software. The data were corrected for absorption using the SADABS⁷⁷ program. Decay of reflection

intensity was not observed. The structures were solved using difference Fourier techniques. The initial solutions revealed the metal center and the majority of all other non-hydrogen positions. The remaining atomic positions were determined from subsequent Fourier syntheses. All hydrogen atoms were placed in ideal positions and refined using a riding model. Relevant crystal and collection data for **1•tpy** can be found in Tables 29 and 30.

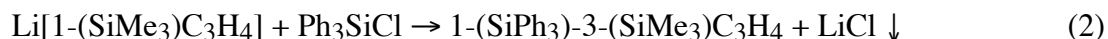
Computational Details. Geometry optimization calculations were performed using the GAUSSIAN 03W suite of programs.⁶⁸ Pre-optimization with calcium replacing ytterbium was performed prior to final geometry optimization of the complexes. For ytterbium complexes, the B3PW91 functional, which incorporates Becke's three-parameter exchange functional⁷⁸ with the 1991 gradient-corrected correlation functional of Perdew and Wang⁷⁹, was used. The effective core potential Gaussian basis set SDD was used for geometry optimization and natural population analysis in these complexes. For calculations of electron density distribution for tpy, tpyCN, and tpy(CN)₂, geometry optimization was performed using semi-empirical methods (PM3). Atomic coordinates for calculated structures can be found in Tables 38–40.

Table 6. Summary of notation for complexes.

Complex	Label	Complex	Label
	1		2
	1•tpy		2•tpyCN
	1•tpyCN		3
	1•tpy(CN)₂		3•tpyCN

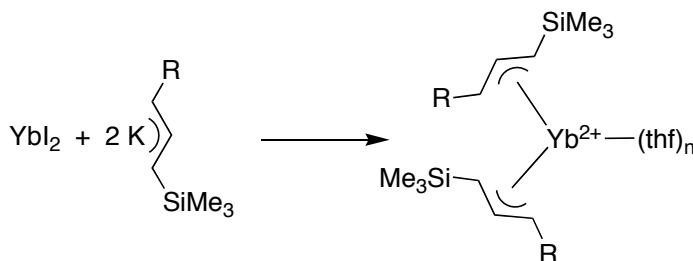
Results and Discussion

Synthesis. Potassium complexes of allyl ligands serve as convenient starting materials for the synthesis of ytterbium-allyl complexes. The lithium salt of the asymmetric allyl ligand, $[1-(\text{SiMe}_3)\text{C}_3\text{H}_4]^-$, was synthesized as described by Fraenkel⁶ in 1990; subsequent transmetalation with $\text{KO}t\text{-Bu}$ yielded the potassium salt. The potassium complex of the symmetric allyl $[1,3-(\text{SiMe}_3)_2\text{C}_3\text{H}_3]^-$ was prepared as described in literature.^{6,19} The trimethylsilyl-, triphenylsilyl-substituted ligand, $[1-(\text{SiPh}_3)\text{-}3-(\text{SiMe}_3)\text{C}_3\text{H}_3]^-$ was prepared through a method similar to that of the symmetric trimethylsilylated allyl ligand.^{6,19} The disubstituted propene was synthesized by deprotonation of allyltrimethylsilane, followed by addition of chlorotriphenylsilane, as shown in eqs 1 and 2. The hydrocarbon was then deprotonated with $n\text{-BuLi}$, and transmetalated with $\text{KO}t\text{-Bu}$ to form the potassium salt (eq 3).



Diallylytterbium complexes with each of these three allyl ligands were synthesized by treatment of two equivalents of the corresponding potassium allyl complex with YbI_2 or $\text{Yb}(\text{OTf})_2(\text{thf})_3$ in THF at $-30\text{ }^\circ\text{C}$ (Scheme 1). The resulting ytterbium complexes consist of two η^3 -bound allyl ligands and one (**3**) or two (**1** and **2**) THF molecules, as indicated by the crystal structure (for **1** and **3**) and ^1H NMR (**2**). Crystallographic data for **1** has

been reported previously.¹⁹ X-ray quality crystals of **3** were grown from a concentrated hexanes solution at $-30\text{ }^{\circ}\text{C}$. The structure was afflicted with severe disorder, and only the atom connectivity could be established.



Scheme 1. Reaction scheme for the synthesis of diallyl ytterbium complexes, **1** ($\text{R} = \text{SiMe}_3$, $n = 2$), **2** ($\text{R} = \text{H}$, $n = 2$), and **3** ($\text{R} = \text{SiPh}_3$, $n = 1$).

To synthesize the terpyridine adducts of these allyl complexes, **1**, **2**, and **3** were treated with three terpyridine derivatives: 2,2':6',2''-terpyridine (tpy), 4'-cyano-2,2':6',2''-terpyridine (tpyCN), and 6,6''-dicyano-2,2':6',2''-terpyridine (tpy(CN)₂) (Figure 5), as shown in Scheme 2. A color change from purple occurred immediately upon addition of the terpyridine ligand (to dark green for tpy, dark blue for tpyCN, and dark red-brown for tpy(CN)₂). Despite the use of large frequency windows, the C₃ allyl and terpyridyl resonances of these complexes were not evident in their ¹H NMR spectra. This is indicative of a paramagnetic f¹³-π*¹ configuration resulting from charge transfer from the Yb(II) (f¹⁴) metal center to the tpy ligand. The absorption bands in the UV-Vis-NIR spectra of adducts of **1** are found in the Experimental Section. They show π-π* and π*-π* transitions that demonstrate electron-transfer between the ytterbium (donor) and terpyridyl ligand (acceptor). Neither the parent allyl complexes (**1–3**) nor their terpyridyl derivatives display the reversible redox behavior exhibited by their Cp* analogs.

Chemical isolation of cationic complexes was attempted using common oxidizing agents (e.g., AgOTf); however, these reactions provide intractable solids. We anticipate that this redox instability is due to the propensity of the allyl groups to reductively eliminate, providing hexadiene products.^{12,80}

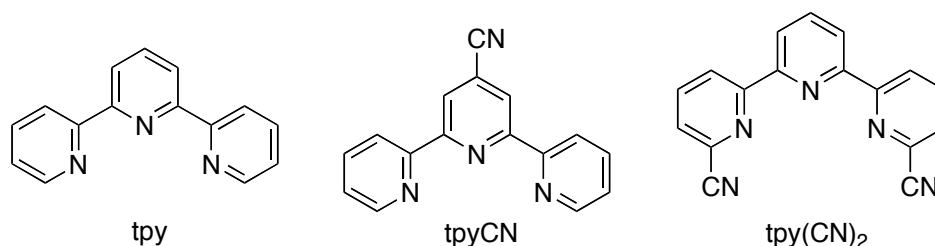
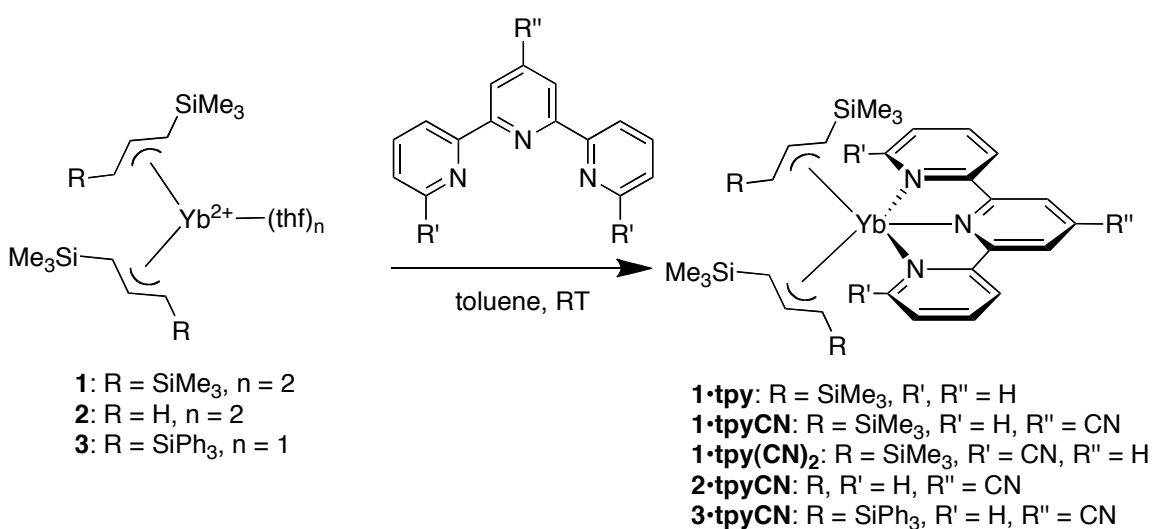


Figure 5. Terpyridine ligands: 2,2':6',2''-terpyridine (tpy), 4'-cyano-2,2':6',2''-terpyridine (tpyCN), and 6,6''-dicyano-2,2':6',2''-terpyridine (tpy(CN)₂).



Scheme 2. Reaction scheme for the synthesis of terpyridine adducts of diallylytterbium complexes, **1•tpy**, **1•tpyCN**, **1•tpy(CN)₂**, **2•tpyCN**, and **3•tpyCN**.

Structural Characterization of 1•tpy. X-ray quality crystals of **1•tpy** were grown in a concentrated solution of hexanes at -30 °C overnight; the structure is shown in

Figure 6. The two allyl ligands in **1•tpy** are in an *anti*-configuration with an average C–C–C angle of 121.4(2)° (Table 7). This value has contracted relative to that of **1** (128.9°)¹⁹, which suggests a slight rehybridization of the allyl moiety that is consistent with a greater extent of electron donation to the ytterbium center. The allyl ligands are π -bound to the ytterbium center with Yb–C bond lengths ranging from 2.52(2) to 2.62(2) Å (Table 7). These distances are shorter than the analogous distances for **1** (Yb–C 2.741(9)–2.754(9) Å, Table 3).¹⁹ This is to be expected given that the metal center in **1** is divalent, whereas for **1•tpy** electron transfer from the Yb(II) center to the tpy ligand has occurred (as evidenced by characterization discussed in the following sections) leading to an effectively trivalent metal center. The tpy ligand is η^3 -bound to the metal center with Yb–N bond lengths from 2.27(2) to 2.39(2) Å. The analogous distances in Cp*₂Yb(tpy) are slightly longer (2.41(1)–2.42(1) Å).⁷¹ Crystallographic data reveal that the more compact allyl ligands allow for closer ligand binding than is possible with the sterically bulky methylated cyclopentadienyl ligands. In both complexes, the bond from ytterbium to the central nitrogen atom (Yb–N_c) is shorter than the bonds to the outer nitrogen atoms (Yb–N₁). This conforms with an observed trend for calculated structures of [Ln(tpy)]³⁺ complexes where (Ln–N_c) < (Ln–N₁) for heavy lanthanides, (Ln–N_c) > (Ln–N₁) for light lanthanides, and (Ln–N_c) \approx (Ln–N₁) for elements in the middle of the series.⁸¹ In the series of structures studied, the distance between the two outer nitrogen atoms remains almost constant, indicating that steric constraints dictate Ln–N distances; i.e., smaller lanthanides can fit in between the outer nitrogen atoms, thus shortening Ln–N_c lengths.⁸²

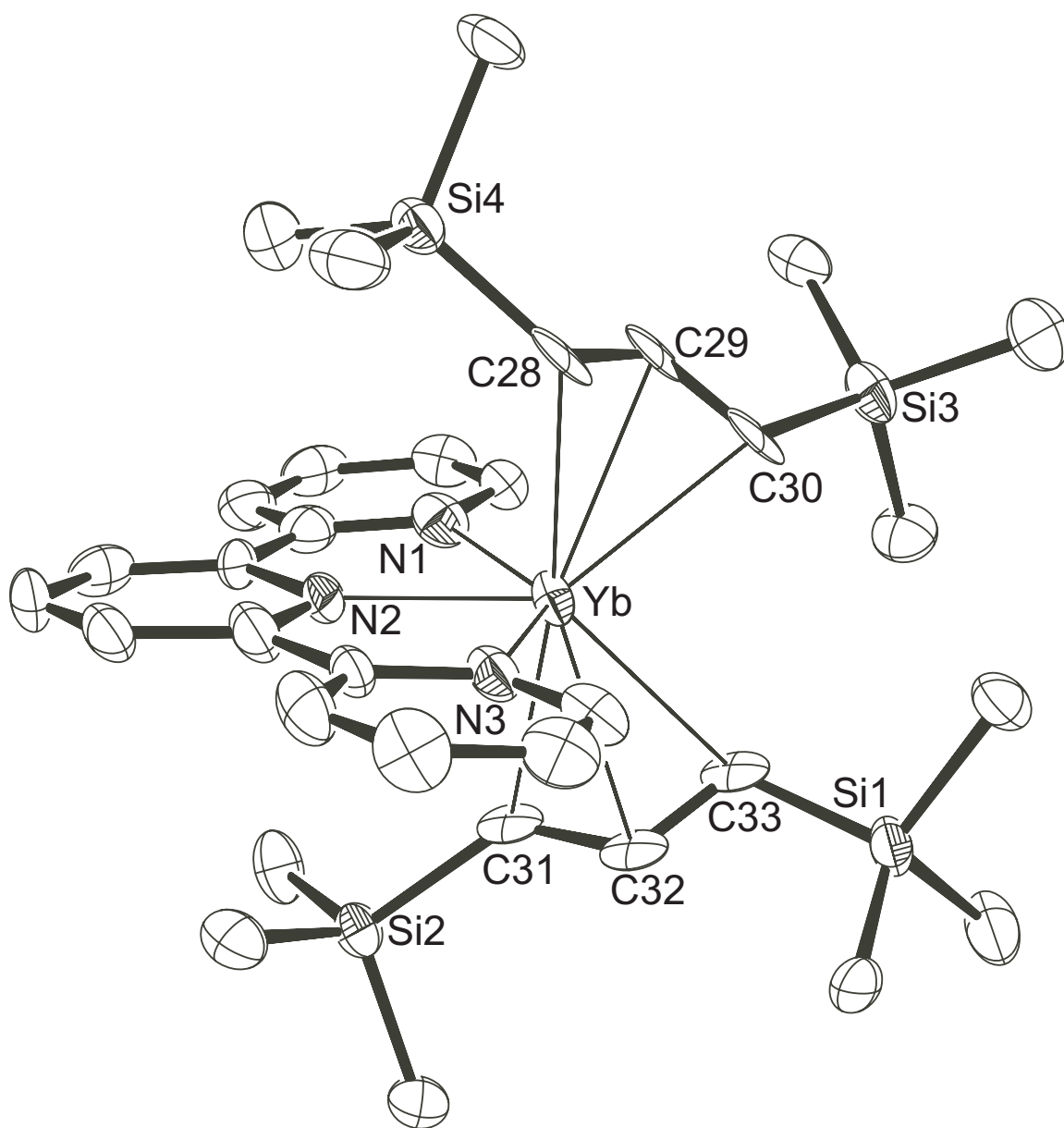


Figure 6. ORTEP of **1•tpy**, with thermal ellipsoids at the 50% level. Hydrogen atoms have been omitted for clarity.

Table 7. Selected bond distances (Å) and angles (°) for **1•tpy**. A_{cent} is defined as the centroid comprising three allyl carbon atoms.

Atoms	Distance	Atoms	Angle
Yb–N1	2.387(15)	C–C–C(allyl, avg)	121.4(2)
Yb–N2	2.269(13)	N1–C–C–N2	–5.8
Yb–N3	2.376(14)	N3–C–C–N2	–3.4
Yb–C28	2.617(17)	A _{cent} –Yb–A _{cent}	135.9
Yb–C29	2.615(15)		
Yb–C30	2.575(15)		
Yb–C31	2.631(15)		
Yb–C32	2.632(15)		
Yb–C33	2.518(15)		

IR Spectroscopy. The C≡N moiety on tpyCN and tpyCN₂ provides an excellent means to gauge the extent of charge transfer for the allyl derivatives. The C≡N stretching frequencies for **1–3•tpyCN**, **1•tpy(CN)₂**, and the neutral and anionic forms of the free ligands (tpyCN, tpy(CN)₂) are presented in Table 8.²⁷ The tpyCN adducts of the asymmetrically substituted allyl complexes (**2•tpyCN** and **3•tpyCN**) have stretching frequencies very close to that reported for YbCp*₂(tpyCN) (Table 8). This correspondence is not surprising, because allyls are believed to have similar electron-donating ability to cyclopentadienyl ligands.⁷ Surprisingly, however, the C≡N stretching frequency for **1•tpyCN** (2130 cm⁻¹) is ~40 wavenumbers lower than the analogous Cp* derivative and is even lower than the C≡N stretching frequency for the anionic form of

the free ligand ([tpyCN]⁻; $\nu_{\text{C}\equiv\text{N}} = 2149 \text{ cm}^{-1}$). It seems that the additional trimethylsilyl group on the allyl ligand of **1•tpyCN** increases the electron density donation to the metal center, which in turn increases electron transfer to the tpyCN ligand as compared to **2•tpyCN** (only 1 SiMe₃ per allyl). This mirrors the trend that is observed for allyl carbonyl complexes of transition metals. The bis(1,3-trimethylsilyl)-substituted allyl metal complexes (e.g., Fe[1,3-(SiMe₃)₂C₃H₃]₂(CO)₂) have lower CO stretching frequencies than their unsubstituted analogues.⁸ The electron withdrawing ability of SiPh₃, which leads to a decrease in electron donation to the tpyCN ligand, accounts for the high C≡N stretching frequency of **3•tpyCN** relative to **1•tpyCN**.⁸³

Table 8. IR C≡N stretching frequencies. All spectra obtained in mineral oil except that of YbCp*₂(tpyCN), which was measured in toluene.

Compound	$\nu_{\text{C}\equiv\text{N}} \text{ (cm}^{-1}\text{)}$
tpyCN	2238
[tpyCN] ⁻	2149
1•tpyCN	2130
2•tpyCN	2171
3•tpyCN	2164
YbCp* ₂ (tpyCN) ²⁷	2172
tpy(CN) ₂	2238
[tpy(CN) ₂] ⁻	2130
1•tpy(CN)₂	2125

There are fewer complexes available for comparison in the case of tpy(CN)₂, as the analogous YbCp*₂(tpy(CN)₂) complex has not been isolated, but the overall trend of the

IR data is similar to that of the diallylytterbium adducts of tpyCN. Specifically, the C≡N stretching frequency of **1•tpy(CN)₂** (2125 cm⁻¹) is slightly lower (~5 cm⁻¹) than that of anionic tpy(CN)₂. This frequency provides a great deal of information about the connectivity of the tpy(CN)₂ ligand, where three bonding modes are plausible for the ligand (Figure 7). Coordination in an η¹ fashion to the nitrile group (Figure 7(a)) is unlikely, as we would anticipate an increase in the C≡N stretch, as has been observed for YbCp*₂I(NCtpy) and other η¹-nitrile complexes.^{27,84,85} Asymmetric binding of the type shown in Figures 7(a) and 7(b) would provide two distinct C≡N stretches. Therefore, the motif in Figure 7(c) is the most reasonable binding mode for tpy(CN)₂ in **1•tpy(CN)₂**.

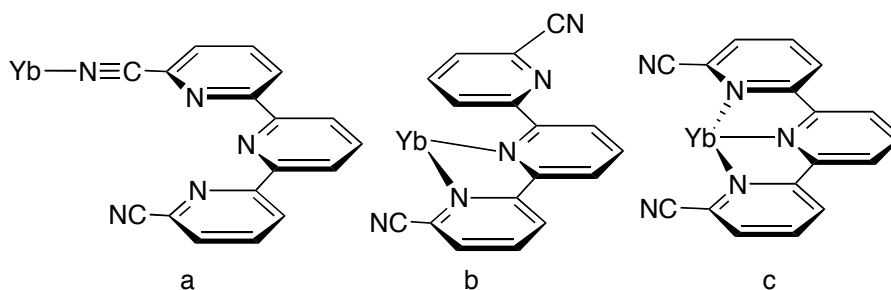


Figure 7. Possible binding modes for tpy(CN)₂.

To substantiate this binding motif, the geometry of a model of **1•tpy(CN)₂** was optimized using density functional theory (B3PW91/SDD).⁶⁸ The resulting structure is similar to that of the crystal structure of **1•tpy**, where the tpy(CN)₂ ligand is η³-bound to the ytterbium center (Figure 7(c)). In the calculated structure (Figure 8(a)), the distance between the metal and the nitrile groups (Yb-C(avg) = 3.575 Å) indicates that steric crowding around the ytterbium does not prevent the terpyridine ligand from being η³-

bound to the ytterbium center. Interestingly, in the calculated structure, the pyridine rings of the $\text{tpy}(\text{CN})_2$ ligand are slightly twisted ($\sim 20^\circ$ between the two outer rings) out of the plane of the normally planar terpyridine ligand, as shown in Figure 8(b). This may be a consequence of electron transfer to the ligand.

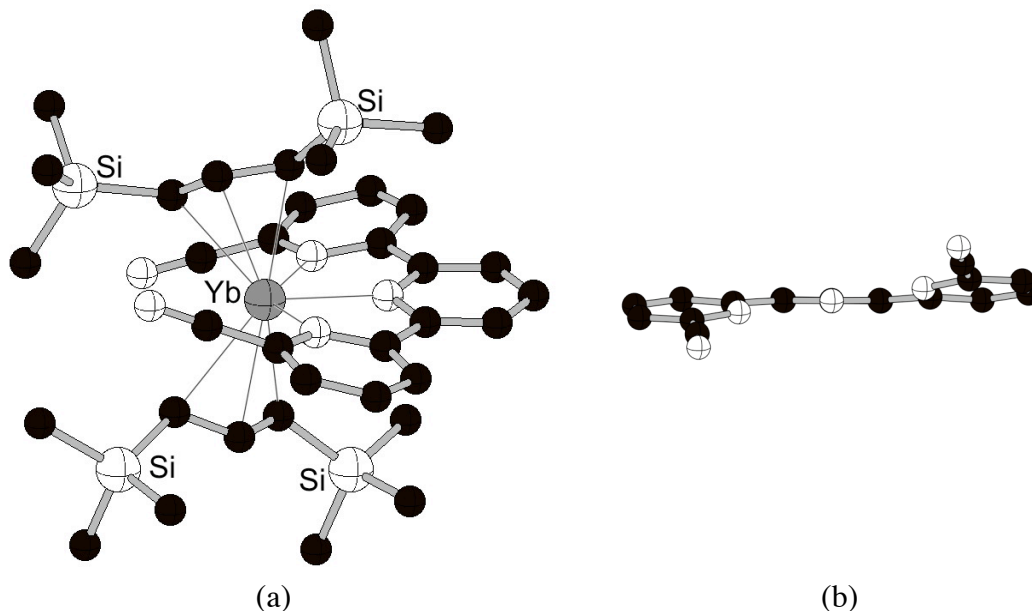


Figure 8. Geometry optimized structure of $1\bullet\text{tpy}(\text{CN})_2$ (a) and side-on view of $\text{tpy}(\text{CN})_2$ ligand in optimized structure (b). Hydrogen atoms have been omitted for clarity.

Magnetic Susceptibility. The magnetic susceptibility (χ) for compound $1\bullet\text{tpy}$ was measured as a function of temperature and is presented in Figure 9. The interpretation of the magnetic data is based on the premise that the neutral electronic configuration is $f^{13}\pi^*1$. The χ^{-1} vs T plot for $1\bullet\text{tpy}$ departs dramatically from the Curie law and exhibits a temperature dependent profile reminiscent of previously examined monometallic analogs such as $\text{YbCp}^*_2(\text{L})$ ($\text{L} = \text{bpy}^{26}, \text{tpy}^{27}, \text{tpyCN}^{27}$). This type of temperature dependent behavior has been ascribed to a valence tautomeric (VT) equilibrium^{86,87} between the

magnetic $f^{13-\pi^*1}$ and non-magnetic $f^{14-\pi^*0}$ forms of the monometallic complex. Field dependent χ vs T measurements of **1•tpy** (at 0.1 and 5 T) do not diverge above 15 K, suggesting that there is no ferromagnetic impurity in the material. Below 15 K, the 5 T data display a maximum at approximately 5 K that is indicative of antiferromagnetic exchange coupling between Yb(III) and ligand radical anion.

For charge transfer complexes of ytterbocene, the $f^{13-\pi^*1}$ contribution was estimated by comparing the χT values for the neutral monometallics to their cationic congeners in which the configuration is solely $f^{13-\pi^*0}$. A correction of $0.375 \text{ emu K mol}^{-1}$ was made to the neutral, monometallic species to account for the ligand radical spin contribution. The ratio of the corrected χT value for the neutral complex divided by the pure f^{13} monocation χT value provided room-temperature f^{13} percentages of 28% and 69% for YbCp*₂(bpy) and YbCp*₂(tpy), respectively. Unfortunately, the redox instability of the diallylytterbium complexes (as evidenced by the irreversible nature of the electrochemistry of **1•tpy** and the inability to isolate a chemically oxidized congener) prevents the determination of the χT value of the monocationic complex. However, the room-temperature magnetic moment of **1•tpy** ($3.58 \mu_B$) is close to that reported for YbCp*₂(tpy) ($3.77 \mu_B$); both room temperature moments are less than the value expected for an uncoupled Yb(III) ion and an organic radical ($4.85 \mu_B$). At 350 K, the magnetic moment of the YbCp*₂(tpy) complex rises to $4.10 \mu_B$, which is substantially closer to the uncoupled value. It is likely that **1•tpy** displays similar behavior at higher temperature, but magnetic data beyond 300 K was not obtained for **1•tpy** due to its thermal instability.

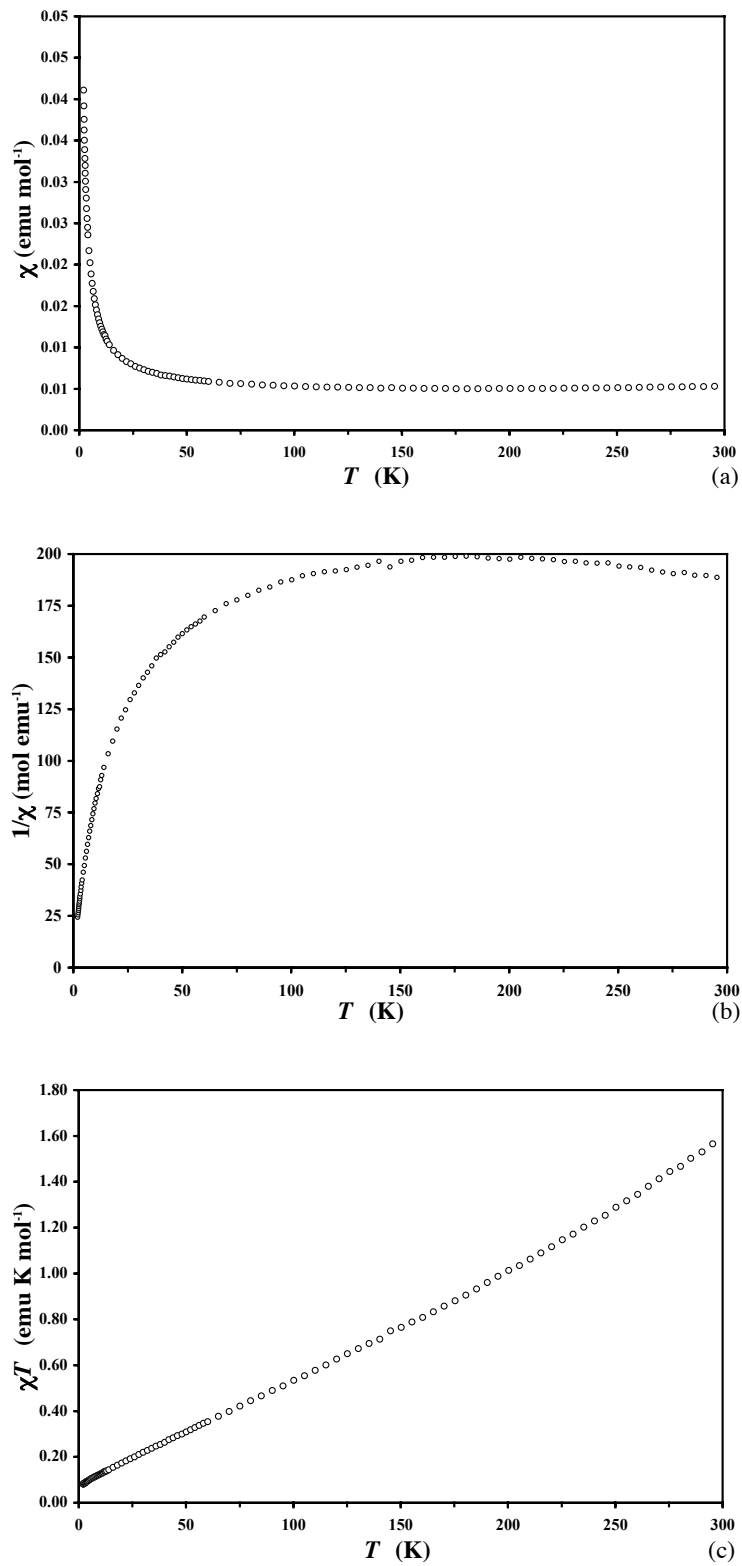


Figure 9. Plots of χ vs T (a), χ^{-1} vs T (b), and χT vs T (c) for **1•tpy**. The data were measured in an applied field of 0.1 T.

Theoretical Calculations. To gain further insight into the structures of these terpyridine adducts, the geometries of **1•tpy**, **2•tpy**, and $\text{YbCp}^*_2(\text{tpy})$, were optimized at the B3PW91/SDD level of theory (Figure 10).⁶⁸ Selected bond distances for each complex are summarized in Table 9. As expected, bond distances of the allyl complexes are shorter than those of the ytterbocene adduct. The allyl ligands have less steric bulk so they can bind closer to the ytterbium center; additionally, this compactness allows the terpyridine to bind closer to the metal in the allyl complexes than it can when Cp^* is present. This trend is mirrored in the crystal structures of $\text{YbCp}^*_2(\text{tpy})$ and **1•tpy**. Shorter bond lengths in the allyl ytterbium complexes should allow for increased charge transfer from the Yb(II) center to tpy, as compared to $\text{YbCp}^*_2(\text{tpy})$. Based on bond distance alone, the complex with the shortest bond distances (i.e., the least bulky allyl adduct, **2•tpy**) should display the largest charge transfer (see Table 9).

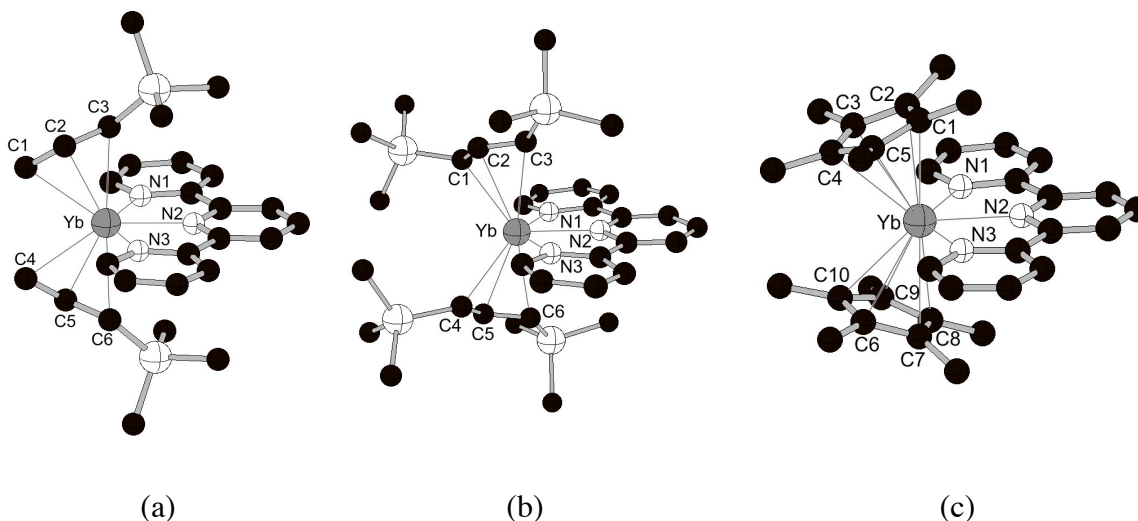


Figure 10. Geometry optimized structures of **1•tpy** (a), **2•tpy** (b), and $\text{YbCp}^*_2(\text{tpy})$ (c). Hydrogen atoms have been omitted for clarity

Table 9. Selected bond distances (Å) for geometry optimized structures of **1•tpy**, **2•tpy**, and YbCp*₂(tpy).

Atoms	Distance	Atoms	Distance
1•tpy		YbCp*₂(tpy)	
Yb–N1	2.420	Yb–N1	2.474
Yb–N2	2.366	Yb–N2	2.475
Yb–N3	2.420	Yb–N3	2.474
Yb–C1	2.695	Yb–C1	2.794
Yb–C2	2.683	Yb–C2	2.794
Yb–C3	2.725	Yb–C3	2.817
Yb–C4	2.695	Yb–C4	2.843
Yb–C5	2.683	Yb–C5	2.850
Yb–C6	2.725	Yb–C6	2.817
2•tpy		Yb–C7	2.794
Yb–N1	2.462	Yb–C8	2.794
Yb–N2	2.422	Yb–C9	2.850
Yb–N3	2.459	Yb–C10	2.843
Yb–C1	2.732		
Yb–C2	2.743		
Yb–C3	2.792		
Yb–C4	2.730		
Yb–C5	2.740		
Yb–C6	2.793		

The C≡N stretching frequency of **2•tpyCN** is close to that of YbCp*₂(tpyCN) and **3•tpyCN**, which shows that steric restraints are not the only factor influencing the donating ability of ytterbium complexes. As previously described, the electron donating ability of the trimethylsilyl groups also plays a role in charge transfer, where a lower C≡N stretching frequency is observed in **1•tpyCN** (2 SiMe₃ per allyl ligand) than for **2•tpyCN** (1 SiMe₃ per allyl ligand). Attempts at quantifying the electron donation of the trimethylsilyl groups and the charge on the ytterbium center by the use of atomic charge criteria with DFT calculations were unsuccessful.

In other theoretical work, the geometry of each of the unbound terpyridine ligands (tpy, tpyCN, and tpy(CN)₂) was optimized, and the electron density of its lowest unoccupied molecular orbital (LUMO) was calculated (Figure 11). To track changes upon addition of an electron, the electron density of the singly occupied molecule orbital (SOMO) of each ligand was also calculated. In the LUMO of all three ligands, there is no electron density on the central nitrogen. Interestingly, however, in the SOMO of tpy and tpy(CN)₂, electron density is present on the central nitrogen. This indicates that the charge transfer complexes discussed in this work (where tpy's LUMO is populated) should exhibit stronger binding to the central nitrogen atom than complexes where the electron transfer has not occurred. This phenomenon is observable by comparing the difference between Yb–N_c and Yb–N₁ bond lengths in YbCp*₂(tpy) ($\Delta = 0.01 \text{ \AA}$) and **1•tpyCN** ($\Delta = 0.12 \text{ \AA}$). In the latter complex, the Yb–N_c distance is significantly shorter than the Yb–N₁ distance, presumably due to increased charge transfer to the tpy ligand, making its electron density picture more analogous to the SUMO (with electron density on the central nitrogen) than the LUMO picture.

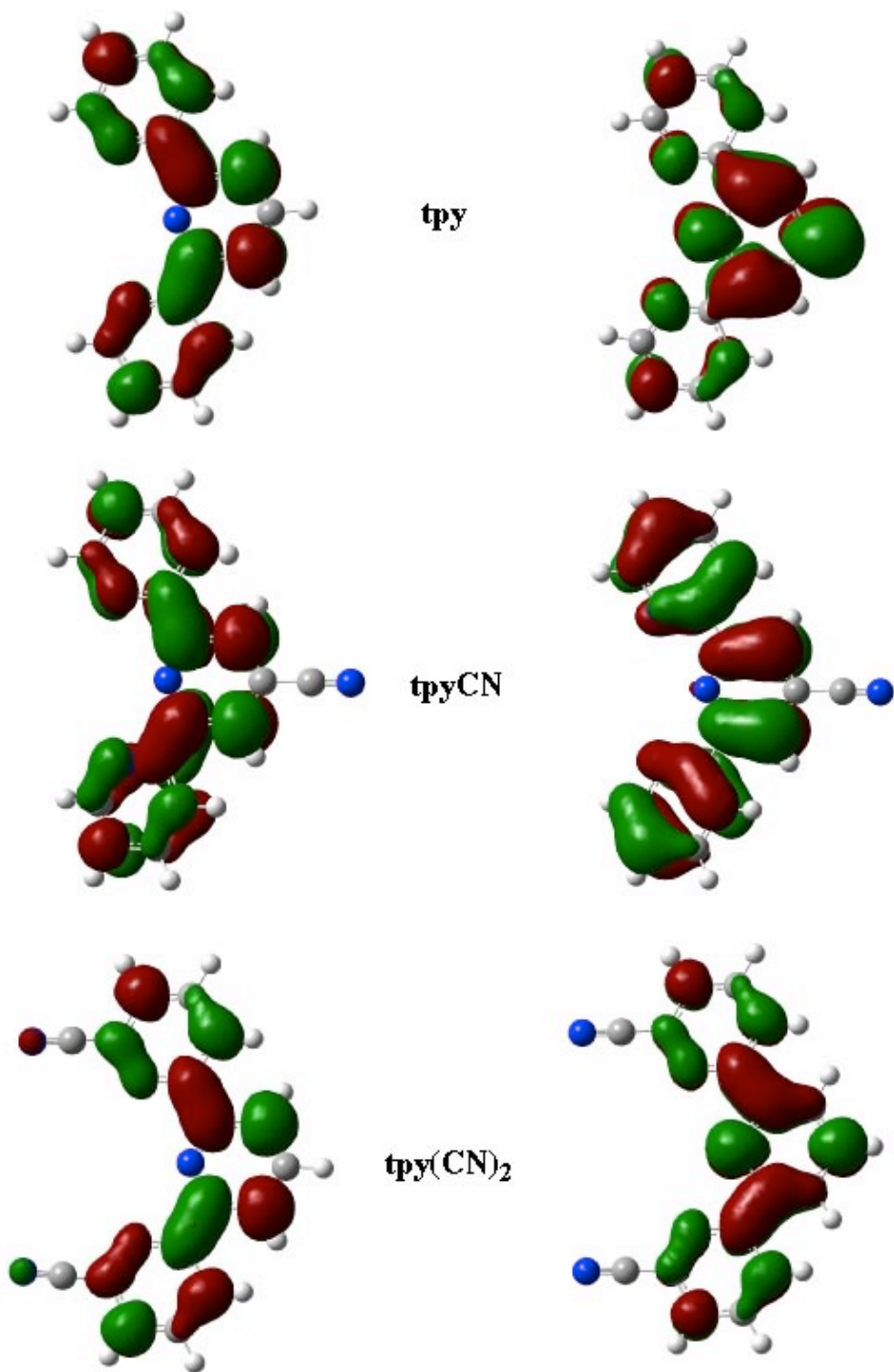


Figure 11. Electron density of LUMO (left) and SOMO (right) of tpy, tpyCN, and tpy(CN)₂.

Conclusion

A new series of charge transfer complexes of ytterbium has been prepared using bulky allyl ligands. The electronic properties of these complexes were tuned by varying the allyl substitution, as evidenced by changes in the C≡N stretching frequencies of the nitrile-substituted terpyridine adducts. Ytterbium complexes with the bis(1,3-trimethylsilyl)allyl ligand have a remarkably low C≡N stretching frequency, indicating a high degree of electron transfer from the metal center to the terpyridine ligand. The complex $\text{Yb}[1,3-(\text{SiMe}_3)_2\text{C}_3\text{H}_3]_2(\text{tpy})$ displays magnetic behavior consistent with the valence tautomer model previously proposed for $\text{YbCp}^*_2(\text{tpy})$. These terpyridyl adducts represent the first observations of charge transfer character in diallylytterbium complexes, supporting the probability that similar electronic properties could be found in analogous species.

CHAPTER III

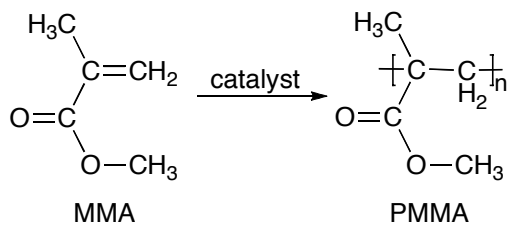
GROUPS I AND II AND LANTHANIDE METAL ALLYL COMPLEXES AS PRE-CATALYSTS IN THE POLYMERIZATION OF METHYL METHACRYLATE

Introduction

Neutral allyl lanthanide complexes have emerged in recent years as promising candidates for materials precursors and polymerization catalysts. The neodymium compound $\text{Nd}(\text{C}_3\text{H}_5)_3$, for example, is a stereospecific initiator for the polymerization of butadiene,⁸⁸ and the analogous lanthanum species is only slightly less selective.⁸⁹ Owing to the large radii of the lanthanide ions³⁰ and the sterically compact nature of the allyl anion, however, neutral $\text{Ln}(\text{C}_3\text{H}_5)_3$ species remain comparatively rare. However, a broader variety of neutral complexes is available with the use of substituted allyl ligands, such as the bulky bis(1,3-trimethylsilyl)allyl anion (A'). This ligand is used to stabilize chromium, iron, cobalt, and nickel complexes whose corresponding monomeric parent allyl $\text{M}(\text{C}_3\text{H}_5)_2$ complexes are unknown.¹²⁻¹⁴

The first reported lanthanide complex with the bis(1,3-trimethylsilyl)allyl ligand, $\text{SmA}'_2(\text{thf})_2$, was isolated from the reaction of SmI_2 and two equiv of KA' ; its use as an initiator for the polymerization of methyl methacrylate (MMA) was also investigated (Scheme 1).²² Unfortunately, the complex was poorly characterized and had limited catalytic activity. More recently, the complex $[\{\text{K}(\text{thf})_2\}\{\text{SmA}'_3(\text{thf})_2\}]_2$ was synthesized from the treatment of $\text{SmI}_2(\text{thf})_2$ with three equivalents of KA' ; it crystallizes with a cyclic structure, comprising two samarium and two potassium centers.³⁶ Interestingly,

this complex, as well as salt complexes of the general types $K[LnA'_3]^{36}$ and $[Ln\{(C_3H_3-SiMe_3)_2SiMe_2\}_2\{\mu-K(thf)\}(thf)_x]_{\infty}^{90}$, show higher than expected activity relative to $SmA'_2(thf)_2^{22}$ as initiators in MMA polymerization.



Scheme 1. Polymerization of methyl methacrylate (MMA).

The inconsistency in the activity of neutral and charged lanthanide allyl complexes led to an investigation of the catalytic properties of other lanthanide allyl complexes, as well as an exploration of the effect of the counterion on polymerization activity. In doing this, Group I complexes (KA' , LiA' , and CsA') and lanthanide allyl complexes ($SmA'_2(thf)_2$, $EuA'_2(thf)_2$, $YbA'_2(thf)_2$, $CeA'_3(thf)$, $NdA'_3(thf)$, and $TbA'_3(thf)$) were synthesized, characterized, and studied as catalysts for the polymerization of MMA.

Because the ionic radii of $Ca(II)$ and $Yb(II)$ (1.00 and 1.02 Å for CN 6, respectively)³⁰ are almost identical, organometallic complexes containing these metals tend to have similar bond distances and angles.²⁸ Examination of the crystal structure of $MA'_2(thf)_2$ complexes of calcium and ytterbium, however, reveals that the average M–C distance for each complex differs by 0.126 Å (see Chapter I).^{7,19} To explore the possible consequences of this structural change, the catalytic activity of $CaA'_2(thf)_2$ was examined. In addition, the catalytic activity of the analogous strontium complex was also explored.

Experimental

General Considerations. All manipulations were performed with the rigorous exclusion of air and moisture using Schlenk or glovebox techniques. Proton and ^{13}C NMR spectra were recorded at ambient temperature on a Bruker DPX-300 MHz at 300 and 75.5 MHz, respectively. PMMA samples were studied at either ambient temperature or, when necessary, 50 °C. Assignment of the tacticity of each PMMA sample was made by integrating the methyl region in the ^1H NMR spectra.⁹¹⁻⁹³ Elemental analyses (C, H) were performed by Desert Analytics (Tucson, AZ); complexometric methods were used for metals.⁴¹

Materials. Bis(1,3-trimethylsilyl)propene was prepared as described by Fraenkel.⁶ The synthesis of $\text{K}[1,3-(\text{SiMe}_3)_2\text{C}_3\text{H}_3]$ (KA' , **2**) by transmetallation of LiA' has been previously described,⁹⁴ although experimental details were not provided; a complete procedure is included below. LiA' (**1**),⁶ CsA' (**3**),⁸ $\text{CaA}'_2(\text{thf})_2$ (**4**),⁷ $\text{SrA}'_2(\text{thf})_2$ (**5**),⁸ $\text{SmA}'_2(\text{thf})_2$ (**6**),¹⁹ $\text{EuA}'_2(\text{thf})_2$ (**7**),¹⁹ $\text{YbA}'_2(\text{thf})_2$ (**8**),¹⁹ $\text{CeA}'_3(\text{thf})$ (**9**),¹⁹ $\text{NdA}'_3(\text{thf})$ (**10**),¹⁸ $\text{TbA}'_3(\text{thf})$ (**11**)¹⁹, and $1,3-(\text{SiMe}_3)_2\text{C}_3\text{H}_4$ ⁶ were prepared as previously described. Methyl methacrylate (MMA) was stirred over CaH_2 , vacuum transferred, and stored in a glovebox freezer at -30 °C prior to use. For lanthanide complexes, HPLC-grade solvents, stored under argon in stainless-steel cylinders, were purified by passing them, under argon pressure, through a stainless-steel system consisting of either two 4.5 in. \times 24 in. (1 gal) columns of activated A2 alumina (THF) or one column of activated A2 alumina and one column of activated BASF R3-11 catalyst (hexanes).⁹⁵ For Group I and II complexes, hexanes and toluene were distilled under nitrogen from potassium benzophenone ketyl;⁴² anhydrous tetrahydrofuran (THF) was purchased from Aldrich

and used as received. Deuterated solvents (toluene- d_8 and C_6D_6) were vacuum distilled from Na/K (22/78) alloy and stored over Type 4A molecular sieves. All other reagents were obtained from commercial sources and used as received.

Synthesis of KA' (2). In a 250 mL Schlenk flask equipped with a stirring bar, 1,3-(SiMe₃)₂C₃H₄ (10.02 g, 53.7 mmol) was degassed, and hexanes (100 mL) was added. After cooling the solution to 0 °C in an ice bath, *n*-BuLi (21.5 mL, 53.7 mmol) was added dropwise over 15 min. After the solution was stirred for 6 h while allowing it to warm to room temperature, KO*t*-Bu (6.09 g, 54.3 mmol) was slowly added, and the solution was stirred for 10 h. A pale peach colored solid was produced that was filtered over a medium-porosity glass frit. The solid was washed with hexanes until the filtrate was colorless. The solid was then dried to yield 9.90 g of off-white product (82%). ¹H NMR (25 °C, 300 MHz, C₆D₆): δ 0.23 (s, 18H, SiMe₃), 2.78 (d, *J* = 15.9 Hz, 2H, CHCHCH), 6.69 (t, *J* = 15.9 Hz, 1H, CHCHCH); ¹³C NMR (25 °C, 75 MHz, C₆D₆): δ 2.52 (SiMe₃), 68.68 (CHCHCH), 155.74 (CHCHCH). Anal. Calcd for C₉H₂₁KS₂: C, 48.14; H, 9.43. Found: C, 47.63; H, 9.42. Redissolution of the powder in dimethoxyethane (dme) followed by slow evaporation at room temperature produced colorless crystals of **2•dme**.

Attempted synthesis of [K(thf)_n][CaA'3]. Synthesis of CaA'2(thf)₂ (4). A 125 mL Schlenk flask was charged with CaI₂ (0.114 g, 0.388 mmol), THF (50 mL), and a stirring bar. An addition funnel was prepared with **2** (0.255 g, 1.136 mmol) in THF (40 mL). After assembly in the glovebox, the apparatus was placed on a Schlenk line. After cooling the CaI₂ solution to -78 °C, the solution of **2** was added dropwise with stirring over 30 min. After warming to room temperature overnight, the orange reaction mixture was evaporated to dryness, then extracted with toluene. The extract was filtered through a

medium porosity frit, and the removal of toluene under vacuum yielded a pale orange solid product. ^1H NMR spectrum indicated isolation of **4** and unreacted **2**.

Attempted synthesis of $[\text{K}(\text{thf})_n][\text{SrA}'_3]$. Synthesis of $\text{SrA}'_2(\text{thf})_2$ (5**).** A 125 mL Schlenk flask was charged with SrI_2 (0.131 g, 0.384 mmol), THF (50 mL), and a stirring bar. An addition funnel was prepared with **2** (0.250 g, 1.114 mmol) in THF (40 mL). After assembly in the glovebox, the apparatus was placed on a Schlenk line. After cooling the SrI_2 solution to $-78\text{ }^\circ\text{C}$, the solution of **2** was added dropwise with stirring over 30 min. After warming to room temperature overnight, the orange reaction mixture was evaporated to dryness, then extracted with toluene. The extract was filtered through a medium porosity frit, and the removal of toluene under vacuum yielded a pale orange solid product. ^1H NMR spectrum indicated isolation of **5** and unreacted **2**.

Elemental Analysis of $\text{SmA}'_2(\text{thf})_2$ (6**), $\text{EuA}'_2(\text{thf})_2$ (**7**), $\text{CeA}'_3(\text{thf})$ (**9**), and $\text{TbA}'_3(\text{thf})$ (**11**).** Complexometric methods of elemental analysis were used to characterize complexes **6**, **7**, **9**, and **11** (Table 10).⁴¹

Table 10. Elemental analysis data for $\text{SmA}'_2(\text{thf})_2$ (**6**), $\text{EuA}'_2(\text{thf})_2$ (**7**), $\text{CeA}'_3(\text{thf})$ (**9**), and $\text{TbA}'_3(\text{thf})$ (**11**).

Complex	Calc. Anal. (Ln%)	Exp. Anal. (Ln%)
$\text{SmA}'_2(\text{thf})_2$ (6)	22.59	22.13
$\text{EuA}'_2(\text{thf})_2$ (7)	22.78	22.65
$\text{CeA}'_3(\text{thf})$ (9)	18.23	18.67
$\text{TbA}'_3(\text{thf})$ (11)	20.18	20.03

¹H NMR Studies of 2 and 6. For a 1:2 ratio of complex **2** to complex **6**, **2** (15 mg, 0.067 mmol) was added to **6** (86 mg, 0.132 mmol) in an NMR tube. Approximately 0.5 mL of toluene-*d*₈ was added, and the tube was shaken to facilitate mixing. After twenty minutes, the ¹H NMR spectrum was taken at room temperature. ¹H NMR (25 °C, 300 MHz, tol-*d*₈): δ -24.62 (br s, 4H, *CHCHCH*), -0.39 (br s, 18H, SiMe₃), 1.39 (s, 8H, thf), 2.36 (br s, 36H, SiMe₃), 3.95 (s, 8H, thf), 14.27 (br s, 2H, *CHCHCH*).

The same method was used to prepare a 1:1 ratio of complex **2** (2 mg, 0.009 mmol) to complex **6** (7 mg, 0.010 mmol). ¹H NMR (25 °C, 300 MHz, tol-*d*₈): δ -23.99 (br s, 4H, *CHCHCH*), -0.30 (br s, 18H, SiMe₃), 1.35 (s, 8H, thf), 2.56 (br s, 36H, SiMe₃), 3.48 (s, 8H, thf), 14.31 (br s, 2H, *CHCHCH*).

A 2:1 ratio of complex **2** to complex **6** was prepared in the same manner using 3 mg (0.013 mmol) of **2** and 4 mg of **6** (0.006 mmol). ¹H NMR (25 °C, 300 MHz, tol-*d*₈): δ -23.80 (br s, 4H, *CHCHCH*), -0.13 (br s, 18H, SiMe₃), 1.36 (s, 8H, thf), 2.65 (br s, 36H, SiMe₃), 3.46 (s, 8H, thf), 14.01 (br s, 2H, *CHCHCH*).

General Polymerization Reaction and Polymer Workup. Unless otherwise noted, MMA (4–5.4 mL, 37.4–50.5 mmol) was added via syringe to a solution of catalyst (~1000 mol MMA: 1 mol catalyst) in toluene (approx. 20 mL) at 0 °C. Polymerization reactions were allowed to run for lengths of time between 30 s and 35 min, after which methanol (approx. 250 mL) was added to quench the reaction mixture and precipitate PMMA. For lanthanide catalysts, the resulting solid was filtered, concentrated to dryness, dissolved in chloroform and precipitated with methanol to give a white solid that was dried under vacuum prior to GPC analysis. For Group I and II catalysts, solid PMMA was dried under vacuum prior to GPC analysis.

GPC determinations. Molecular weights were determined in tetrahydrofuran (THF) or dimethylformamide (DMF; only the PMMA sample generated from **10** was measured in this solvent) by gel permeation chromatography (GPC). The GPC consisted of an Alliance 2690 pump equipped with a 2410 Differential Refractive Index Detector. The column set utilized for DMF consisted of two Polymer Labs PL Mixed B GPC Columns at 80 °C at a flow rate of 1.0 mL/min. The columns used for the THF analysis consisted of Shodex 806, 804 and 802.5 columns at 40 °C at a flow rate of 1.0 mL/min. The molecular weights were calculated relative to the retention times of narrow MW polystyrene standards or polyethylene oxide standards using Waters Corporation's Millennium32 software. The shape of the MW distribution for the PMMA sample generated from **7** indicated that this polymer was uniform. However, the PMMA sample generated from **8** has a high molecular weight shoulder, and the PMMA sample generated from **10** is broad with shoulders possessing high and low molecular weight components. Also, for PMMA generated by **6**, the GPC chromatogram was very broad. Note: the PMMA sample from **10** did not completely dissolve in either DMF or THF. The cloudy solution was filtered through a 0.45 micron syringe filter. The PMMA samples generated from **6** and **9** were also filtered to remove undissolved solids prior to analysis. Other samples were not filtered and appeared to dissolve completely.

General Procedures for X-ray Crystallography. Data collection and structure solution were conducted at the X-Ray Crystallographic Laboratory at the University of Minnesota. All calculations were performed using the current SHELXTL⁴³ suite of programs. A suitable crystal was located and attached to the tip of a glass capillary and mounted on a CCD area detector diffractometer for data collection at 173(2) K. A

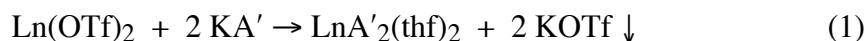
preliminary set of cell constants was calculated from reflections harvested from three sets of 20 frames. These initial sets of frames were oriented such that orthogonal wedges of reciprocal space were surveyed. Data collection of a randomly oriented region of reciprocal space was carried out using MoK α radiation (graphite monochromator). The intensity data were corrected for absorption with SADABS.⁴⁵ Final cell constants were calculated from strong reflections from the actual data collection after integration (SAINT).⁴⁶ Relevant crystal and collection data parameters for **2•dme** can be found in Tables 31 and 32.

Results and Discussion

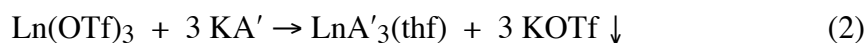
Synthesis. In 1990, Fraenkel described the synthesis and subsequent deprotonation with *n*-BuLi of bis(1,3-trimethylsilyl)propene to produce Li[1,3-(SiMe₃)₂C₃H₃] (LiA', **1**).⁶ Transmetalation of **1** with KO*t*-Bu yields the potassium salt KA' (**2**), a highly air- and moisture-sensitive off-white solid. Complex **2** has been treated with various metal halides and triflates to produce allyl complexes with metals throughout the periodic table.^{6,7,9,12-23,36} For example, treatment of MI₂ with two equivalents of **2** in THF at -78 °C yields the diallyl complex MA'₂(thf)₂ (M = Ca, **4**; Sr **5**).^{7,8}

Analogous diallyllanthanide complexes (LnA'₂(thf)₂, Ln = Sm (**6**), Eu (**7**), Yb(**8**)) were prepared by treating Ln(OTf)₂ with two equivalents of **2** in THF at -30 °C (eq 1). After overnight stirring, THF was removed under reduced pressure from the reaction mixture, the residue was extracted with hexanes, and the solutions were filtered to remove KOTf. Concentration of the filtrate to approximately 5 mL and cooling to -30 °C overnight allowed for the growth of X-ray quality crystals of each product in moderate to

good yield (48–74%). The corresponding lanthanide diiodides can be used as well, with no difference in yield. When Yb(III) or Eu(III) triflate precursors were treated with **2**, reduction to the lanthanide(II) product was observed, but the yield of the allyl complex was reduced (< 50%).



Lanthanide triflates of cerium, neodymium, and terbium were treated with three equivalents of **2** under similar reaction conditions to produce thf-solvated triallyllanthanide complexes ($\text{LnA}'_3(\text{thf})$, Ln = Ce (**9**), Nd (**10**),¹⁸ Tb (**11**)) in 41–80% yield (eq 2). All of these air- and moisture-sensitive lanthanide allyl complexes are highly colored (**6**: dark green; **7**: red; **8**: blue; **9**: brick red; **10**: green; **11**: orange). These complexes are stable for several days under inert atmosphere at ambient temperature and stable indefinitely under inert atmosphere at reduced temperature (< -25 °C).



Structural Characterization of 2•dme. Owing to its extensive use as a starting material for these reactions, the solid state structure of **2** was of considerable interest. Crystals of **2•dme** were grown by dissolving solid **2** in dimethoxyethane and allowing the solution to evaporate at room temperature. Colorless needle-like crystals grew overnight, which were shown to be the oligomerized product of **2** with coordinated dme (Figure 12).

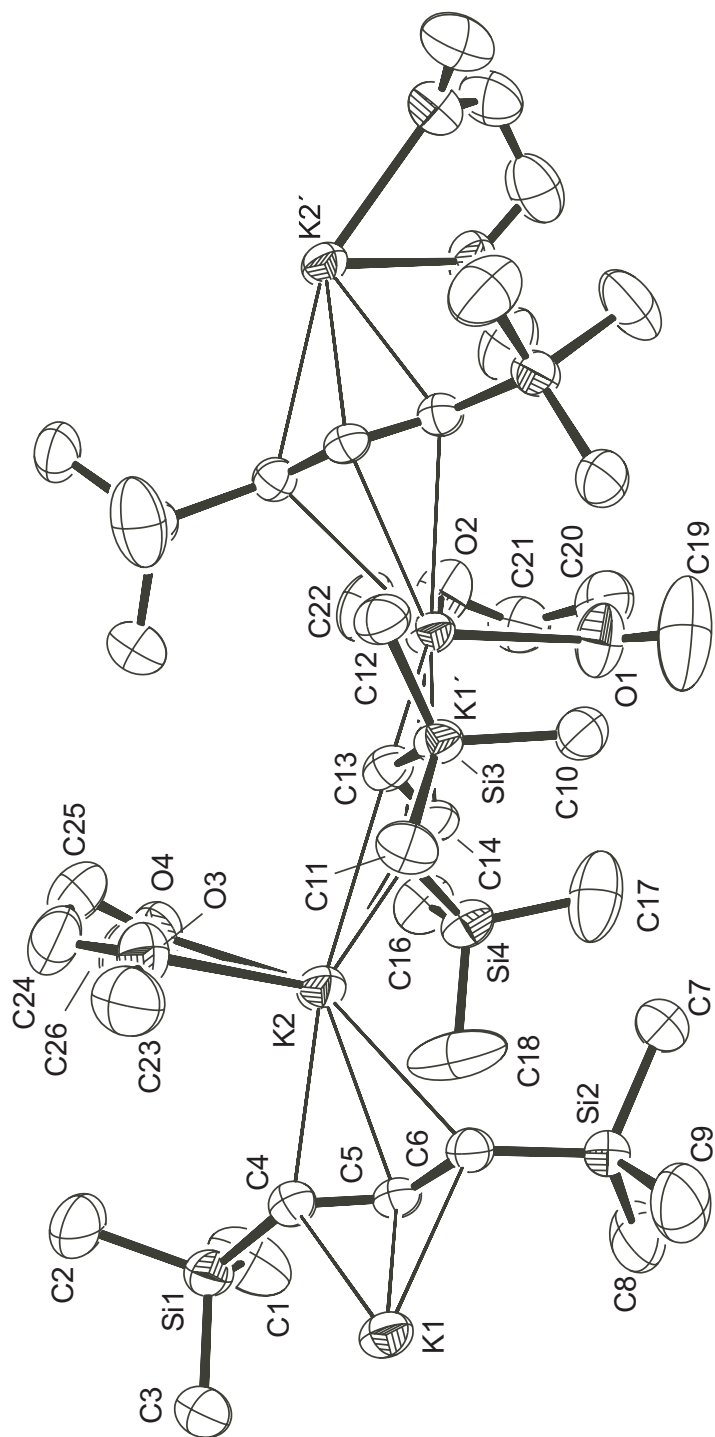


Figure 12. ORTEP of **2•dme**, with thermal ellipsoids at the 50% level. Hydrogen atoms have been omitted for clarity.

As is typical for organometallic coordination polymers of the heavy alkali metals, the potassium ions constitute a zig-zag chain, with K1–K2–K1 and K2–K1–K2 angles of 153.3° and 141.9°, respectively (cf. the K–K'–K'' angle of 138.0° in [K(C₅H₅)]_∞⁹⁶ and the K–K'–K'' angle of 150.7° in [K(C₅(SiMe₃)H₄)]_∞⁹⁷). The K–C distances of 2.98–3.10 Å are similar to those for potassium cyclopentadienides (cf. 2.988 Å to 3.079 Å in [K(C₅(SiMe₃)H₄)]_∞ and 2.933 to 3.101 Å in [K(C₅(SiMe₃)₃H₂)]_∞⁹⁸), an indication of the comparably ionic bonding in the complexes.

Coordination of the allyl anion to potassium causes relatively little perturbation in its geometry, as suggested by the average C–C–C angle 130.7(3)°, which is close to the 130.3° angle calculated for the free [A']⁻ anion.⁷ The SiMe₃ groups in **2•dme** are arranged in a *syn, syn* configuration. As is generally found for such substituents,^{13,23} the silicon atoms Si1 and Si2 are near the C₃ plane; their average 0.10 Å displacements are reflected in the nearly linear C–C–C–Si torsion angles of 176.3° (avg); the values for Si3 and Si4 are similar.

Polymerization Reactions. Complexes **1–10** were studied as single-component catalysts for the polymerization of methyl methacrylate (MMA). Typical experiments were run in ~20 mL toluene at 0 °C (Table 11). The microstructures of the polymers were analyzed with ¹H NMR spectroscopy.⁹¹⁻⁹³ The molecule weight and polydispersity of each polymer was determined with GPC. As a control, the iodide and/or triflate salt of each metal was subjected to similar polymerization conditions; no poly(methyl methacrylate) (PMMA) was formed from these salts.

Table 11. Results of MMA polymerization (in ~20 mL toluene at 0 °C) with allyl complexes. TOF = (mol monomer consumed) (mol catalyst)⁻¹ h⁻¹.

Complex	Time (min)	Conv'n (%)	TOF	M _w	M _n	M _w /M _n	Tacticity		
							rr	mr	mm
LiA' (1)	0.5	49.5	7400	–	–	–	15	31	54
KA' (2)	0.5	82.5	104000	215000	110000	1.95	23	54	23
CsA' (3)	0.5	72.6	16000	–	–	–	35	52	13
CaA' ₂ (thf) ₂ (4)	0.5	76.8	19000	–	–	–	14	28	58
SrA' ₂ (thf) ₂ (5)	0.5	36.4	8000	–	–	–	12	31	57
SmA' ₂ (thf) ₂ (6) ^a	0.5 300	5.3 12.3	1200 –	23700 63200	32400 13600	7.3 4.65	31 –	30 –	39 –
EuA' ₂ (thf) ₂ (7)	30	24.6	2400	131000	41200	3.2	21	41	38
YbA' ₂ (thf) ₂ (8)	35	41.4	100	378400	98100	3.9	26	51	23
CeA' ₃ (thf) (9)	30	13.6	67	148000	9070	16.3	23	30	47
NdA' ₃ (thf) (10)	30	16.8	63	272400	87200	3.1	23	27	50
[Li(thf) ₄][CeA' ₃] ^b	30	64.1	2400	613600	70600	8.7	25	28	47
[{K(thf) ₂ }{SmA' ₃ }] ₂ ^c	0.5	69.2	83100	87600	43800	2.0	24	54	22
2 SmA' ₂ (thf) ₂ (6) + KA' (2)	0.5	24.4	4590	42800	22100	1.93	20	47	32
SmA' ₂ (thf) ₂ (6) + KA' (2)	0.5	75.8	17000	62500	39700	1.57	22	51	27
SmA' ₂ (thf) ₂ (6) + 2 KA' (2)	0.5	83.3	18800	46500	29400	1.58	22	54	23

^a Values italicized represent those for PMMA prepared by Yasuda, see reference 22. ^b See reference 18 and Chapter I. ^c See reference 36 for all data except tacticity.

In these experiments, the turnover frequency (TOF) and the tacticity of the resultant polymers are influenced by several attributes of the catalyst; among these are the catalyst's metal size, M–C bond lengths, metal charge, and metal family. From Table 11, it is obvious that the combination and competition of these factors convolutes the results,

making it difficult to fully identify trends and anomalies in the data. Poorly understood mechanistic details of propagation of PMMA further inhibit full understanding of the discrepancies in PMMA results.⁹⁹

Metal family. As illustrated in Table 11, trends in both activity and stereocontrol exist for each family of metal catalysts. Lanthanide complexes **6–10** yield, in all cases, atactic PMMA, a lack of stereocontrol that has been previously reported for similar lanthanide complexes.^{36,90} Group II complexes **4** and **5** give slightly isotactic PMMA (58 and 57% mm, respectively). The Group I catalysts are the only metal family with variety in the tacticity of polymer produced; complexes **2** and **3** give atactic polymer, while LiA' (**1**) yields isotactic PMMA (54% mm). It should be noted that variations in polymerization activity and stereocontrol with isomorphous catalysts of the same group have been previously reported.^{99,100} The turnover frequency (TOF) for all of the Group I and II complexes is higher than that for the lanthanide complexes. Complex **2** has the highest TOF (104,000 h⁻¹) of any of the complexes studied; **4** is the next highest with a TOF of 19,000 h⁻¹.

Metal size. Throughout the series of lanthanide catalysts, with the exception of **7**, activity decreases with metal size. This has been attributed to increased steric congestion with smaller radii, which restricts access to the metal center.¹⁹ To further investigate this trend, unsolvated triallyllanthanide complexes YA'₃ and ErA'₃ were also studied as initiators for MMA polymerization; both complexes were inactive. Since these metal centers are smaller than those in lanthanide complexes **6–10** (Y(III) = 0.90 Å; Er(III) = 0.89 Å for CN 6),³⁰ these results support the idea that smaller metal centers lead to lower catalytic activity, presumably due to an increase in steric crowding.

Although the Group II and divalent lanthanide complexes are isomorphous and have similar metal radii ($\text{Ca(II)} \approx \text{Yb(II)} = 1.02 \text{ \AA}$; $\text{Sr(II)} \approx \text{Sm(II)} \approx \text{Eu(II)} = 1.17 \text{ \AA}$ for CN 6),³⁰ there is a substantial difference between the TOFs for the Group II and the divalent lanthanide complexes. Group II complexes (**4** and **5**) have TOF values significantly higher than those for divalent lanthanide complexes **6**, **7**, and **8**. Additionally, the size/TOF trend for each group differs; i.e., the Group II complex with the smallest metal center has the highest TOF, while the complexes with the largest lanthanide metals have the highest TOF.

Comparisons between calcium(II) and ytterbium(II) complexes have been previously made due to similarities in their metal radii, IR spectra, gas-phase behavior, and structures.²⁸ This work, however, shows a significant difference between the catalytic behavior of calcium and ytterbium complexes **4** and **8**; while **4** yields isotactic PMMA at a high rate ($19,000 \text{ h}^{-1}$), **8** gives atactic PMMA and has one of the lowest TOFs of all of the complexes studied (100 h^{-1}). Variations in the bond lengths of **4** and **8** ($\Delta = \sim 0.09 \text{ \AA}$) have been described in Chapter I and may account for the difference in activity and polymer microstructure for the two initiators.

This is not the first example where differences in the catalytic behavior of calcium and ytterbium complexes have been observed. For example, MMA polymerization with $\text{CaCp}^*_2(\text{thf})_2$ in toluene yields atactic PMMA,¹⁰¹ while $\text{YbCp}^*_2(\text{thf})_2$ gives syndiotactic PMMA (84% rr).¹⁰² Similarly, styrene polymerization with the chiral catalyst $\text{Yb}[1-(\text{NMe}_2)-2-(\mu\text{-CHSiMe}_3)\text{C}_6\text{H}_4][9-(\text{SiMe}_3)\text{fluorenyl}](\text{thf})$ yields polymer with lower syndiotacticity than the isomorphous calcium complex (67 and 86% rr,

respectively).^{28,103} It is evident that the propagation mechanism in each polymerization differs for calcium and ytterbium catalysts.

Metal charge. In general, TOF decreases with the charge on the catalyst's metal center; i.e., monovalent catalysts tend to have higher activity than divalent ones, which are in turn more active than trivalent complexes. Although there are a few exceptions among the Group I and II complexes, this trend is particularly obvious among the lanthanide allyl complexes, where the polymerization activity of the divalent complexes (**6**, **7**, and **8**) is notably higher than that of the trivalent species (**9** and **10**), as shown in Table 11. Higher charges lead to stronger bonds between the metal and ligands, which may decrease polymerization activity. However, increasing a metal's charge also involves an increase in the number of ligands bound to the metal; thus, more steric congestion around the metal center may reduce activity as described above. It is impossible to separate these effects, as there is a direct correlation in the number of ligands and metal charge in all of the catalysts studied. Nevertheless, with the exception of **1** and **4**, a direct relationship between metal charge and polymerization activity is observable for these allyl complexes.

Mixed Metal Catalysts. The salt complexes containing two metal centers are more efficient catalysts than the neutral complexes with the same lanthanide metal; they exhibit TOF values that are 10–100 times greater. A similar increase in activity was seen for $\text{Li}(\text{thf})_3(\mu\text{-Cl})\text{Ln}[\text{N}(\text{SiMe}_3)_2]_3$ ($\text{Ln} = \text{Nd}, \text{Sm}, \text{Eu}$), when compared to analogous neutral $\text{Ln}[\text{N}(\text{SiMe}_3)_2]_3$ complexes.¹⁰⁴ As described above, **2** displays the highest TOF for MMA polymerization of all tested compounds; hence for the salt complexes, in particular $[\{\text{K}(\text{thf})_2\}\{\text{SmA}'_3\}]_2$ ³⁶, there may exist two centers of monomer reactivity which may

explain the elevated TOF values seen for this complex. To test this assumption, catalyst mixtures of independently prepared **2** and **6** in varying ratios were used to polymerize MMA.

The TOFs of the mixtures of **2** and **6** are not as high as when **2** is used independently; however, higher TOFs accompany increased amounts of **2** in the catalyst mixtures. In solution, **2** and **6** seem to be interacting in such a way that the catalytic activity of **2** is retarded. To explore this, the ^1H NMR spectra of the three ratios of **2** and **6** were compared to those of **2**, **6**, and $[\{\text{K}(\text{thf})_2\}\{\text{SmA}'_3\}]_2$. Individual ^1H NMR resonances of **2** and **6** are not found in the spectra of mixtures of the two compounds. Resonances for the mixtures of **2** and **6** are very similar to those assigned for $[\{\text{K}(\text{thf})_2\}\{\text{SmA}'_3\}]_2$,³⁶ indicative that mixing **2** and **6** in toluene leads to an aggregate complex similar to $[\{\text{K}(\text{thf})_2\}\{\text{SmA}'_3\}]_2$. For example, the ^1H NMR peaks assigned to SiMe_3 groups are within a narrow range for all ratios (δ 2.36–2.65, -0.39– -0.13) and the peaks for $[\{\text{K}(\text{thf})_2\}\{\text{SmA}'_3\}]_2$ fall within this range (δ 2.65, -0.25). Similarly, the peaks corresponding to the allylic protons are close (ratios: δ 14.01–14.31, -24.62– -23.80; $[\{\text{K}(\text{thf})_2\}\{\text{SmA}'_3\}]_2$: δ 13.88, -25.84). Furthermore, the polydispersities of the combinations of **2** and **6** ($M_w/M_n = 1.57$ – 1.93) are lower than either **2** or **6** by itself, implying that the two species are not functioning as separate initiators.

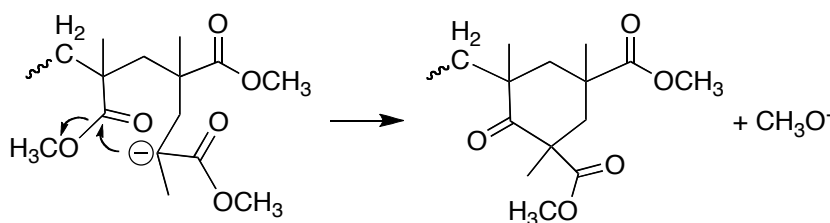
Although an interaction clearly exists between **2** and **6** when both initiators are dissolved in toluene, the mixtures do not behave exactly like $[\{\text{K}(\text{thf})_2\}\{\text{SmA}'_3\}]_2$. The latter has substantially heightened polymerization activity compared with all of the combinations of **2** and **6**.³⁶ To further show that the combinations of **2** and **6** do not reproduce the $[\{\text{K}(\text{thf})_2\}\{\text{SmA}'_3\}]_2$ complex, a 1:1 ratio of **2** and **6** was allowed to stir in

THF overnight. Upon removal of the solvent, the mixture was tested for MMA polymerization under the previously described conditions. The activity was similar to the 1:1 ratio, and hence significantly lower than the activity of separately prepared $[\{K(thf)_2\}\{SmA'_3\}]_2$. To ensure that differences in reaction conditions are not the cause of this discrepancy, $[\{K(thf)_2\}\{SmA'_3\}]_2$ was synthesized and its activity in the polymerization of MMA was reevaluated. It was found to be as active as previously published (e.g., a TOF of 82,600 h⁻¹ compared to the reported value of 83,100 h⁻¹).³⁶

Since **2** had the highest activity of any of the complexes studied, but yielded atactic polymers, and **4** and **5** produced slightly isotactic PMMA, attempts were made to synthesize mixed metal complexes with heightened activity, while maintaining control over the tacticity of the polymer. Towards this goal, CaI₂ and SrI₂ were each treated with three equivalents of **2** in THF at -78 °C. Evaporation of solvent, followed by extraction in and removal of toluene, yielded pale orange solid products. Unfortunately, in both cases, the ¹H NMR spectra of the products indicated the synthesis of the diallyl complex (**4** or **5**) and excess starting material (**2**).

Polymerization Conditions. The effect of temperature and solvent on polymerization with **1**, **2**, and **4** was also investigated (Table 12). For **2** and **4**, the highest activity is observed when the experiment is run in toluene at 0 °C, and higher activity is always seen with toluene than THF. Maximum activity at 0 °C is not surprising, as this has been observed in similar studies of MMA polymerization,^{101,104} and it may be the “ceiling temperature” for MMA at this concentration.⁹⁹ At room temperature (i.e., no regulation of the reaction’s temperature), the heat released from the highly exothermic polymerization reaction may be causing catalyst decomposition or side reactions.

Temperatures lower than room temperature also inhibit cyclization reactions from occurring at the end of the growing polymer chain (Scheme 2); such cyclization, or “backbiting,” is detrimental to propagation and decreases polymerization activity.^{99,105} Polymerization reactions were also performed at $-78\text{ }^{\circ}\text{C}$ with **2**; these runs exhibited lower activity than trials at $0\text{ }^{\circ}\text{C}$, presumably due to reaction retardation at such a low temperature.



Scheme 2. Unfavorable cyclization reaction on growing PMMA chain terminus.

With **2** and **4**, lower activity was observed when reactions were run in THF (Table 12). While atactic polymers were isolated with **2** in both solvents at all temperatures, polymerization with **4** in THF led to decreased stereoselectivity compared to reactions in toluene. Observation of decreased activity in polar solvents is caused by ion solvation, which reduces the number of free ions available to react with monomer.¹⁰⁶ Furthermore, ion solvation can alter the environment around the ion and influence the stereochemistry of the growing polymer chain.

Complex **1** does not follow the same trend as **2** and **4**; i.e., heightened activity is seen when THF is used as the solvent (Table 12). Additionally, **1** yields slightly isotactic polymers (54 and 62% mm at $0\text{ }^{\circ}\text{C}$ and RT, respectively) in toluene, but syndiotactic polymer is produced in THF (64% rr). This increase in activity and change in polymer

tacticity is not unprecedented; it has been observed with $\text{Li}(\text{thf})_3(\mu\text{-Cl})\text{Ln}[\text{N}(\text{SiMe}_3)_2]_3$ ($\text{Ln} = \text{Nd}, \text{Sm}, \text{Eu}$) and $\text{Y}[\text{Me}_2\text{C}(2,7\text{-}(t\text{-Bu})_2\text{Flu})(\text{Cp})][\text{CH}(\text{SiMe}_3)_2]$ catalysts.^{104,107} In living anionic polymerization with lithium enolates, varying the polarity of the solvent led to controllable changes in the stereochemistry throughout the polymer chain.¹⁰⁸ Similar block copolymers with alternating stereochemistry are likely to be obtained with **1** if the solvent is alternated between THF and toluene throughout the polymerization experiment.

Table 12. Results of MMA polymerization (in ~20 mL solvent, 0.5 min) with allyl complexes. TOF = (mol monomer consumed) (mol catalyst)⁻¹ h⁻¹.

Complex	Temp., °C	Solv.	Conv'n (%)	TOF	Tacticity		
					rr	mr	mm
LiA' (1)	0	Tol.	49.5	7400	15	31	54
LiA' (1)	0	THF	50.1	9000	63	33	4
LiA' (1)	25	Tol.	45.1	2500	9	29	62
KA' (2)	-78	Tol.	87.1	69000	22	53	25
KA' (2)	-78	THF	60.1	47000	24	57	19
KA' (2)	0	Tol.	82.5	104000	23	54	23
KA' (2)	0	THF	87.3	29000	30	56	14
KA' (2)	25	Tol.	56.2	28000	19	57	24
KA' (2)	25	THF	73.2	31000	30	57	14
CaA' ₂ (thf) ₂ (4)	0	Tol.	76.8	19000	14	28	58
CaA' ₂ (thf) ₂ (4)	0	THF	18.4	11000	42	42	16
CaA' ₂ (thf) ₂ (4)	25	Tol.	24.3	8100	10	30	59

The production of syndiotactic PMMA with **1** in THF is a notable result, as an increase in the syndiotacticity of PMMA leads to a higher glass transition temperature (T_g). The T_g for 100% syndiotactic PMMA is estimated to be between 135 and 145 °C,¹⁰¹ while PMMA samples produced by free radical polymerization (62% rr) typically display a T_g of only 105 °C.¹⁰⁹ In future work, optimization of polymerization conditions with **1** could eventually lead to highly syndiotactic PMMA, a desirable goal for polymer chemists.

Conclusion

Trimethylsilylated allyl complexes with Groups I and II and lanthanide metals have been explored as single component initiators in the polymerization of MMA. The potassium allyl complex produces atactic PMMA with a high turnover frequency (104,000 h⁻¹). Group I and II metal complexes have high activity compared to lanthanide allyl species, and the heightened activity of lanthanate and mixed metal complexes is likely due to the presence of Group I metals. Interestingly, activity with the lithium allyl complex increases in THF (relative to trials in toluene) and slightly syndiotactic polymer (63% rr) is produced in this solvent. Further investigation of this, and other bulky allyl complexes, could lead to highly stereoselective polymerization of MMA and other monomers.

CHAPTER IV

SYNTHESIS AND REACTIVITY OF TRIALLYLYTTTRIUM AND DENSITY FUNCTIONAL THEORY CALCULATIONS OF ^{89}Y NMR CHEMICAL SHIFTS FOR ORGANOYTTTRIUM COMPLEXES

Introduction

The diallylyttrium complex $\text{Y}[1,3-(\text{SiMe}_3)_2\text{C}_3\text{H}_3]_2\text{Cl}$ has been reported as an efficient catalyst for the polymerization of butadiene.²¹ Unfortunately, only limited characterization of the complex was reported, inhibiting full understanding of its catalytic role. Its potential use as a catalyst for the polymerization of other monomers (including methyl methacrylate and ethylene) has prompted further characterization of the complex. In doing this, density functional theory calculations of ^{89}Y NMR chemical shifts were used in combination with experimental methods.

Metal-centered NMR spectroscopy is an increasingly accessible complement to the non-metal nuclei (^1H , ^{13}C , ^{31}P , etc.) routinely used in the NMR characterization of organometallic and coordination complexes.¹¹⁰⁻¹¹⁴ The chemical shifts of metal nuclei are frequently more sensitive to small changes in geometry and coordination number than are those of ligands and can reveal subtle changes in the solution composition of complexes.^{115,116} These benefits are applicable to compounds of yttrium, virtually all of which contain the diamagnetic, tripositive Y(III) ion ($[\text{Kr}]5s^04d^0$). Yttrium complexes support an extensive range of ligands, including cyclopentadienyl rings,¹¹⁷⁻¹²¹ alkyls,¹²²⁻¹²⁴ allyls,^{125,126} dienes,¹²⁷ hydrides,^{128,129} alkoxides¹³⁰⁻¹³³ and aryloxides,¹³⁴ halides,¹³⁴ phosphides,¹³⁵ amides,¹³⁶ chalcogenides,¹³⁷ and even such “non-traditional”

species as N_2 .^{35,138,139} This ligand variety has contributed to the use of yttrium compounds as catalysts and in materials chemistry.^{122,140-145} Yttrium compounds are often structurally similar to those of the late lanthanide elements (the ionic radii of Y(III) and Ho(III) are virtually identical (ca. 0.90 Å)).^{28,30} Consequently, yttrium complexes are useful in modeling the structures and reactions of related compounds of the paramagnetic heavy lanthanides.¹⁴⁶⁻¹⁴⁸

As a monoisotopic species with $I = -1/2$ and a wide chemical shift range (ca. 1300 ppm),²⁹ the ^{89}Y nucleus is an attractive nucleus for NMR study. That it has not been routinely used in the characterization of yttrium complexes is a consequence of several factors, including its low receptivity (0.681 relative to ^{13}C) and resonance frequency (e.g., 24.5 MHz at a magnetic field strength of 11.7 T ($^1\text{H} = 500$ MHz)). In addition, the yttrium nucleus' relaxation time (T_1) is long,^{29,149-151} leading to problems with detection and to the necessity for lengthy experiments. There are techniques available that can be used to address some of these problems; e.g., spin-echo sequences will minimize probe ringing associated with low frequency nuclei, and the addition of relaxation agents can shorten relaxation times.^{117,152} It should be noted that solid state CP/MAS ^{89}Y NMR spectroscopy does not suffer from the problems of long relaxation times; therefore, spectra with good signal to noise ratios are obtainable in minutes, as distinct from the several hours or even days often required by solution experiments.^{153,154} However, information obtained in the solid state (particularly the chemical shift) is not directly comparable to that from solution spectra.

Upfield NMR shifts have been observed with higher coordination numbers in beryllium and aluminum complexes,^{155,156} but the correlation between ^{89}Y chemical

shifts and the metal coordination number is unclear. Neutral base adducts can produce both greater shielding¹⁵⁷ and deshielding¹⁵⁸ of the metal nucleus. Over a decade ago, Schaverien used NMR data to estimate the group contribution of various ligands to ⁸⁹Y chemical shifts and found they moved farther upfield with increased electronegativity and π -donating ability of the ligands.¹³¹ The trend was quantified in values such as +300 ppm for alkyls, +190 ppm for amides, +56 ppm for aryloxides, and -100 ppm for the C₅Me₅ ring. Schaverien excluded from his compilations ⁸⁹Y NMR data obtained in ethereal solvents (primarily THF) because of the possibility that the formation of adducts or other reaction products would obscure the ligand contributions.

Direct calculation of yttrium chemical shifts would be a valuable tool in the characterization of organometallic yttrium complexes. The compounds of a variety of main-group and transition metals, including ⁹Be,¹⁵⁵ ⁵¹V,¹⁵⁹ ⁵⁵Mn,¹⁶⁰ ⁵⁷Fe,^{161,162} ¹⁰³Rh,^{163,164} ²⁰⁵Tl,¹⁶⁵ and ¹⁹⁵Pt¹⁶⁵ have been studied with DFT methods,¹⁶⁶ although this approach has not yet been applied to complexes of yttrium. Density functional theory in combination with the GIAO (gauge-including atomic orbitals)^{167,168} method has been used to predict the ⁸⁹Y chemical shifts of a variety of organoyttrium species and to aid in characterizing a bis(1,3-trimethylsilyl)allyl yttrium complex.

Experimental

General Considerations. All operations were performed in an atmosphere of nitrogen using standard glovebox or Schlenk techniques. ¹H and ¹³C NMR spectra were obtained on a Bruker DPX-300 spectrometer at 300 and 75.5 MHz, respectively, and were referenced to the residual ¹H and ¹³C resonances of C₆D₆ (δ 7.15 and 128.0) or ¹H

resonance of THF-*d*₈ (δ 1.73, 3.58). ⁸⁹Y NMR spectra were obtained on a Bruker DPX-400 spectrometer at 19.6 MHz and were externally referenced to 2 M YCl₃ in D₂O. The spectra were acquired with a 30° pulse and a 60 s delay, with accumulation times of about 48 h. Post-processing baseline correction using NUTS (Acorn NMR, Inc., Livermore, CA) was performed with a linear prediction of the first 128 data points of ⁸⁹Y NMR acquisition. To test the accuracy of this experimental ⁸⁹Y NMR method, Y[N(SiMe₃)₂]₃ was synthesized and its ⁸⁹Y NMR spectrum was obtained. The observed shift was at 570 ppm, which exactly matches with the literature value.¹³¹ Elemental analysis was performed by the Micro-Mass Facility at the University of California, Berkeley, CA. Transmission electron microscopy (TEM) analysis was conducted using a Phillips CM 20 microscope operating at 200 kV. The sample for TEM study was dissolved in THF, added dropwise to a nickel TEM grid covered with holey carbon film as a substrate (SPI Supplies), and dried. Energy dispersive X-ray spectrometry (EDS) analysis was obtained using an EDAX DX-4 package integrated onto the TEM. Samples were tilted at 15° for analysis at 200 kV during TEM analysis and were analyzed over a 1 μ m area.

Materials. K[1,3-(SiMe₃)₂C₃H₃]¹⁹ and Y[N(SiMe₃)₂]₃¹⁶⁹ were prepared as previously reported. Hexanes were distilled under nitrogen from potassium benzophenone ketyl.⁴² Anhydrous tetrahydrofuran (THF) was purchased from Aldrich and used as received. Deuterium oxide was purchased from Cambridge Isotope Laboratories and used as received. After vacuum distillation from Na/K (22/78) alloy, C₆D₆ and THF-*d*₈ were stored over Type 4A molecular sieves. All other reagents were obtained from commercial sources and used as received.

Synthesis of Y[1,3-(SiMe₃)₂C₃H₃]₃ (15). A 125 mL Schlenk flask was charged with YCl₃ (0.839 g, 4.30 mmol), THF (50 mL), and a stirring bar. An addition funnel was prepared with K[1,3-(SiMe₃)₂C₃H₃] (1.904 g, 8.49 mmol) in THF (40 mL). After assembly in a glovebox, the apparatus was placed on a Schlenk line, where the YCl₃ solution was cooled to -78 °C. The K[1,3-(SiMe₃)₂C₃H₃] solution was added dropwise with stirring over 30 min, after which the reaction was allowed to continue stirring as it warmed to room temperature overnight. The orange reaction mixture was then evaporated to dryness, and the residue extracted with hexanes. The extract was filtered, and removal of hexanes under vacuum produced a yellow oil that yielded yellow-orange crystals of Y[1,3-(SiMe₃)₂C₃H₃]₃ on standing overnight (1.92 g, 70%). Anal. Calc. C₂₇H₆₃Si₆Y: C, 50.26; H, 9.84; Cl, 0.00. Found: C, 48.49, H, 9.87; Cl, 0.17. Pure Y[1,3-(SiMe₃)₂C₃H₃]₂Cl requires C, 43.66; H, 8.55; Cl, 7.16. The somewhat lower than expected carbon analysis and the trace amount of Cl may indicate the presence of unreacted YCl₃ or the formation of a minor amount of Y[1,3-(SiMe₃)₂C₃H₃]₂Cl. ¹H NMR (25 °C, 300 MHz, C₆D₆): δ 0.22 (s, 54H, SiMe₃); 3.58 (d, *J* = 16.2 Hz, 6H, CHCHCH); 7.46 (t, *J* = 16.2 Hz, 3H, CHCHCH). The spectrum was invariant from -65 to 45 °C in THF-*d*₈. ¹³C NMR (25 °C, 75 MHz, C₆D₆): δ 1.12 (SiMe₃); 95.29 (CHCHCH); 163.13 (CHCHCH). ⁸⁹Y NMR (25 °C, 19.6 MHz, C₆D₆, 0.28 M): δ 470.5. Despite disorder in the allyl ligands, crystallographic data were consistent with the formation of Y[1,3-(SiMe₃)₂C₃H₃]₃.

Synthesis of Y[1,3-(SiMe₃)₂C₃H₃]₃ (15). Method B. The procedure follows that of Method A of the attempted synthesis of Y[1,3-(SiMe₃)₂C₃H₃]₂Cl except for the

following alterations. The reaction was run at room temperature rather than $-78\text{ }^{\circ}\text{C}$, and 0.310 g (1.59 mmol) of YCl_3 was treated with 0.691 g (3.08 mmol) of $\text{K}[1,3\text{-(SiMe}_3)_2\text{C}_3\text{H}_3]$. Yellow-orange crystals formed overnight in a concentrated hexanes solution. The reaction yielded 0.70 g of product (70%). The ^1H NMR spectrum was identical to that of the product in Method A.

Synthesis of $\text{Y}[1,3\text{-(SiMe}_3)_2\text{C}_3\text{H}_3]_3$ (15). Method C. A 125 mL Schlenk flask was charged with $\text{K}[1,3\text{-(SiMe}_3)_2\text{C}_3\text{H}_3]$ (0.757 g, 3.37 mmol) in THF (50 mL) and a stirring bar. An addition funnel was prepared with YCl_3 (0.319 g, 1.63 mmol) in THF (40 mL). After assembly in the glove box, the apparatus was placed on a Schlenk line. After the $\text{K}[1,3\text{-(SiMe}_3)_2\text{C}_3\text{H}_3]$ solution was cooled to $-78\text{ }^{\circ}\text{C}$, the YCl_3 solution was added dropwise with stirring over 30 min. After warming to room temperature overnight, the orange reaction mixture was evaporated to dryness, then extracted with hexanes. The extract was filtered, and removal of hexanes under vacuum yielded a yellow oil that formed yellow-orange crystals overnight. The reaction yielded 0.61 g of product (58%). The ^1H NMR spectrum was identical to that of the product in Method A.

Synthesis of $\text{Y}[1,3\text{-(SiMe}_3)_2\text{C}_3\text{H}_3]_3$ (15). Method D. The procedure follows that of Method C of the attempted synthesis of $\text{Y}[1,3\text{-(SiMe}_3)_2\text{C}_3\text{H}_3]_2\text{Cl}$ except for the following alterations. The reaction was run at room temperature rather than $-78\text{ }^{\circ}\text{C}$, 0.343 g (1.76 mmol) of YCl_3 was treated with 0.808 g (3.60 mmol) of $\text{K}[1,3\text{-(SiMe}_3)_2\text{C}_3\text{H}_3]$. Yellow-orange crystals formed overnight in a concentrated hexanes solution. The reaction yielded 0.47 g of product (48%). The ^1H NMR spectrum and crystal structure were identical to that of the product in Method A.

Synthesis of Y[1,3-(SiMe₃)₂C₃H₃]₃ (15). Method E. A 125 mL Schlenk flask was charged with YCl₃ (0.783 g, 4.01 mmol), THF (50 mL), and a stirring bar. An addition funnel was prepared with K[1,3-(SiMe₃)₂C₃H₃] (2.209 g, 9.84 mmol) in THF (40 mL). After assembly in the glove box, the apparatus was placed on a Schlenk line. After the YCl₃ solution was cooled to -78 °C, the K[1,3-(SiMe₃)₂C₃H₃] solution was added dropwise with stirring over 30 min. After warming to room temperature overnight, the yellow reaction mixture was evaporated to dryness, then extracted with hexanes. The extract was filtered, and removal of hexanes under vacuum yielded an orange oil (0.76 g, 71%). The ¹H NMR spectrum was identical to that of the product in Method A.

Synthesis of Y[1,3-(SiMe₃)₂C₃H₃]₃ (15). Method F. A 125 mL Erlenmeyer flask was charged with YCl₃ (0.435 g, 2.23 mmol), DME (100 mL), and a stirring bar. To this stirred flask, K[1,3-(SiMe₃)₂C₃H₃] (1.111 g, 4.95 mmol) was added slowly at room temperature. After stirring overnight, the reaction mixture was evaporated to dryness, then extracted with hexanes. The extract was filtered, and removal of hexanes under vacuum yielded an orange oil (1.08 g, 75%). The ¹H NMR spectrum was identical to that of the product in Method A.

Attempted reaction of Y[1,3-(SiMe₃)₂C₃H₃]₃ (15) with PMe₃. A 125 mL Schlenk flask was charged with Y[1,3-(SiMe₃)₂C₃H₃]₃ (0.190 g, 0.29 mmol), hexanes (50 mL), and a stirring bar. AgI•PMe₃ (0.128, 0.41 mmol) was added to a Schlenk tube. The two flasks were connected, brought out of the glovebox, and placed onto the Schlenk line. The Schlenk flask with the Y[1,3-(SiMe₃)₂C₃H₃]₃ solution was cooled to 0 °C. The Schlenk tube with AgI•PMe₃ was heated with a heat gun, where upon it began to boil and turn orange. Heat was stopped once it appeared to no longer boil. There was no

noticeable change in the appearance of the $\text{Y}[1,3-(\text{SiMe}_3)_2\text{C}_3\text{H}_3]_3$ solution. The apparatus was brought into the glovebox. The $\text{Y}[1,3-(\text{SiMe}_3)_2\text{C}_3\text{H}_3]_3$ solution was evaporated to dryness under vacuum. The ^1H NMR spectrum of the product indicated that no reaction had occurred.

Reaction of $\text{Y}[1,3-(\text{SiMe}_3)_2\text{C}_3\text{H}_3]_3$ (15) with AlMe_3 . A 125 mL Schlenk flask was charged with $\text{Y}[1,3-(\text{SiMe}_3)_2\text{C}_3\text{H}_3]_3$ (0.200 g, 0.31 mmol), hexanes (50 mL), and a stirring bar. At room temperature, 0.155 mL (0.31 mmol) of 2M AlMe_3 in hexanes was syringed into the $\text{Y}[1,3-(\text{SiMe}_3)_2\text{C}_3\text{H}_3]_3$ solution with stirring. The yellow reaction mixture immediately became cloudy and then turned pale yellow indicating a reaction between the two substrates had occurred.

General Procedures for X-ray Crystallography. Data collection and structure solution were conducted at the X-Ray Crystallographic Laboratory at the University of Minnesota. All calculations were performed using the current SHELXTL⁴³ suite of programs. A suitable crystal was located and attached to the tip of a glass capillary and mounted on a CCD area detector diffractometer for data collection at 173(2) K. A preliminary set of cell constants was calculated from reflections harvested from three sets of 20 frames. These initial sets of frames were oriented such that orthogonal wedges of reciprocal space were surveyed. Data collection of a randomly oriented region of reciprocal space was carried out using $\text{MoK}\alpha$ radiation (graphite monochromator). The intensity data were corrected for absorption with SADABS.⁴⁵ Final cell constants were calculated from strong reflections from the actual data collection after integration (SAINT).¹⁷⁰ Relevant crystal and collection data parameters for $\text{Y}[1,3-(\text{SiMe}_3)_2\text{C}_3\text{H}_3]_3$ can be found in Tables 33–35.

Computational Methods. Geometry optimization and NMR shift calculations were performed with the GAUSSIAN 03W suite of programs⁶⁸ and the GIAO (gauge-including atomic orbitals) method.¹⁶⁷ For geometry optimizations, the B3PW91 functional, which incorporates Becke's three-parameter exchange functional¹⁷¹ with the 1991 gradient-corrected correlation functional of Perdew and Wang,¹⁷² was used. This hybrid functional has previously been shown to provide realistic geometries for organometallic species.^{173,174} For yttrium, the DFT-optimized double-zeta basis set of Godbout (DGDZVP; ([18s12p9d])/[6s5p3d]) was used; for atoms other than yttrium, the standard 6-311G(d,p) basis sets were employed. Atomic coordinates for calculated structures can be found in Tables 41–44 and ref 175.

For the shielding calculations, the larger triple-zeta basis set of Ahlrich (TZVPalls2; (19s14p9d)/[8s6p5d])¹⁷⁶ was used for yttrium; the 6-311+G(2p,d) basis was used for other atoms. Typical calculations require at least 24 h on a single 3.2 MHz processor machine (e.g., for $\text{Y}(\text{C}_5\text{H}_4\text{Me})_2(\text{Me})(\text{thf})$, geometry optimization required 18 h (510 basis functions) and the shielding calculation an additional 23.5 h (687 basis functions)).

As the optimum functional for transition metal shielding constants can vary depending on the metal,¹⁶⁶ six hybrid and two GGA DFT functionals were evaluated for this study. The hybrids included B3PW91, B3LYP, O3LYP,¹⁷⁷ B97-1,¹⁷⁸ the one-parameter mPW1PW91,¹⁷⁹ and the parameter-free PBE1PBE.¹⁸⁰ The GGA functionals included BP86, BPW91, and OLYP.¹⁷⁷ Test calculations (described in detail below) performed on the $\text{Y}^{3+}(\text{aq})$ ion and with several organometallic molecules led to the selection of O3LYP as the functional of choice, although its superiority over most of the others was not large. It provides a strongly linear correlation between calculated and

observed chemical shifts, but substantial scaling was still required to provide quantitatively reasonable shift values.

Results and Discussion

Experimental Chemical Shifts. Table 13 provides a compilation of reported ^{89}Y chemical shifts of both organometallic and, for comparative purposes, some coordination compounds in nonaqueous solvents. The previously noted lack of correlation between chemical shift and coordination number (see the Introduction) is apparent in the data in Table 13. The linear correlation coefficient (r^2) between the two sets of numbers is 0.25, so that there is no useful covariance between them. Organometallic species occupy both extremes of the 1270 ppm range, but as noted earlier,^{131,181} cyclopentadienyl species are the most shielded, and are found in the range of ca. -370 to 80 ppm; purely sigma-bound species are the most deshielded, with the homoleptic alkyl complex $\text{Y}[\text{CH}(\text{SiMe}_3)_2]_3$ possessing the largest reported shift ($+895$ ppm).

In addition to the group contributions described by Schaverien,¹³¹ some further correlations can now be identified (Tables 14 and 15). For example, starting with the contribution of $+190$ ppm from the $\text{N}(\text{SiMe}_3)_2$ group, the shift of $\text{Y}[\text{N}(\text{SiMe}_3)_2]_3(\text{OPPh}_3)$ suggests a contribution of -25 ppm from the OPPh_3 group. Similar reasoning using the chemical shifts of $\text{Y}(\text{BHT})_3$ and $\text{Y}(\text{BHT})_3(\text{OPMe}_2\text{Ph})$ indicates a value of -23 ppm from the OPMe_2Ph group. If the average of -24 ppm is used as a starting point for the contribution of a OPR_3 group ($\text{R} = \text{aryl or alkyl}$), then the value observed for $\text{Y}(\text{OSiPh}_3)_3(\text{OPn-Bu}_3)_2$ implies that $+90$ ppm is an appropriate value for OSiPh_3 . This

value is consistent with the expectation that alkoxides, with an average contribution of +56 ppm, are better σ -donors than are the corresponding aryl silyloxides.¹⁸²

The difficulty in assessing the effects of ethereal solvents (primarily THF) on ^{89}Y NMR data is illustrated by the changes in the chemical shifts of $[\text{Y}(\text{C}_5\text{H}_4\text{Me})_2\text{E}]_2$ (in toluene- d_8) and $\text{Y}(\text{C}_5\text{H}_4\text{Me})_2\text{E}(\text{thf})$ (in THF- d_8) (Tables 14 and 15). When $\text{E} = \text{Cl}$, the shifts of the two compounds differ by only 5 ppm, despite the disruption of the dimer in THF and the coordination of the additional ligand. When $\text{E} = \text{Me}$, the shift difference is 55 ppm. In both cases, the shift of the solvated species is upfield, but which of these changes is the more typical of the influence of solvent is unknown. It may be impossible to quantify the effect of coordinated (but rapidly exchanging) THF ligands on the chemical shift when THF is also the solvent. If the group contribution to the chemical shift from THF is arbitrarily set to zero, a second internally consistent set of values can be derived (Table 15). It seems clear that the qualitative trends involving sigma donation and chemical shift that are observed in aromatic solvents persist in THF, although the two scales of values (Tables 14 and 15) are not directly comparable.

It should also be noted from the data in Table 13 that charged complexes are shifted substantially from the neutral species. Based on the series of $[\text{Y}(\text{CH}_2\text{SiMe}_3)_n(\text{thf})_4]^{(3-n)+}$ complexes and the group contributions in Table 15, a positive charge is associated with a downfield shift of ca. 75 ppm, and a dipositive charge with a ca. 115 ppm shift. It is possible that $\text{Y}(\text{C}_5\text{Me}_5)_2(\mu\text{-Cl})_2\text{K}(\text{thf})_2$ should be represented in solution as the solvent-separated ion pair $[\text{K}(\text{thf})_n]^+[(\text{C}_5\text{Me}_5)_2\text{YCl}_2]^-$, and that the strong upfield shift of the complex (–324 ppm) stems from the negative charge on the yttrium fragment. The

limited amount of data currently available makes it impossible to be more definitive about the effects of charge on the ^{89}Y chemical shift.

Selection of the Density Functionals. The initial survey of the functionals focused on the yttrium aquo ion, which serves as the chemical shift standard for ^{89}Y NMR (typically used in 1–3 M aqueous solution of YCl_3). It has been established from both EXAFS and X-ray scattering experiments that the $[\text{Y}(\text{OH}_2)_8]^{3+}$ ion exists at these concentrations,¹⁸³ with eight nearly equal Y–O distances at $2.368 \pm 0.005 \text{ \AA}$.¹⁸³⁻¹⁸⁵ The $[\text{Y}(\text{OH}_2)_8]^{3+}$ ion is also known in the solid state, and in the $[\text{Y}(\text{OH}_2)_8]\text{Cl}_3 \cdot (15\text{-crown-5})$ complex, the cation takes the form of a distorted bicapped trigonal prism with Y–O = 2.31–2.44 \AA , averaging to 2.364 \AA .¹⁸⁶

The presence of Cl^- in aqueous solutions of YCl_3 has a small but measurable effect (up to ca. 6 ppm) on the chemical shift of the $[\text{Y}(\text{OH}_2)_8]^{3+}$ ion.¹⁵⁰ In general, it is unknown how changes in concentrations and temperatures affect chemical shifts in ^{89}Y NMR; rarely are experiments run at more than one temperature or concentration, and the latter is frequently not reported in any case. Cooling from ambient temperature to $-83 \text{ }^\circ\text{C}$ caused a 7.2 ppm downfield shift in the resonance for $\text{Y}[\text{H}(\mu\text{-H})\text{B}(\text{Pz})_2]_3$,¹⁸⁷ for example, but the molecule is fluxional in solution (^1H , ^{13}C NMR evidence), so little can be inferred about the temperature change *per se* on the shift. In addition, the shift of $\text{Y}(\text{C}_5\text{H}_4\text{Me})_2\text{Cl}(\text{thf})$ has been reported at two slightly different concentrations (1.5 and 1.7 M), for which there is a shift difference of 2 ppm;¹⁸¹ in the absence of additional examples, the significance of these changes is unknown.

Table 13. Yttrium complexes and their corresponding ^{89}Y NMR chemical shifts.

Compounds	δ_{exp} (ppm)	CN ^a	Solvent	Ref.
$\text{Y}(\text{C}_5\text{H}_4\text{Me})_3(\text{thf})$	-371	10	THF- <i>d</i> ₈	181
$\text{Y}(\text{C}_5\text{Me}_5)_2(\mu\text{-Cl})_2\text{K}(\text{thf})_2$	-324	8	THF- <i>d</i> ₈	181
$\text{Y}(\text{C}_5\text{Me}_5)_2(\text{OAr})$	-129.3 (25 °C)	7	C ₆ D ₆	131
$\text{Y}(\text{C}_5\text{H}_4\text{Me})_2\text{Cl}(\text{thf})$	-103 (1.5M), -101 (1.7M)	8	THF- <i>d</i> ₈	181
$[\text{Y}(\text{C}_5\text{H}_4\text{Me})_2\text{Cl}]_2$	-97	8	C ₆ D ₅ CD ₃	181
$[\text{Y}(\text{C}_5\text{H}_4\text{Me})_2(\mu\text{-H})(\text{thf})]_2$	-92	9	THF- <i>d</i> ₈	181
$[\text{Y}(\text{C}_5\text{H}_4\text{Me})_2(\mu\text{-C}\equiv\text{CCMe}_3)]_2$	-74	8	THF- <i>d</i> ₈	181
$\{\text{Li}(\text{thf})_4\}\{[\text{Y}(\text{C}_5\text{H}_5)_2(\mu\text{-H})]_3(\mu_3\text{-H})\}$	-67	9	THF- <i>d</i> ₈	181
$[\text{Y}(\text{C}_5\text{H}_4\text{Me})_2(\mu\text{-Me})]_2$	-15	8	C ₆ D ₅ CD ₃	181
$[\text{Y}(\text{OH}_2)_8]^{3+}$	0.00 (reference)	6	D ₂ O	
$\text{Y}(\text{C}_5\text{Me}_5)(\text{O-2,6-}(t\text{-Bu})_2\text{C}_6\text{H}_3)_2$	21.0 (25 °C)	5	C ₆ D ₆	131
$\text{Y}(\text{OCMe}_2i\text{-Pr})_3$	36.8 (37 °C)	4	C ₆ D ₅ CD ₃	158
$\text{Y}(\text{C}_5\text{H}_4\text{Me})_2(\text{Me})(\text{thf})$	40	8	THF- <i>d</i> ₈	181
$\text{Y}(\text{OCMeEt}i\text{-Pr})_3$	45.6 (37 °C)	4	C ₆ D ₅ CD ₃	158
$\text{Y}(\text{OCe}t_3)_3$	47.8 (25 °C)	4	C ₆ D ₅ CD ₃	158
$\text{Y}_3(\text{OCH}_2\text{CH}_2\text{OMe})_5(\text{acac})_4$	62.7 (1), 91.4 (2)	8	C ₆ D ₅ CD ₃	157
$\text{Y}(\text{C}_5\text{Me}_5)_2\text{CH}(\text{SiMe}_3)_2$	78.9 (25 °C)	4	C ₆ D ₆	131
$\text{Y}[\text{H}(\mu\text{-H})\text{B}(3,5\text{-Me}_2\text{Pz})_2]_3$	105.6	9	CDCl ₃	187
$[\text{Y}(\text{OCH}_2\text{CH}_2\text{OMe})_2]_{10}$	134.5	5,7	C ₆ D ₅ CD ₃	157
$\text{Y}(\text{BHT})_3(\text{OPMe}_2\text{Ph})$	148.1	4	C ₆ D ₆	157
$\text{Y}(\text{OSiPh}_3)_3(\text{thf})_3$	157.1	6	THF- <i>d</i> ₈	157

$Y_3(Ot\text{-Bu})_9(t\text{-BuOH})_2$	166.8 (37 °C)	6	C_6D_6	158
$[K(dme)_4][Y(OSiPh_3)_4(dme)]$	168.1	6	DME- d_{10}	157
$Y(DPM)_3$	168.3	6	$CDCl_3$	157
$Y(O\text{-}2,6\text{-}(t\text{-Bu})_2C_6H_3)_3$	168.4 (25 °C)	3	C_6D_6	131
$Y(BHT)_3$	170.8 (23 °C)	3	C_6D_6	157
$Y_3(Ot\text{-Am})_9(t\text{-AmOH})_2$	199.1 (37 °C)	6	C_6D_6	158
$Y_5(\mu_5\text{-O})(\mu_3\text{-}Oi\text{-Pr})_4(Oi\text{-Pr})_5$	214.0 (1), 217.7 (4)	5,6	C_6D_6	157
$Y(OSiPh_3)_3(OPn\text{-Bu}_3)_2$	221.6	5	$CDCl_3$	157
$Y[H(\mu\text{-H})B(Pz)_2]_3$	238.8 (ambient)	9	CD_2Cl_2	187
$Y[H(\mu\text{-H})B(Pz)_2]_3$	246.0 (−83 °C)	9	CD_2Cl_2	187
$Y(OSiMe_2t\text{-Bu})_3(thf)_3$	266.6	6	$CDCl_3$	157
$[Y(CH_2SiMe_3)(thf)_4][BPh_4]_2$	409.2	5	THF- d_8	188
$[YMe(thf)_6][BPh_4]_2$	433.2	7	pyr- d_5	188
$Y[1,3\text{-}(SiMe_3)_2C_3H_3]_3$	470.5	3	C_6D_6	this work
$Y[N(SiMe_3)_2]_3(OPPh_3)$	544.4 (23 °C)	4	$C_6D_5CD_3$	157
$Y[N(SiMe_3)_2]_3$	570.0 (23 °C)	3	$CDCl_3$	157
$[Y(CH_2SiMe_3)_2(thf)_4][BPh_4]$	660.0	6	THF- d_8	188
$[Y(CH_2SiMe_3)_2(thf)_4][BPh_3(CH_2SiMe_3)]$	660.2	6	THF- d_8	188
$[Y(CH_2SiMe_3)_2(thf)_4][Al(CH_2SiMe_3)]$	666.4	6	THF- d_8	188
$Y(CH_2SiMe_3)_3(thf)_2$	882.7	5	THF- d_8	188
$Y[CH(SiMe_3)_2]_3$	895.0 (25 °C)	3	$C_6D_5CD_3$	131

^a Formal coordination number. All cyclopentadienyl rings are known or assumed to be η^5 , and assigned a CN of 3. Abbreviations: acac = acetylacetonate, BHT = O-2,6-*t*-Bu₂-4-MeC₆H₂, dme = dimethoxyethane, DPM = 2,2,6,6-tetramethyl-3,5-heptanedionato, Pz = pyrazolyl ring, *t*-Am = *tert*-amyl, thf = tetrahydrofuran.

Table 14. Empirical group contributions to ^{89}Y NMR chemical shift for aromatic solvents (benzene or toluene).

Group	Contribution (ppm)	Ref.
C_5Me_5	-100	189
OPR_3 (R = aryl or alkyl)	-24	this work
$\text{OCMe}_2i\text{-Pr}$	+12	189
$\text{OCMeEt}i\text{-Pr}$	+15	189
OCe_3	+16	189
$\text{O-2,6-}t\text{-Bu}_2\text{C}_6\text{H}_3$	+56	189
$\text{O-2,6-}t\text{-Bu}_2\text{C}_6\text{H}_2\text{-4-Me}$	+57	189
OSiPh_3	+90	this work
$\text{N}(\text{SiMe}_3)_2$	+190	189
$\text{CH}(\text{SiMe}_3)_2$	+298	189

Table 15. Empirical group contributions to ^{89}Y NMR chemical shift in $\text{THF-}d_8$.

Group	Contribution (ppm)
$\text{C}_5\text{H}_4\text{Me}$	-124
THF	0 (assumed)
OSiPh_3	+52
Cl	+146
CH_3	+288
$\text{CH}_2(\text{SiMe}_3)$	+294

The $Y[(OH_2)_8]^{3+}$ ion was optimized starting from the coordinates in $[Y(OH_2)_8]Cl_3 \cdot (15\text{-crown-5})$, which yielded a square antiprismatic structure with nearly exact S_8 symmetry; the symmetry was made exact in subsequent testing. Table 16 lists the shielding constants calculated with the functionals for the $[Y(OH_2)_8]^{3+}$ ion and three of the organometallic molecules used in this study that together encompass a nearly 1000 ppm shift range. Trial linear fits on the calculated and experimental chemical shifts of the organometallic complexes led to the selection of O3LYP, mPW1PW91, PBE1PBE, and OLYP as the most promising; additional testing led to the selection of O3LYP for use in subsequent calculations.

Table 16. Shielding constants (σ_{calc} , ppm) from various GGA and hybrid functionals. All geometries were calculated at the B3PW91/DGDZVP level. The experimental chemical shifts in ppm from $[Y(OH_2)_8]^{3+}$ are indicated below the compounds.

Functional	$[Y(OH_2)_8]^{3+}$ (0.0 ppm)	$[Y(C_5H_4Me)_2(\mu\text{-Cl})_2]$ (-97 ppm)	$Y(C_5H_4Me)_2(Me)(thf)$ (40 ppm)	$Y[CH(SiMe_3)_2]_3$ (895.0 ppm)
B97-1	2800.9	2797.7	2597.1	1477.9
O3LYP	2775.4	2702.8	2539.5	1441.4
mPW1PW91	2808.7	2789.8	2623.5	1518.1
PBE1PBE	2807.7	2794.1	2627.0	1522.6
B3LYP	2784.9	2747.7	2579.8	1451.9
B3PW91	2783.2	2755.1	2587.1	1471.1
OLYP	2708.4	2617.3	2454.4	1346.6
BPW91	2661.7	2607.9	2439.4	1299.6
BP86	2653.1	2604.9	2435.6	1281.2

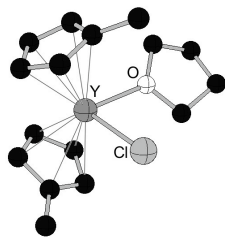
The determination of accurate geometries is a key element in the effectiveness of computational NMR as a characterization tool, and comparatively high levels of theory must be used to obtain them.¹⁹⁰ Although hundreds of single-crystal X-ray structures of organometallic and coordination compounds of yttrium are known, there are few for which both ⁸⁹Y NMR data and solid state structural data have been reported. Figure 13 contains the geometry-optimized structures and selected bond lengths of the complexes used in this study. In general, the combination of B3PW91/DGDZVP (on Y); 6-311G(d,p) (other atoms) consistently overestimates Y–E bond distances, but not by more than 1.6% (Table 17). The exceptions are neutral oxygen donor ligands, for which the overestimation is larger. The average Y–OH₂ bond length in the [Y(OH₂)₈]³⁺ standard is overestimated by 0.047 Å (2.0%); discrepancies in the average Y–O(thf) distances range up to 4.6% (in Y(CH₂SiMe₃)₃(thf)₃, **14**). Inherent difference between gas-phase (calculated) and condensed phase structures account for some of the error, but it is specifically the distances to neutral ligands that are less accurately modeled. In the case of **14**, for example, the calculated Y–C(alkyl) distances are within 0.007 Å (0.3%) of experiment.

Calculated NMR Chemical Shifts. It is often sufficient to calculate a theoretical shift by subtracting the absolute shielding of a complex from that of a calculated reference. However, if the calculated value of the reference is inaccurate, all the predicted shifts will possess systematic error.¹⁹² For this reason, a scaling method previously developed for ¹³C NMR chemical shifts¹⁹³ was applied to the ⁸⁹Y NMR data. In this procedure, the predicted chemical shifts (δ_{calc}) were determined by plotting experimental ⁸⁹Y chemical shifts (δ_{exp}) for the organometallic complexes against theoretical chemical

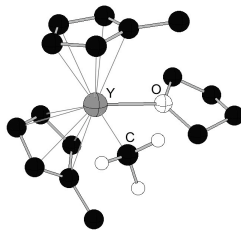
shieldings (σ_{calc}) (Figure 14). The slope (m) and y -intercept (i) of the least-squares correlation line were then used to calculate predicted chemical shifts, as in eq 1.

Table 17. Calculated and experimental (X-ray data) Y–X bond distances (Å). Experimental value for $\text{Y}(\text{C}_5\text{Me}_5)(\text{OPh})_2$ is for the $\text{Y}(\text{C}_5\text{Me}_5)(\text{O}-2,6-(t\text{-Bu})_2\text{C}_6\text{H}_3)_2$ complex.

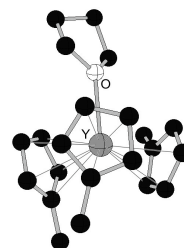
Bond		$[\text{Y}(\text{C}_5\text{H}_4\text{Me})_2(\mu\text{-H})(\text{thf})_2]$ (6) ¹²⁸	$\text{Y}(\text{C}_5\text{Me}_5)(\text{OPh})_2$ (8) ¹³⁰	$\text{Y}(\text{C}_5\text{Me}_5)_2\text{-CH}(\text{SiMe}_3)_2$ (9) ¹⁹¹
Y–C(Cp)	calc.	2.703	2.630	2.711
	expt.	2.69(2)	2.652(3)	2.669(4)
Y–O	calc.	2.550	2.081	
	expt.	2.460(8)	2.059(3), 2.096(4)	
Y–H	calc.	2.131, 2.185		
	expt.	2.18(8)		
Y–C	calc.			2.483
	expt.			2.468(7)
		$\text{Y}[\text{CH}(\text{SiMe}_3)_2]_3$ (10) ¹³⁵	$\text{Y}(\text{CH}_2\text{SiMe}_3)_3(\text{thf})_3$ (14) ¹²⁵	$\text{Y}[\text{N}(\text{SiMe}_3)_2]_3$ ¹³⁶
Y–C	calc.	2.382	2.434 (avg)	
	expt.	2.357(7)	2.427(19)	
Y–O	calc.		2.583 (avg)	
	expt.		2.451(1), 2.457(1), 2.500(1)	
Y–N	calc.			2.237
	expt.			2.223(1)



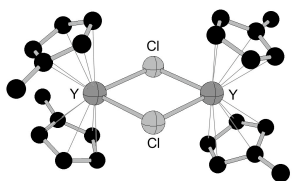
Y(C₅H₄Me)₂Cl(thf) (1)
 Y–C = 2.663 Å (avg)
 Y–Cl = 2.583 Å
 Y–O = 2.436 Å



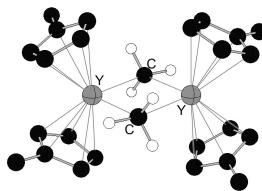
Y(C₅H₄Me)₂(Me)(thf) (2)
 Y–C = 2.685 Å (avg)
 Y–Me = 2.414 Å
 Y–O = 2.437 Å



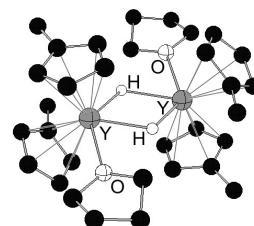
Y(C₅H₄Me)₃(thf) (3)
 Y–C = 2.747 Å (avg)
 Y–O = 2.575 Å



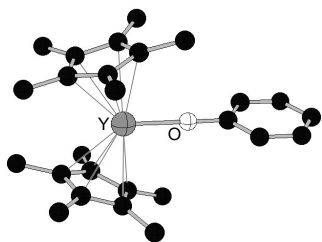
[Y(C₅H₄Me)₂(μ-Cl)]₂ (D₂) (4)
 Y–C = 2.645 Å (avg)
 Y–Cl = 2.734 Å



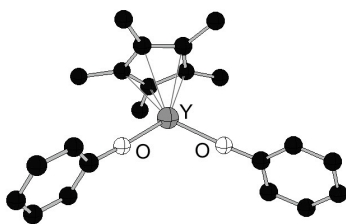
[Y(C₅H₄Me)₂(μ-Me)]₂ (C_i) (5)
 Y–C = 2.678 Å (avg)
 Y–Me = 2.561, 2.562 Å



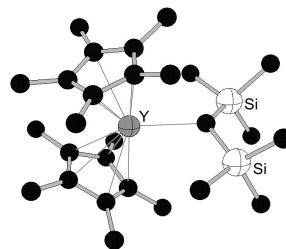
[Y(C₅H₄Me)₂(μ-H)(thf)]₂ (C_i) (6)
 Y–C = 2.703 Å (avg)
 Y–H = 2.131, 2.185 Å
 Y–O = 2.550 Å



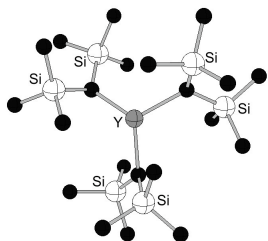
Y(C₅Me₅)₂(OPh) (C_s) (7)
 Y–C = 2.662 Å (avg)
 Y–O = 2.103 Å



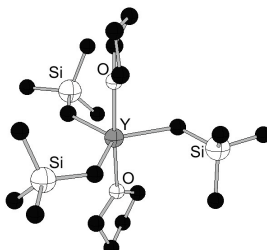
Y(C₅Me₅)(OPh)₂ (C_s) (8)
 Y–C = 2.630 Å (avg)
 Y–O = 2.081 Å



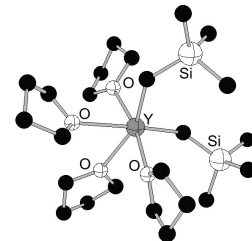
Y(C₅Me₅)₂[CH(SiMe₃)₂] (C_s) (9)
 Y–C(Cp) = 2.711 Å (avg)
 Y–C = 2.483 Å



Y[CH(SiMe₃)₂]₃ (C₃) (10)
 Y–C = 2.382 Å



Y(CH₂SiMe₃)₃(thf)₂ (11)
 Y–C = 2.433 Å (avg)
 Y–O = 2.418 Å (avg)



[Y(CH₂SiMe₃)₂(thf)₄]⁺ (12)
 Y–C = 2.387 Å (avg)
 Y–O = 2.477 Å (avg)

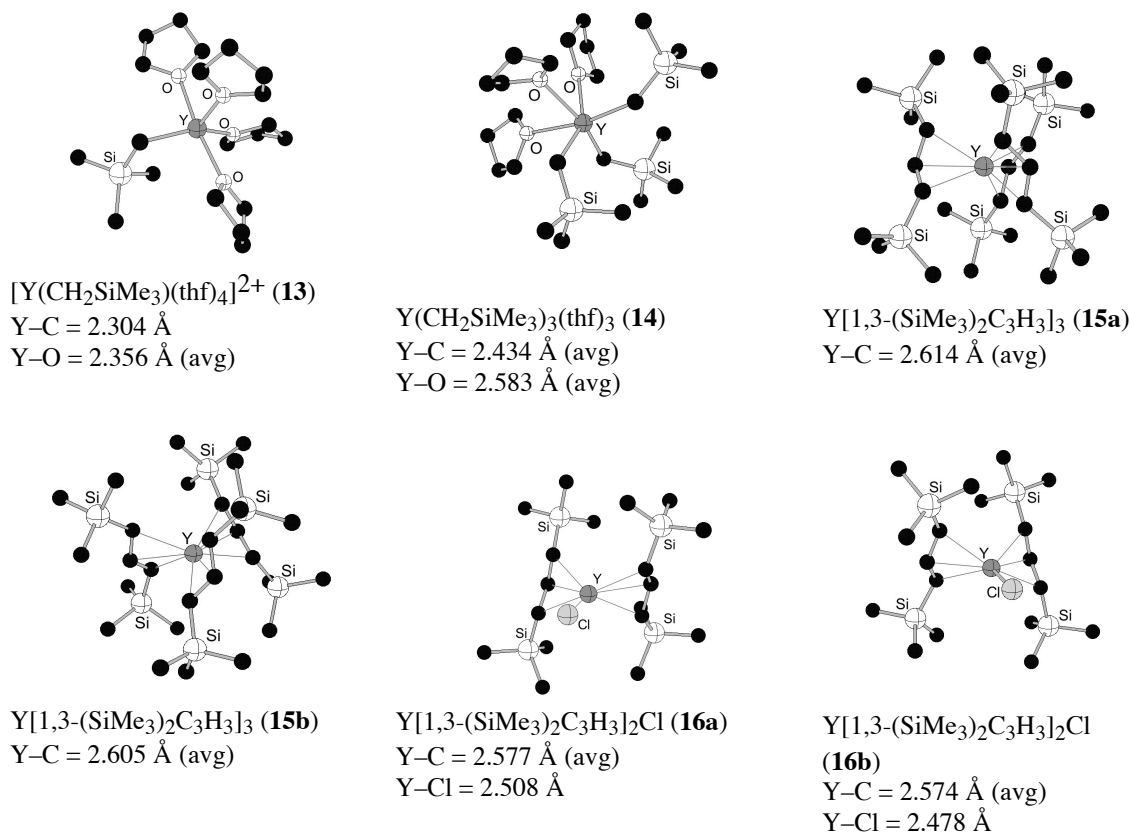


Figure 13. Geometry optimized structures of complexes **1-16** and selected bond lengths. In most cases, hydrogen atoms have been removed for clarity. Symmetry constraints (if any) applied during geometry optimization are listed in parenthesis before the compound's number.

$$\delta_{\text{calc}} = m\sigma_{\text{calc}} + i \quad (1)$$

The values from the geometry-optimized complexes **1-13** were used to calculate the line equation. The linear least squares fit is given in eq 2, from which the δ_{calc} values in Table 18 were derived.

$$\delta_{\text{calc}} = -0.8093\sigma_{\text{calc}} + 2063.6 \quad (r^2 = 0.991) \quad (2)$$

The strong linearity over the large range indicates that the scaled DFT/GIAO combination accounts for most of the contributions to the chemical shift. Nevertheless, the deviation of the gradient from the ideal value of -1.0 indicates that there are still deficiencies in the approach, possibility involving the functionals or basis sets (especially for Y) or both. It should be stressed, however, that the linear relationship between the calculated and experimental chemical shifts means that the error is systematic, and hence the results are still useful for discussing ligands effects on chemical shifts.

Comparisons of calculated and experimental shifts. Experimental and predicted ^{89}Y NMR shifts of the complexes studied are listed in Table 18. For complexes **9** and **10**, the ^{89}Y NMR shift was calculated both from a single point calculation using the crystallographic data and from the geometry optimized structure.

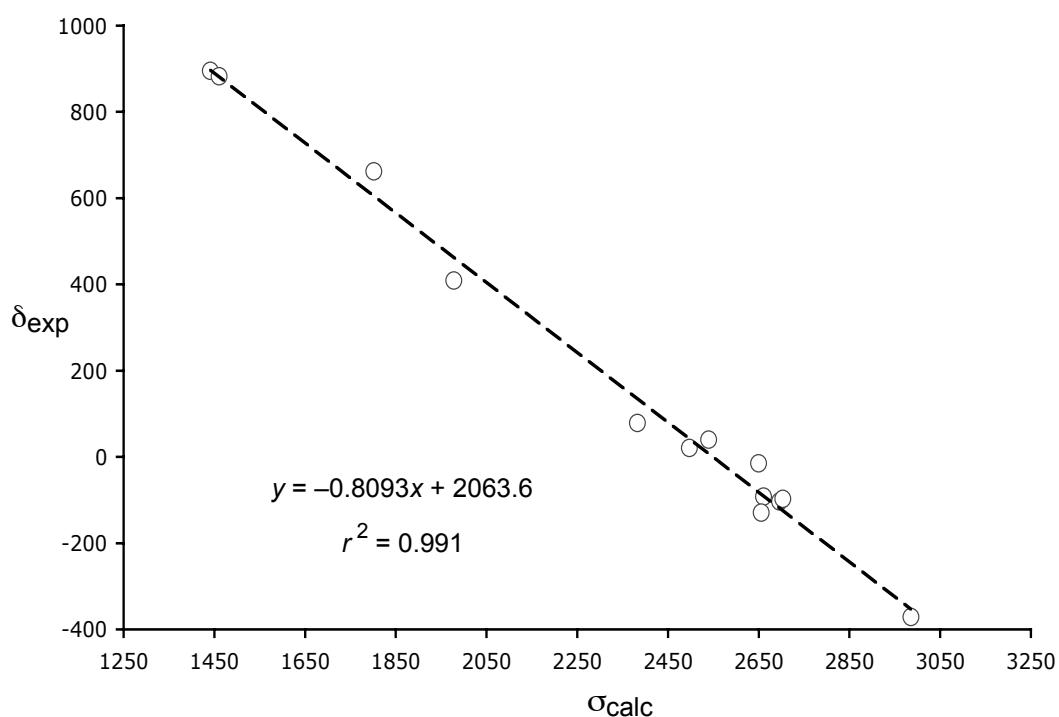


Figure 14. Plot of experimental chemical shifts (δ_{exp}) versus calculated chemical shieldings (σ_{calc}) for geometry optimized organometallic complexes.

(a) *Complexes 1–6*:¹⁸¹ $\text{Y}(\text{C}_5\text{H}_4\text{Me})_2\text{Cl}(\text{thf})$ (**1**), $\text{Y}(\text{C}_5\text{H}_4\text{Me})_2(\text{Me})(\text{thf})$ (**2**), $\text{Y}(\text{C}_5\text{H}_4\text{Me})_3(\text{thf})$ (**3**), $[\text{Y}(\text{C}_5\text{H}_4\text{Me})_2(\mu\text{-Cl})]_2$ (**4**), $[\text{Y}(\text{C}_5\text{H}_4\text{Me})_2(\mu\text{-Me})]_2$ (**5**), $[\text{Y}(\text{C}_5\text{H}_4\text{Me})_2(\mu\text{-H})(\text{thf})]_2$ (**6**). With the exception of **5**, the predicted ^{89}Y NMR shifts for these methylcyclopentadienyl complexes are within 35 ppm of the experimental shifts (Table 18). Compared to the large window of ^{89}Y NMR shifts (ca. 1300 ppm), these values represent errors of less than 3%. The use of THF as a solvent does not appear to affect the calculations in a systematic fashion; both under- and overestimations of the chemical shifts are found for samples measured in THF-*d*₈ (e.g., $\Delta\delta = -31.6$ ppm for **2**, and $\Delta\delta = 18.2$ ppm for **3**). In agreement with trends reported for cyclopentadienyl complexes of other metals, the ^{89}Y resonances for these complexes are shifted upfield compared to the σ -bound complexes.^{155,156} The discrepancy between the observed and calculated values for the dimeric **5** is roughly twice that of the other cyclopentadienyl complexes. A trial calculation on the monomeric $\text{Y}(\text{C}_5\text{H}_4\text{Me})_2\text{Me}$ produced an even larger error, so that partial dissociation in solution is evidently not part of the reason for the difference.

(b) *Complexes 7,8*:¹⁸⁹ $\text{Y}(\text{C}_5\text{Me}_5)_2(\text{OAr})$ (**7**), $\text{Y}(\text{C}_5\text{Me}_5)(\text{OAr})_2$ (**8**). Complexes **7** and **8** both contain bulky substituted cyclopentadienyl (C_5Me_5) and aryloxy (*O*-2,6-*t*- $\text{Bu}_2\text{C}_6\text{H}_3$) ligands. To explore the effect on the predicted ^{89}Y chemical shift of substitution of the cyclopentadienyl and aryloxy rings, the geometry of a simplified version of **7** (i.e., $\text{Y}(\text{C}_5\text{H}_5)_2(\text{OC}_6\text{H}_5)$) was optimized and its ^{89}Y NMR shift was calculated. Given the changes in the model, it is not surprising that the error ($\Delta\delta$) of -161.0 ppm from the fully substituted **7** is larger than that observed with complexes **1–6**.

Table 18. Predicted shielding constants (σ_{calc}) and chemical shifts (δ_{calc}) in ppm.

Complex	σ_{calc}	δ_{calc}	δ_{exp} (solvent)	$\Delta\delta^a$	CN ^b
Y(C ₅ H ₄ Me) ₂ Cl(thf) (1)	2696.1	-118.4	-103 (THF- <i>d</i> ₈) ¹⁸¹	-15.4	8
Y(C ₅ H ₄ Me) ₂ (Me)(thf) (2)	2539.5	8.4	40 (THF- <i>d</i> ₈) ¹⁸¹	-31.6	8
Y(C ₅ H ₄ Me) ₃ (thf) (3)	2985.8	-352.8	-371 (THF- <i>d</i> ₈) ¹⁸¹	18.2	10
[Y(C ₅ H ₄ Me) ₂ (μ -Cl)] ₂ (4)	2702.8	-123.8	-97 (C ₆ D ₅ CD ₃) ¹⁸¹	-26.8	8
[Y(C ₅ H ₄ Me) ₂ (μ -Me)] ₂ (5)	2649.9	-81.0	-15 (C ₆ D ₅ CD ₃) ¹⁸¹	-66.0	8
[Y(C ₅ H ₄ Me) ₂ (μ -H)(thf)] ₂ (6)	2660.4	-89.5	-92 (THF- <i>d</i> ₈) ¹⁸¹	2.5	9
Y(C ₅ Me ₅) ₂ (OPh) (7)	2655.1	-85.2	-129.3 ^c (C ₆ D ₆) ¹³¹	44.1	7
Y(C ₅ Me ₅)(OPh) ₂ (8)	2497.1	42.7	21 ^c (C ₆ D ₆) ¹³¹	21.7	5
Y(C ₅ Me ₅) ₂ CH(SiMe ₃) ₂ (9) ^{191,d}	2382.7	135.3	78.9 (C ₆ D ₆) ¹³¹	56.4	7
Y(C ₅ Me ₅) ₂ CH(SiMe ₃) ₂ (9) ^e	2520.1	24.1	78.9 (C ₆ D ₆) ¹³¹	-54.8	7
Y[CH(SiMe ₃) ₂] ₃ (10) ^{135, d}	1441.4	897.1	895.0 (C ₆ D ₅ CD ₃) ¹³¹	2.1	3
Y[CH(SiMe ₃) ₂] ₃ (10) ^e	1431.6	905.0	895.0 (C ₆ D ₅ CD ₃) ¹³¹	10.0	3
Y(CH ₂ SiMe ₃) ₃ (thf) ₂ (11)	1460.2	881.9	882.7 (THF- <i>d</i> ₈) ¹⁸⁸	-0.8	5
[Y(CH ₂ SiMe ₃) ₂ (thf) ₄] ⁺ (12)	1801.5	605.6	662.2 ^f (THF- <i>d</i> ₈) ¹⁸⁸	-56.6	6
[Y(CH ₂ SiMe ₃)(thf) ₄] ²⁺ (13)	1977.6	463.1	409.2 (THF- <i>d</i> ₈) ¹⁸⁸	53.9	5
Y(CH ₂ SiMe ₃) ₃ (thf) ₃ (14)	1613.6	757.7	882.7 ^g (THF- <i>d</i> ₈) ¹⁸⁸	-125.0	6

^a $\Delta\delta = \delta_{\text{calc}} - \delta_{\text{exp}}$. ^bFormal coordination number. All cyclopentadienyl rings are known or assumed to be η^5 , and assigned a CN of 3. ^cThis value is for OPh = O-2,6-*t*-Bu₂C₆H₃. ^dCalculation with geometry optimized structure. ^eSingle point calculation. ^fThis value was derived from averaging ⁸⁹Y NMR shifts of **12** with various counterions.¹⁸⁸ ^gThis value is for complex **11**, but is listed for **14** for comparison.

The geometry and chemical shift for a model of **7** with an unsubstituted phenoxide ligand and fully methylated cyclopentadienyl ligands (i.e., Y(C₅Me₅)₂(OC₆H₅)) was then

calculated; the predicted chemical shift is -85.2 ppm ($\Delta\delta = 44.1$ ppm), a substantial improvement over the unsubstituted cyclopentadienyl model.

When a similar modification was made for **8**; i.e., using a model with a methylated cyclopentadienyl ligand and an unsubstituted phenoxide ligand ($\text{Y}(\text{C}_5\text{Me}_5)(\text{OC}_6\text{H}_5)_2$), there was relatively good agreement between the predicted and experimental shifts ($\Delta\delta = -21.7$ ppm). The results for **7** and **8** indicate the presence of the methyl groups on the cyclopentadienyl ligand is crucial to accurately predicting of chemical shifts for complexes with methylated cyclopentadienyl groups. However, the absence of the more distant *t*-butyl groups on the phenoxide ligands (three bonds from the yttrium center) does not seem to have detrimental effects on ^{89}Y shift prediction.

(c) *Complexes 9,10*:¹⁸⁹ $\text{Y}(\text{C}_5\text{Me}_5)_2[\text{CH}(\text{SiMe}_3)_2]$ (**9**), $\text{Y}[\text{CH}(\text{SiMe}_3)_2]_3$ (**10**). In the case of complex **9**, the calculated ^{89}Y NMR shift differs by 56.4 ppm from the experimental value. Using the coordinates from the crystal structure, a single point calculation was also performed and resulted in a predicted shift of 24.1 ppm ($\Delta\delta = -54.8$ ppm). It seems neither the geometry optimized or the crystal structure for **9** lead to highly accurate predictions of the experimental chemical shift.

For the trialkyl complex **10**, the ^{89}Y NMR shift of 897.1 ppm for the geometry-optimized structure differs by only 2.1 ppm from the experimental value ($\delta_{\text{exp}} = 895.0$ ppm).¹⁸⁹ The ^{89}Y NMR shift was also calculated directly from the crystal structure coordinates;¹³⁵ the value (905.0 ppm) is only 10.0 ppm from the literature value (Table 18). It is surprising that the predicted chemical shift from the crystal coordinates and the geometry optimized structure of **10** differ by only ~ 8 ppm, while the analogous difference for **9** is ~ 110 ppm. For **9**, the average Y–C bond length to the cyclopentadienyl and alkyl

ligands in the optimized structure were off by 0.042 and 0.015 Å, respectively (Table 17). The Y–C length in **10** was overestimated by 0.025 Å in the optimized structure. As the Y–C bonds to the alkyl ligand are estimated more accurately in **9** than in **10**, the discrepancy in the bond length to the cyclopentadienyl ligand must have a large influence on the chemical shift for **9**. This discrepancy causes the difference in the predicted shifts for the optimized and single point calculations of **9**.

(d) *Complexes 11-14*:^{125,188} $\text{Y}(\text{CH}_2\text{SiMe}_3)_3(\text{thf})_2$ (**11**), $[\text{Y}(\text{CH}_2\text{SiMe}_3)_2(\text{thf})_4]^+$ (**12**), $[\text{Y}(\text{CH}_2\text{SiMe}_3)\text{Y}(\text{thf})_4]^{2+}$ (**13**), $\text{Y}(\text{CH}_2\text{SiMe}_3)_3(\text{thf})_3$ (**14**). The predicted ⁸⁹Y NMR shifts for the alkyl complexes **11–13** differed by up to 60 ppm from the experimental values (Table 18). Of the three complexes, the shift for the neutral complex **11** is the closest to its experimental value ($\Delta\delta$ for **11** = –0.8 ppm). It is certainly possible that discrepancies in the predicted shifts for **12** and **13** are due to the influence of counterions in solution. Such effects are not accounted for in these (gas phase) calculations.

The coordination environment of the neutral **11** is variable; two coordinated THF molecules are observed in solution (¹H NMR),¹⁹⁴ but three THFs are coordinated in the crystal structure.¹²⁵ For this reason, the effect of the addition of the third THF molecule (**14**) on the predicted chemical shift was investigated. The addition of a third THF molecule to the structure of **11** to form **14** moves the calculated shift upfield by approximately 120 ppm, yielding a shift far from the experimental value ($\Delta\delta = 125.0$ ppm). The inaccuracy of this value coupled with the highly accurate prediction for **11** indicates that three coordinated THF molecules are primarily a result of solid-state forces and that only two solvent molecules are closely associated with the yttrium center in solution.

(e) $Y[N(SiMe_3)_2]_3$:¹³⁶ Although not an organometallic complex, the amido complex $Y[N(SiMe_3)_2]_3$ was also studied for comparison purposes. The average Y–N bond length of the geometry optimized structure is only 0.014 Å longer (0.6%) than that of the crystal structure (Table 19),¹³⁶ yet the discrepancy between the predicted and observed¹⁸⁹ chemical shift ($\Delta\delta = -171$ ppm) is large (Table 20). The shift prediction with the single point calculation of the crystal structure is improved over the geometry optimized model, but the value is still inaccurate ($\Delta\delta = -127$ ppm).

(f) $Y(thd)_3$:¹⁹⁵ While most of this work focuses on the prediction of ⁸⁹Y chemical shifts for organometallic complexes, the coordination complex $Y(thd)_3$ (thd = 2,2,6,6-tetramethyl-3,5-heptanedionato) was also studied. As illustrated in Figure 15(a), in the crystal structure of $Y(thd)_3$, the oxygen atoms are arranged around the yttrium center in a trigonal prismatic geometry (Y–O = 2.160(17)–2.298(12) Å).¹⁹⁵ However, when the geometry of the molecule is optimized, the ligands rearrange such that the oxygen atoms are in a pseudo-octahedral conformation around the metal center (Figure 15(b); Y–O = 2.254–2.277 Å). Unlike all of the aforementioned organometallic examples, this is an example of a drastic difference between a molecule's crystal structure and optimized geometry; the pseudo-octahedral conformation most likely reflects the molecule's geometry in solution. Although the Y–O bond lengths of the optimized structure do not differ greatly from the crystal structure (Table 19), its predicted ⁸⁹Y NMR shift ($\delta -8.5$ ppm) is not as accurate as that of a single point calculation ($\delta 84.9$ ppm) of the crystal structure (Table 20).

Table 19. Calculated and experimental (X-ray data) bond distances. All values in Å.

Y[N(SiMe ₃) ₂] ₃ ¹³⁶		Y(thd) ₃ ¹⁹⁵	
Y–N		Y–O	
calc.	2.237	calc.	2.254–2.277
exp.	2.223(1)	exp.	2.160(17)–2.298(12)

Although the geometry optimized models of Y[N(SiMe₃)₂]₃ and Y(thd)₃ both lead to more accurate chemical shift predictions than the single point calculations from the crystal structures, the calculated shifts of both complexes have much higher discrepancy from the experimental values than any of the organometallic complexes. It seems that the ionic bonding in coordination compounds does not lead to the same chemical shift correlation as that of organometallic complexes. Therefore, for accurate shift predictions to be made for non-organometallic compounds, the shielding constants for a series of coordination complexes must be calculated to obtain a proper correlation equation.

Table 20. Predicted shielding constants (σ_{calc}) and chemical shifts (δ_{calc}) in ppm for coordination complexes.

Complex	σ_{calc}	δ_{calc}	δ_{exp} (solvent)	$\Delta\delta^a$	CN ^b
Y[N(SiMe ₃) ₂] ₃ ^c	2057.1	398.8	570 (CDCl ₃) ¹⁵⁷	–171.2	3
Y[N(SiMe ₃) ₂] ₃ ^{136,d}	2003.0	442.6	570 (CDCl ₃) ¹⁵⁷	–127.4	3
Y(thd) ₃ ^c	2560.4	–8.5	168.3 (CDCl ₃) ¹⁵⁷	–176.8	6
Y(thd) ₃ ^{195,d}	2445.0	84.9	168.3 (CDCl ₃) ¹⁵⁷	–83.4	6

^a $\Delta\delta = \delta_{\text{calc}} - \delta_{\text{exp}}$. ^bFormal coordination number. ^cCalculation with geometry optimized structure. ^dSingle point calculation.

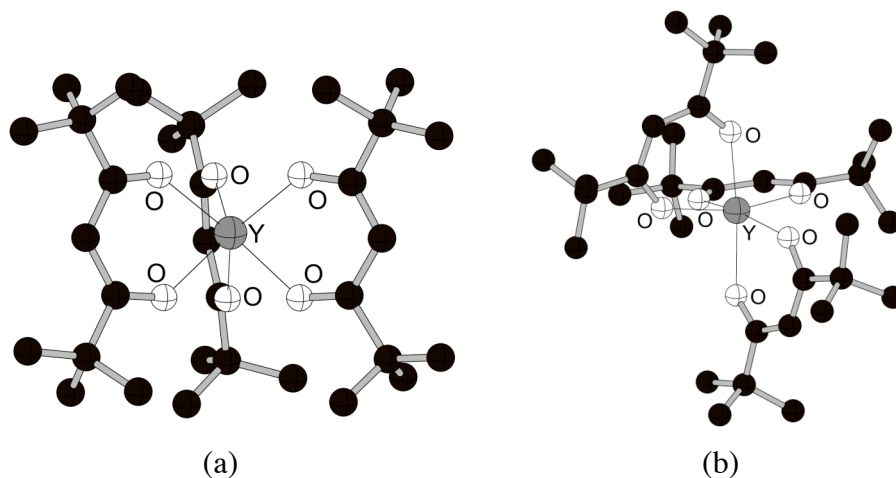
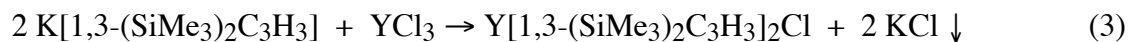


Figure 15. Crystal (a) and geometry optimized (b) structure of $\text{Y}(\text{thd})_3$.

Case Study. Our own interest in ^{89}Y NMR spectroscopy stems from experiments with metal complexes containing bulky allyl ligands, particularly 1,3- $(\text{SiMe}_3)_2\text{C}_3\text{H}_3$.^{12,15,19,23} Unlike cyclopentadienyl ligands, for which it is usually possible to predict the preferred products of reactions involving electropositive metals from the molar ratio of reactants, reactions with bulky allyl ligands do not always give the stoichiometrically expected products.^{12,126} For example, in an attempt to synthesize $\text{La}[1,3-(\text{SiMe}_3)_2\text{C}_3\text{H}_3]_3$, Bochmann and coworkers treated three equivalents of $\text{K}[1,3-(\text{SiMe}_3)_2\text{C}_3\text{H}_3]$ with LaCl_3 .¹²⁶ Instead of obtaining the expected triallyllanthanum product, $\text{La}[1,3-(\text{SiMe}_3)_2\text{C}_3\text{H}_3]_2\text{Cl}(\text{thf})$ was produced, even with excess $\text{K}[1,3-(\text{SiMe}_3)_2\text{C}_3\text{H}_3]$.¹²⁶ Given that four of the bulky allyl ligands can fit around the smaller $\text{Th}(\text{IV})$ ion,²³ steric crowding around the lanthanum center that would prevent the coordination of a third allyl ligand would seem unlikely. An unexpected kinetic stability of the bis(allyl')lanthanum chloride is possibly responsible for its resistance to further substitution.

In an attempt to remake the previously reported¹²⁶ complex $\text{Y}[1,3\text{-(SiMe}_3)_2\text{C}_3\text{H}_3]_2\text{Cl}$, two equivalents of $\text{K}[1,3\text{-(SiMe}_3)_2\text{C}_3\text{H}_3]$ were allowed to react with YCl_3 in THF at $-78\text{ }^\circ\text{C}$ (eq 3):



A hexanes extract of the filtered reaction mixture yielded a yellow oil that crystallized overnight. Elemental analysis (0.17% Cl), X-ray EDS (mass ratio of Y:Cl = 42.1 : 1), or an aqueous AgNO_3 test (a slight haze was observed) all suggested that substantially less than the 7.2% Cl required by $\text{Y}[1,3\text{-(SiMe}_3)_2\text{C}_3\text{H}_3]_2\text{Cl}$ was present.

Variations in the temperature or the order of addition of reagents, as described in the Experimental Section, produced in every case yellow oils that had identical ^1H NMR spectra. When YCl_3 was treated with three equivalents of $\text{K}[1,3\text{-(SiMe}_3)_2\text{C}_3\text{H}_3]$, the yellow oil produced had an ^1H NMR spectrum identical with those from the 1:2 reactions.

Crystals of the product from the reaction with the allyl reagent added to the yttrium chloride at low temperature (eq 3) and that from the reaction following the literature procedure exactly (yttrium chloride added to the allyl reagent at room temperature) were examined with X-ray crystallography. Both had the same unit cell dimensions and space group. Unfortunately, the structure is afflicted by substantial, and not completely resolvable, disorder; the silicon atoms are arranged in a roughly octahedral manner around the yttrium center (Figure 16). The crystallographic data, although not definitive, are consistent with the chloride tests for the formation of $\text{Y}[1,3\text{-(SiMe}_3)_2\text{C}_3\text{H}_3]_3$. The

^{89}Y NMR spectrum of the isolated complex was obtained in toluene- d_8 and contained a single peak at 470.5 ppm.

Geometries of several different bis(trimethylsilyl)-substituted triallylyttrium (**15**) and diallylyttrium chloride (**16**) complexes were first minimized with molecular mechanics, and then optimized with the DFT methods described above. A model for **15** (**15a**) was constructed in which one of the allyl ligands was oriented antiparallel to the other two (Figure 16). This was the arrangement reached when the major peaks in the disorder model of the X-ray structure were used as starting coordinates. It is also the arrangement found in the structure of $\text{Tm}[1,3-(\text{SiMe}_3)_2\text{C}_3\text{H}_3]_3$, which is disordered as well ($R_1 = 0.0335$), but resolvably so (see Chapter I). The predicted ^{89}Y shift was found to be 402.0 ppm ($\Delta\delta = -68.5$ ppm). For comparison, the alternate model **15b** was constructed, in which the allyl ligands point in the same direction around the metal center (approximate C_3 symmetry, although none was imposed). The predicted shift for this conformation was 362.2 ppm, $\Delta\delta = -108.3$ ppm from the experimental value. Based on the X-ray data, we believe it likely that **15a** represents the actual structure more closely than does **15b**, although frequency calculations indicated that both structures are minima on the potential energy surface ($N_{\text{imag}} = 0$) and differ negligibly in total energy (2.2 kcal mol $^{-1}$).

It is possible that **16** could occur in monomeric or dimeric forms. In the latter case, the two yttrium centers would be expected to be within ca. 4.5 Å of each other, based on known $[\text{YCp}'_2(\mu\text{-Cl})]_2$ examples.^{120,121,132} In the only known organoyttrium complex with a single chloride bridge, $(\text{C}_5\text{Me}_5)_2\text{Y}(\mu\text{-Cl})\text{YCl}(\text{C}_5\text{Me}_5)_2$, the metals are separated by 5.35 Å.¹⁹⁶ Despite the disorder in the ligands, the metal centers in the crystal structure (Figure 16) are well located, and have a closest approach of 8.63 Å. A dinuclear structure

for the complex would appear to be ruled out, although it is possible that an extensively disordered chloride might not be recognized. For **16**, calculations with the ligands pointing in eclipsed (**16a**) and staggered (**16b**) conformations around the yttrium center were completed. The predicted ^{89}Y NMR shifts for these complexes are 645.4 ($\Delta\delta = 174.9$ ppm) and 637.2 ppm ($\Delta\delta = 166.7$ ppm), respectively. The discrepancy between either of these values and the experimental shift is larger than that of the predicted shifts for **15a** and **15b**. The NMR results support the formation of the triallylyttrium complex from the experimental work described above, although the agreement between predicted and measured shifts, even in the best case (**15a**), is not as strong as with the cyclopentadienyl complexes.

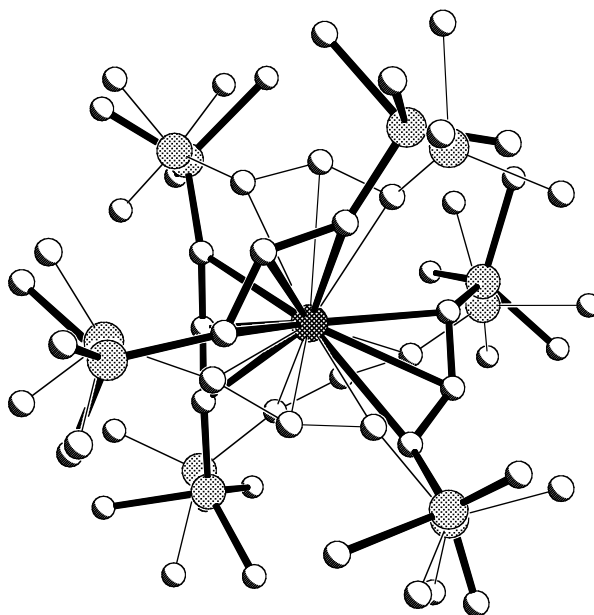


Figure 16. Figure of $\text{Y}[1,3-(\text{SiMe}_3)_2\text{C}_3\text{H}_3]_3$ (**15**), with two disordered parts (bold and non-bold) shown.

Polymerization Studies with 15. Interest in the isolation of **15** arose from its potential as a polymerization catalyst. Unfortunately, attempts at polymerization of

methyl methacrylate with **15** were unsuccessful. As described in Chapter III, the presence of three allyl ligands leads to steric congestion around the metal center that presumably prevents binding of the monomer. The lack of reaction of **15** with PMe_3 further supports the inaccessibility of the metal center.

Complex **15** was also investigated under various conditions as a catalyst for the polymerization of ethylene.¹⁹⁷ The highest activity was observed when an acidic support was used without the use of a co-catalyst or co-monomer. When methylaluminoxane (MAO) was added as a co-catalyst, very low activity and polymer yield were observed; addition of $\text{Al}(i\text{-Bu})_3$ also appears to reduce catalytic activity. In a separate experiment, when **15** was treated with $\text{Al}(i\text{-Bu})_3$, the ^1H NMR spectrum of the product indicated the formation of an $\text{Al}(\text{allyl}')(\textit{i}\text{-Bu})_2$ species, as well as an unidentified yttrium species.¹²⁶ Loss of yellow color in a 1:1 solution of **15** and AlMe_3 in toluene corresponds to a similar result. The reduction in activity of **15** in the presence of alkyl aluminum complexes may be attributed to such interactions, which detrimentally modify the structure of the catalyst. Although **15** was the only complex of this type tested as an ethylene polymerization catalyst, other $\text{Ln}[1,3\text{-}(\text{SiMe}_3)_2\text{C}_3\text{H}_3]_3$ complexes are likely to have similar activity.

Conclusion

Calculation of ^{89}Y NMR shifts with DFT/GIAO methods is feasible for a variety of organometallic molecules. Despite remaining systematic error in the absolute values of the shielding constants, a strongly linear fit between calculated and observed shifts exists across a nearly 1300 ppm range. For most complexes, agreement within ± 70 ppm

between calculated and experimental shifts is found. Agreement between predicted and experimental ^{89}Y NMR shifts supports the identification of $\text{Y}[1,3-(\text{SiMe}_3)_2\text{C}_3\text{H}_3]_3$, the unexpected product of a 2:1 mixture of allyl and yttrium precursors. Characterization of this allyl complex is important, as it is an active ethylene polymerization catalyst and analogous lanthanide complexes may exhibit comparable efficiency.

CHAPTER V

SYNTHETIC, STRUCTURAL, AND COMPUTATIONAL STUDIES OF BULKY ALLYL COMPLEXES OF VANADIUM

Introduction

In 1966, Wilke et al. summarized the work to date on homoleptic π -allyl complexes of the first row transition metals; most of these complexes were thermally unstable, despite sometimes favorable formal electron counts.² For example, under an inert atmosphere, triallylcobalt (an 18 electron species) decomposes above -40 °C, and triallylvanadium ($14 e^-$) deflagrates at temperatures above -30 °C. Because of such thermal instability, homoleptic allyl complexes of some first row metals (e.g., manganese) have yet to be isolated, even four decades after Wilke's report.

Nonetheless, in recent years, the synthesis of thermally stable allyl complexes has been achieved by placing bulky substituents on the allyl ligand. Using this approach, the first bis(π -allyl)iron(II) complex, $\text{Fe}[1,3-(\text{SiMe}_3)_2\text{C}_3\text{H}_3]_2$, was isolated and crystallographically characterized in 2001; it is indefinitely stable at room temperature under an inert atmosphere.¹³ In the same paper, the first monomeric bis(π -allyl)chromium(II) complex, $\text{Cr}[1,3-(\text{SiMe}_3)_2\text{C}_3\text{H}_3]_2$, was reported; the unsubstituted allyl chromium(II) analog exists as a dimer.⁷⁰ Other isostructural first row complexes that are now known include $\text{Co}[1,3-(\text{SiMe}_3)_2\text{C}_3\text{H}_3]_2$ and $\text{Ni}[1,3-(\text{SiMe}_3)_2\text{C}_3\text{H}_3]_2$.^{12,14}

Using the bis(1,3-trimethylsilyl)allyl ligand, the synthesis of thermally stable vanadium allyl complexes was attempted. In doing this, a novel vanadium(II) dimeric

species with three bridging allyl ligands and a terminal chloride was isolated and crystallographically characterized. Density functional theory calculations were used to explore the structure of this complex.

Experimental

General Considerations. All operations were performed in an atmosphere of nitrogen using standard glovebox or Schlenk techniques. ^1H NMR spectra were collected on a Bruker NMR spectrometer at 300 MHz.

Materials. $\text{K}[1,3-(\text{SiMe}_3)_2\text{C}_3\text{H}_3]$ was prepared as previously reported.¹⁹ $\text{VCl}_3(\text{thf})_3$ was prepared by refluxing anhydrous VCl_3 (Strem) in THF overnight. Removal of solvent under vacuum resulted in $\text{VCl}_3(\text{thf})_3$ as a red powder in quantitative yield. Carbon monoxide (CP grade) was purchased in a pressurized cylinder from A-L Compressed Gases and passed through a drying column (anhydrous CaSO_4) prior to use. Hexanes were distilled under nitrogen from potassium benzophenone ketyl.⁴² Anhydrous tetrahydrofuran (THF) was purchased from Aldrich and used as received. C_6D_6 was vacuum distilled from Na/K (22/78) alloy and stored over Type 4A molecular sieves. All other reagents were obtained from commercial sources and used as received.

Synthesis of $\text{V}_2[\mu\text{-}\{1,3-(\text{SiMe}_3)_2\text{C}_3\text{H}_3\}]_3\text{Cl}$. $\text{VCl}_3(\text{thf})_3$ (1.823 g, 4.88 mmol) was added to a 250 mL Erlenmeyer flask with 100 mL of THF and a stirring bar. Excess aluminum powder (0.157 g, 5.82 mmol) and KH (0.078 g, 1.94 mmol) were added, resulting in a red solution. After stirring overnight, the reaction mixture turned green-blue, indicating the presence of the $[\text{V}_2\text{Cl}_3(\text{thf})_6]^+$ cation.¹⁹⁸ The cation solution was filtered through a medium-porosity frit to remove excess Al and KH. An addition funnel

with $\text{K}[1,3-(\text{SiMe}_3)_2\text{C}_3\text{H}_3]$ (2.163 g, 9.64 mmol) and THF (50 mL) was prepared. After assembly in the glovebox, the apparatus was placed on a Schlenk line. The $\text{K}[1,3-(\text{SiMe}_3)_2\text{C}_3\text{H}_3]$ solution was added dropwise at $-78\text{ }^\circ\text{C}$ with stirring over 30 min. After allowing the reaction mixture to warm to room temperature overnight, the resulting dark brown solution was evaporated to dryness. The residue was extracted in hexanes and filtered. Removal of solvent yielded a dark oil that appeared red when transilluminated (0.34 g). X-ray quality crystals formed throughout the oil overnight.

Attempted synthesis of $\text{V}[1,3-(\text{SiMe}_3)_2\text{C}_3\text{H}_3]_3$. A 125 mL Schlenk flask was charged with anhydrous $\text{VCl}_3(\text{thf})_3$ (0.139 g, 0.372 mmol), THF (40 mL), and a stirring bar. An addition funnel was prepared with $\text{K}[1,3-(\text{SiMe}_3)\text{C}_3\text{H}_3]$ (0.269 g, 1.199 mmol) in THF (40 mL). After assembly in the glovebox, the apparatus was placed on a Schlenk line. The $\text{K}[1,3-(\text{SiMe}_3)_2\text{C}_3\text{H}_3]$ solution was added dropwise at $-78\text{ }^\circ\text{C}$ with stirring over 30 min. After warming to room temperature overnight, the reaction mixture was evaporated to dryness, then extracted with hexanes. The extract was filtered, and removal of hexanes under vacuum yielded a red-brown oil (0.16 g, 71%).

Attempted synthesis of $\text{V}[1,3-(\text{SiMe}_3)_2\text{C}_3\text{H}_3]_3$. Synthesis of $1,3,4,6-(\text{SiMe}_3)_4\text{C}_6\text{H}_6$. Due to the light sensitivity of VBr_3 , caution was taken to ensure the exclusion of light during this reaction. An aluminum foil-covered 125 mL Schlenk flask was charged with anhydrous VBr_3 (0.450 g, 1.55 mmol), THF (40 mL), and a stirring bar. An addition funnel was prepared with $\text{K}[1,3-(\text{SiMe}_3)\text{C}_3\text{H}_3]$ (1.046 g, 4.66 mmol) in THF (40 mL). After assembly in the glovebox, the apparatus was placed on a Schlenk line. The $\text{K}[1,3-(\text{SiMe}_3)_2\text{C}_3\text{H}_3]$ solution was added dropwise at $-78\text{ }^\circ\text{C}$ with stirring over 30 min. After warming to room temperature overnight, the reaction mixture was

evaporated to dryness, then extracted with hexanes. The extract was filtered, and removal of hexanes under vacuum yielded a red-brown oil. ^1H NMR spectroscopy indicates that the ligand had dimerized to form $[(\text{SiMe}_3)_2\text{C}_3\text{H}_3]_2$.¹² ^1H NMR (25 °C, 300 MHz, C_6D_6): δ 0.088 (s, 18H, outer SiMe_3); 0.149 (s, 18H, inner SiMe_3); 2.02 (m, 2H, $\text{C}(3)\text{HC}(4)\text{H}$); 5.48 (d, $J = 18.6$ Hz, 1H, $\text{C}(1)\text{H}$); 5.61 (d, $J = 18.3$ Hz, 1H, $\text{C}(6)\text{H}$); 5.92 (ddd, $J_1 = 18.6$ Hz, $J_2 = 6.9$ Hz, $J_3 = 2.8$ Hz, 1H, $\text{C}(5)\text{H}$); 6.39 (dd, $J_1 = 18.3$ Hz, $J_2 = 9.95$ Hz, 1H, $\text{C}(2)\text{H}$).

General Procedures for X-ray Crystallography. Data collection and structure solution were conducted at the X-Ray Crystallographic Laboratory at the University of Minnesota. All calculations were performed using the current SHELXTL⁴³ suite of programs. A suitable crystal was located and attached to the tip of a glass capillary and mounted on a CCD area detector diffractometer for data collection at 173(2) K. A preliminary set of cell constants was calculated from reflections harvested from three sets of 20 frames. These initial sets of frames were oriented such that orthogonal wedges of reciprocal space were surveyed. Data collection of a randomly oriented region of reciprocal space was carried out using $\text{MoK}\alpha$ radiation (graphite monochromator). The intensity data were corrected for absorption with SADABS.⁴⁵ Final cell constants were calculated from strong reflections from the actual data collection after integration (SAINT).¹⁷⁰ Relevant crystal and collection data parameters for $\text{V}_2[\mu\text{-}\{1,3\text{-}(\text{SiMe}_3)_2\text{C}_3\text{H}_3\}\}_3\text{Cl}$ can be found in Tables 36 and 37.

Computational Details. Geometry optimization calculations were performed using the GAUSSIAN 03W suite of programs.⁶⁸ The B3PW91 functional, which incorporates Becke's three-parameter exchange functional¹⁷¹ with the 1991 gradient-corrected

correlation functional of Perdew and Wang,¹⁷² was used; this hybrid functional has previously been shown to provide realistic geometries for organometallic species.^{173,174} The DFT-optimized double zeta polarized basis set DGDZVP2 of Godbout¹⁹⁹ was used for geometry optimizations. Stationary points were characterized by the calculation of vibrational frequencies, and all geometries were found to be minima ($N_{\text{imag}} = 0$). Atomic coordinates for calculated structures can be found in Tables 45–47.

Results and Discussion

Synthesis and Structural Characterization of $\text{V}_2[\mu\text{-}\{1,3\text{-(SiMe}_3\text{)}_2\text{C}_3\text{H}_3\}]_3\text{Cl}$. In an attempt to synthesize the divalent complex $\text{V}[1,3\text{-(SiMe}_3\text{)}_2\text{C}_3\text{H}_3]_2$, the V(II) cation $[\text{V}_2\text{Cl}_3(\text{thf})_6]^+$ was synthesized by reduction of $\text{VCl}_3(\text{thf})_3$ in THF with excess aluminum powder and a catalytic amount of potassium hydride.¹⁹⁸ After filtering the solution to remove excess aluminum and potassium hydride, the reaction mixture was treated in situ with two equivalents of $\text{K}[1,3\text{-(SiMe}_3\text{)}_2\text{C}_3\text{H}_3]$ in THF at $-78\text{ }^\circ\text{C}$. The solution immediately turned dark red-brown and was allowed to stir overnight with warming to room temperature. Removal of THF under reduced pressure, followed by dissolution in hexanes, filtration, and evaporation of hexanes under vacuum, yielded a dark red-brown oil. X-ray quality crystals grew in the oil at room temperature overnight.

Two types of crystals were present in the oil; one is of a complex with two vanadium centers bridged by three allyl ligands (Figure 17). Although crystallographic data indicates a chloride atom is bound to one of the metal centers, which balances the charge for an overall neutral complex, only 73% of the electron density is detected. When the chloride is not present, the disordered trimethylsilyl group containing $\text{Si}4/\text{Si}4'$ shifts to

partially occupy the space of the chloride vacancy. Selected bond distances for $V_2[\mu\text{-}\{1,3\text{-(SiMe}_3)_2\text{C}_3\text{H}_3\}\}_3\text{Cl}$ are listed in Table 21. The V–V bond distance of 2.4312(15) Å is indicative of a double bond between the vanadium atoms (cf., bond order of 2 in $V_2Cp_2(\mu\text{-H})_2(\mu\text{-}\eta^4,\eta^4\text{-C}_6\text{H}_6)$: V–V = 2.425(1) Å;²⁰⁰ $V_2Cp_2(\mu\text{-CO})_2(\text{CO})_3$: V–V = 2.462(2) Å).²⁰¹

The second type of crystal in the oil formed from the co-crystallization of dinuclear species. Although the crystal structure was not well defined, X-ray data indicates that there are two molecules in the asymmetric unit. Both have structures that are almost identical to that in the other crystal. However, one molecule has electron density to account for 15% of a chloride atom, and the other molecule is chloride-free. Assuming that the chloride-free complex is neutral (as no counterion is detected in the crystal structure), one V(I) and one V(II) center would have to be present. Using a variety of vanadium precursors, numerous attempts to reproduce the chloride-free divanadium species were made, but none were successful.

Treatment of the $[V_2Cl_3(\text{thf})_6]^+$ cation with various Group I cyclopentadienyl or pentadienyl precursors typically yields monomeric vanadocene or open vanadocene derivatives.^{198,202,203} For example, when $[V_2Cl_3(\text{thf})_6][Zn_2Cl_6]$ is treated with two equivalents of NaCp, bis(cyclopentadienyl)vanadium is isolated.²⁰² Unlike cyclopentadienyl ligands, however, the allyl anion has the ability to bridge the vanadium centers, leading to the divanadium product $V_2[\mu\text{-}\{1,3\text{-(SiMe}_3)_2\text{C}_3\text{H}_3\}\}_3\text{Cl}$. Analogous bridging occurs in the Cr(II) dimers $Cr(\text{C}_3\text{H}_5)_2$ and $Cr[1\text{-(SiMe}_3)\text{C}_3\text{H}_4]_2$, where each chromium atom is π -bound to a terminal allyl ligand and two allyl ligands bridge the

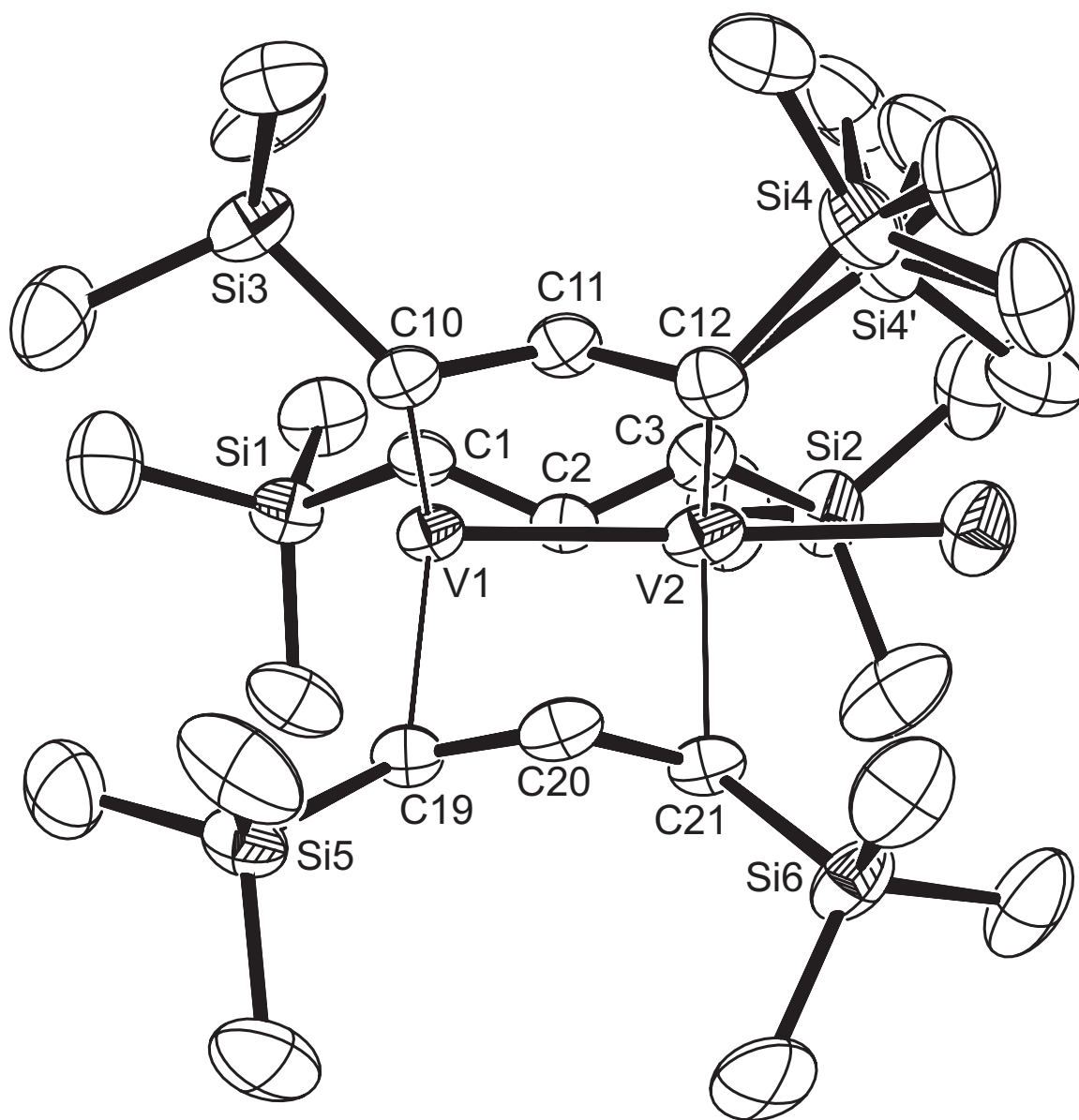


Figure 17. ORTEP of $V_2[\mu\{-1,3-(SiMe_3)_2C_3H_3\}]_3Cl$, with thermal ellipsoids at the 50% level. Hydrogen atoms have been omitted for clarity. Resolvable disorder was found for one trimethylsilyl group (containing Si4/Si4').

Table 21. Selected bond distances (Å) for $V_2[\mu\text{-}\{1,3\text{-(SiMe}_3)_2\text{C}_3\text{H}_3\}\}_3\text{Cl}$.

Atoms	Distance	Atoms	Distance
V1–V2	2.4312(15)	V2–Cl1	2.435(3)
V1–C1	2.018(5)	V2–C3	2.086(6)
V1–C10	2.012(6)	V2–C12	2.084(6)
V1–C19	2.019(6)	V2–C21	2.068(5)
V1–C2	2.254(5)	V2–C2	2.306(6)
V1–C11	2.263(6)	V2–C11	2.290(6)
V1–C20	2.266(5)	V2–C20	2.305(6)

chromium centers.^{15,70} Interestingly, $\text{Cr}[1,3\text{-(SiMe}_3)_2\text{C}_3\text{H}_3]_2$ and $\text{Cr}[1,1',3\text{-(SiMe}_3)_3\text{C}_3\text{H}_2]_2$ both exist as monomers, as dimerization is prevented by the additional trimethylsilyl groups.¹⁵ Although the 12 electron bis(1,3-trimethylsilyl)allyl chromium monomer is a thermally stable complex, the analogous 11 electron vanadium monomer appears to be an unfavorable product and the synthesis of the bimetallic complex occurs under these reaction conditions.

In separate experiments, hexanes solutions of $V_2[\mu\text{-}\{1,3\text{-(SiMe}_3)_2\text{C}_3\text{H}_3\}\}_3\text{Cl}$ were treated with CO and *t*-BuNC; no color change from red-brown was observed in either case. In contrast, analogous reactions with $V(\text{C}_5\text{Me}_5)_2$ lead to immediate color changes; the treatment of $V(\text{C}_5\text{Me}_5)_2$ (red) with CO forms $V(\text{C}_5\text{Me}_5)_2(\text{CO})$ (maroon) and with *t*-BuNC forms $V(\text{C}_5\text{Me}_5)_2(\text{CN})(t\text{-BuNC})$ (black).²⁰⁴ The lack of such color change for $V_2[\mu\text{-}\{1,3\text{-(SiMe}_3)_2\text{C}_3\text{H}_3\}\}_3\text{Cl}$ (i.e., its inability to bind either molecule) reflects the stability of the complex and the steric congestion around the metal centers.

Synthesis of Vanadium(III) Allyl Complexes. In addition to work with divalent vanadium species, attempts were made to synthesize trivalent vanadium allyl complexes. Treatment of VBr_3 with three equivalents of $K[1,3-(SiMe_3)_2C_3H_3]$ in THF at $-78\text{ }^\circ\text{C}$ results in the reduction of the metal and coupling of the allyl ligand to form tetrakis(1,3,4,6-trimethylsilyl)-1,5-hexadiene. This dimerization is also observed in efforts to synthesize allyl complexes using halides of other early transition metals (e.g., Ti(IV), Nb(V), Ta(V)) and similar redox active metals (e.g., Co, Ni).^{12,80} As reported for nickel allyl complexes, ligand dimerization may be the result of surface chemistry on rather insoluble metal starting materials.^{12,205}

To avoid ligand dimerization, the use of alternative V(III) starting material was also investigated. Treatment of $VCl_3(thf)_3$ with three equivalents of $K[1,3-(SiMe_3)_2C_3H_3]$ under the same reaction conditions yields a dark red-brown oil, which is presumably $V[1,3-(SiMe_3)_2C_3H_3]_3$. X-ray quality crystals were not obtained, and the paramagnetism of the compound prevents NMR characterization of the complex. No color change is observed upon treatment of a hexanes solution of the product with CO or *t*-BuNC. As described above, binding of either molecule is likely to involve a change of color from red-brown. The lack of such color change in this work indicates that binding of an additional molecule is prevented by steric congestion around the vanadium center.

Computational Analysis of $V_2[\mu-\{1,3-(SiMe_3)_2C_3H_3\}]_3Cl$. Density functional theory calculations were used to explore the structure of $V_2[\mu-\{1,3-(SiMe_3)_2C_3H_3\}]_3Cl$, including the influence of the trimethylsilyl groups on the bonding. For each calculation, the atomic coordinates from the crystal structure were used as a starting point for geometry optimization. In one study, the trimethylsilyl groups were replaced with

hydrogen atoms prior to optimization. A major difference between the observed and calculated structures is that, in the latter, an allyl ligand has shifted away from the chloride-bound vanadium center to be η^3 -bound to the chloride-free vanadium atom (see Figure 18(a)). The two other allyl ligands bridge the vanadium atoms with similar bond lengths to those in the crystal structure. Optimization also led to a shortening of the V–Cl bond length by 0.17 Å, as well as a decrease in the V–V–Cl angle by approximately 27°, compared to the crystal structure (Table 22). In contrast, the V–V bond length is slightly (~0.06 Å) longer than that in the crystal structure.

Using the same method, a second study was performed where the trimethylsilyl groups were replaced with silyl groups. In this case as well, one of the allyl ligands has shifted towards the chloride-free vanadium atom, but remains slightly closer to the other vanadium atom than for the unsubstituted derivative (see Figure 18(b)). The other two allyl ligands bridge the vanadium atoms with similar V–C bond distances as in the crystal structure. Like the calculation with unsubstituted allyl ligands, the V–Cl distance and V–V–Cl angle have decreased relative to the crystal data (Table 22), and the V–V is slightly longer than the analogous bond in the crystal structure.

In a third calculation, the geometry of $V_2[\mu-\{1,3-(SiMe_3)_2C_3H_3\}]_3Cl$ was optimized (Figure 18(c)). In this case, the V–V and V–Cl distances are significantly closer to the analogous values for the crystal structure (Table 22). The V–V–Cl angle is still ~18° smaller than the ~177° angle in the crystal structure, but has increased by ~8° from the angle in the initial models of the complex. Unlike the first two models, all three allyl ligands in this model bridge the vanadium centers with V–C bond distances similar to those of the crystal structure. Through this series of calculations, it is obvious that

presence of the methyl groups on the trimethylsilyl moieties are instrumental in maintaining the near-linearity of the V–V–Cl angle and the bridging of all three allyl ligands. Thus, the trimethylsilyl groups may account for the structural differences between vanadium complexes with unsubstituted allyl and bis(1,3-trimethylsilyl)allyl ligands.

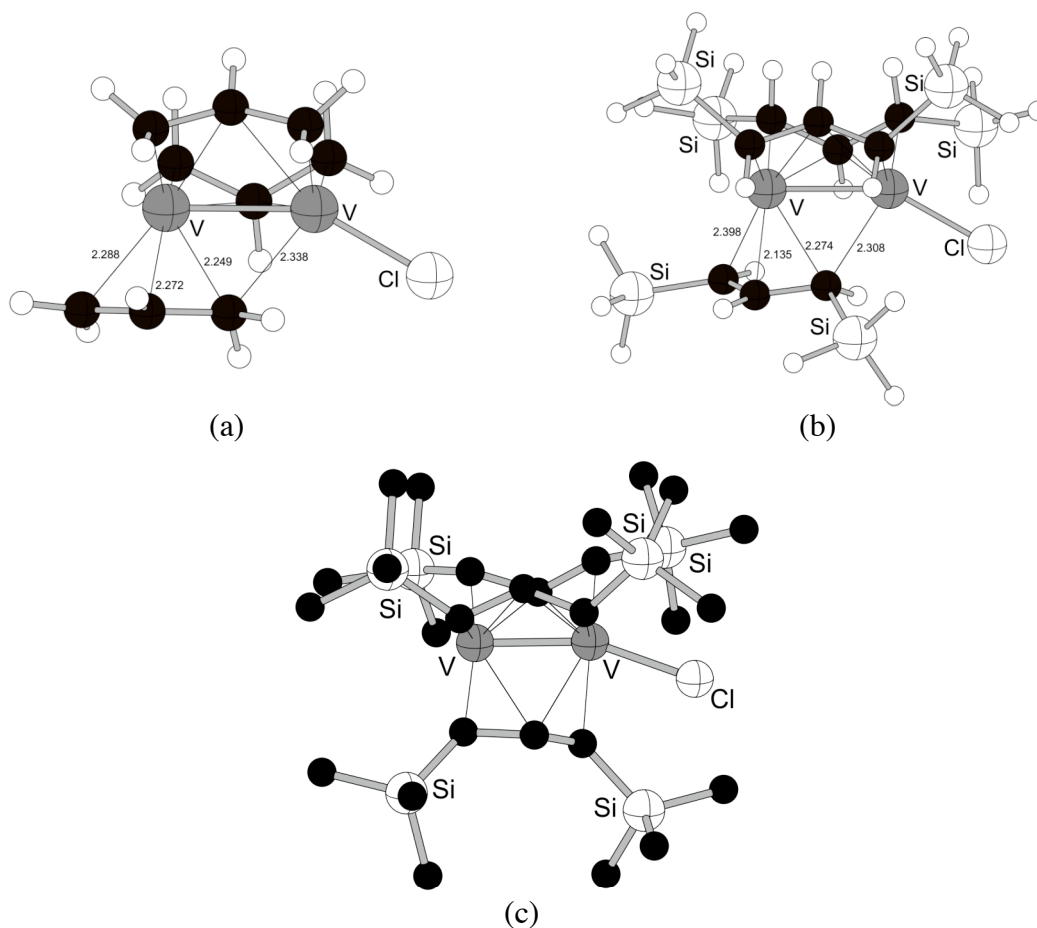


Figure 18. Geometry optimized structures of $V_2[\mu-(C_3H_5)]_3Cl$ (a), $V_2[\mu-\{1,3-(SiH_3)_2C_3H_3\}]_3Cl$ (b), and $V_2[\mu-\{1,3-(SiMe_3)_2C_3H_3\}]_3Cl$ (Hydrogen atoms have been omitted for clarity) (c).

Table 22. Bond distances (Å) and angles (°) from crystal and calculated structures of $V_2[\mu\text{-}\{1,3\text{-}(X)_2C_3H_3\}]_3Cl$, where X = H, SiH₃, SiMe₃.

X	V–V	V–Cl	V–V–Cl
SiMe ₃ (crystal)	2.4312(15)	2.433(3)	177.33(8)
H	2.496	2.261	150.5
SiH ₃	2.448	2.271	151.3
SiMe ₃	2.421	2.310	159.2

Conclusion

The use of the bis(1,3-trimethylsilyl)allyl ligand has led to the isolation of a novel divanadium complex $V_2[\mu\text{-}\{1,3\text{-}(SiMe_3)_2C_3H_3\}]_3Cl$. This result differs from the allyl chemistry of chromium(II), where the steric bulk of the trimethylsilyl groups prevents dimerization. Density functional theory calculations were performed to explore the structure of the vanadium complex; in reference to the experimental geometry, it seems that the methyl groups of the trimethylsilyl moiety are important in preserving the almost linear V–V–Cl angle and in maintaining the bridging position of all three allyl ligands.

Appendix A

CRYSTAL DATA, ATOMIC FRACTIONAL COORDINATES, AND ISOTROPIC
THERMAL PARAMETERS FOR X-RAY STRUCTURAL DETERMINATIONS

Table 23. Crystal data and structure refinement for Tm[1,3-(SiMe₃)₂C₃H₃]₃.

Empirical formula	C ₂₇ H ₆₃ Si ₆ Tm	
Formula weight	725.24	
Temperature	173(2) K	
Wavelength	0.71073 Å	
Crystal system	Hexagonal	
Space group	<i>R</i> -3	
Unit cell dimensions	<i>a</i> = 10.8486(5) Å	$\alpha = 90^\circ$
	<i>b</i> = 10.8486(5) Å	$\beta = 90^\circ$
	<i>c</i> = 30.357(3) Å	$\gamma = 120^\circ$
Volume	3094.1(4) Å ³	
<i>Z</i>	3	
Density (calculated)	1.168 Mg/m ³	
Absorption coefficient	2.338 mm ⁻¹	
<i>F</i> (000)	1134	
Crystal color, morphology	Orange, block	
Crystal size	0.25 × 0.20 × 0.15 mm ³	
Theta range for data collection	2.01 to 25.04°	
Index ranges	-12 ≤ <i>h</i> ≤ 12, -12 ≤ <i>k</i> ≤ 12, -36 ≤ <i>l</i> ≤ 30	
Reflections collected	5724	
Independent reflections	1220 [<i>R</i> (int) = 0.0197]	
Observed reflections	1219	
Completeness to theta = 25.04°	99.8%	
Absorption correction	Multi-scan	
Max. and min. transmission	0.7206 and 0.5926	
Refinement method	Full-matrix least-squares on <i>F</i> ²	
Data / restraints / parameters	1220 / 366 / 139	
Goodness-of-fit on <i>F</i> ²	1.044	
Final <i>R</i> indices [<i>I</i> > 2σ(<i>I</i>)]	<i>R</i> 1 = 0.0335, <i>wR</i> 2 = 0.0888	
<i>R</i> indices (all data)	<i>R</i> 1 = 0.0335, <i>wR</i> 2 = 0.0889	
Largest diff. peak and hole	0.529 and -0.301 e Å ⁻³	

Table 24. Atomic coordinates ($\times 10^4$) and equivalent isotropic displacement parameters ($\text{\AA}^2 \times 10^3$) for $\text{Tm}[1,3-(\text{SiMe}_3)_2\text{C}_3\text{H}_3]_3$. U_{eq} is defined as one third of the trace of the orthogonalized U_{ij} tensor.

atom	x	y	z	U_{eq}
Tm1	0	0	0	66(1)
C4	-4896(16)	-4210(40)	681(13)	119(5)
C5	-2680(50)	-1810(40)	1238(10)	155(9)
C6	-2230(40)	-4240(40)	957(14)	126(5)
Si1	-2948(13)	-3075(18)	782(4)	72(1)
C1	-1800(30)	-2040(20)	333(8)	76(2)
C2	-1610(20)	-2708(12)	-10(8)	87(5)
C3	-1210(30)	-2250(30)	-463(7)	76(2)
Si2	-494(11)	-3045(13)	-875(3)	72(1)
C7	-2030(30)	-4720(20)	-1085(11)	119(5)
C8	390(30)	-1830(30)	-1350(8)	155(9)
C9	800(30)	-3480(40)	-615(10)	126(5)
C13	-4280(30)	-1707(16)	-765(12)	119(5)
C14	-4180(30)	890(30)	-361(10)	155(9)
C15	-2700(30)	1140(40)	-1228(6)	126(5)
Si3	-3145(10)	248(13)	-679(4)	72(1)
C10	-1430(20)	930(30)	-413(8)	76(2)
C11	-1270(30)	1450(20)	-3(8)	87(5)
C12	-20(20)	2270(40)	270(10)	76(2)
Si4	-5(13)	2862(16)	855(4)	72(1)
C16	1080(30)	4842(18)	861(14)	119(5)
C17	800(40)	2140(40)	1245(10)	155(9)
C18	-1840(20)	2330(40)	1047(11)	126(5)
C22	5209(14)	4190(40)	-704(13)	119(5)
C23	2840(40)	1590(30)	-1149(10)	155(9)
C24	2450(40)	4100(40)	-940(13)	126(5)
Si5	3241(10)	3021(15)	-740(4)	72(1)
C19	2250(30)	2180(40)	-245(9)	76(2)
C20	2716(12)	1520(20)	24(9)	87(5)
C21	2230(20)	920(30)	461(7)	76(2)
Si6	2999(15)	30(20)	811(4)	72(1)
C25	3120(30)	-1310(30)	459(12)	119(5)
C26	1860(30)	-890(40)	1297(9)	155(9)
C27	4820(20)	1340(30)	1007(10)	126(5)

Table 25. Crystal data and structure refinement for [Ho{1,3-(SiMe₃)₂C₃H₃}{μ-(1-(SiMe₃)-3-(SiMe₂CH₂)C₃H₃)}]2.

Empirical formula	C ₃₆ H ₈₂ Ho ₂ Si ₈	
Formula weight	1069.60	
Temperature	173(2) K	
Wavelength	0.71069 Å	
Crystal system	Triclinic	
Space group	<i>P</i> -1	
Unit cell dimensions	<i>a</i> = 11.537(5) Å	α = 84.786(5)°
	<i>b</i> = 12.043(5) Å	β = 75.757(5)°
	<i>c</i> = 20.903(5) Å	γ = 69.666(5)°
Volume	2639.5(17) Å ³	
<i>Z</i>	2	
Density (calculated)	1.346 Mg/m ³	
Absorption coefficient	3.178 mm ⁻¹	
<i>F</i> (000)	1088	
Crystal color, morphology	Yellow, block	
Crystal size	0.40 × 0.30 × 0.20 mm ³	
Theta range for data collection	1.00 to 27.50°	
Index ranges	-14 ≤ <i>h</i> ≤ 14, -15 ≤ <i>k</i> ≤ 15, -27 ≤ <i>l</i> ≤ 27	
Reflections collected	31764	
Independent reflections	12002 [<i>R</i> (int) = 0.0333]	
Observed reflections	9613	
Completeness to theta = 27.50°	99.1%	
Absorption correction	Multi-scan	
Max. and min. transmission	0.5292 and 0.3375	
Refinement method	Full-matrix least-squares on <i>F</i> ²	
Data / restraints / parameters	12002 / 14 / 481	
Goodness-of-fit on <i>F</i> ²	1.019	
Final <i>R</i> indices [<i>I</i> > 2σ(<i>I</i>)]	<i>R</i> 1 = 0.0302, <i>wR</i> 2 = 0.0747	
<i>R</i> indices (all data)	<i>R</i> 1 = 0.0439, <i>wR</i> 2 = 0.0819	
Largest diff. peak and hole	1.54 and -0.56 e Å ⁻³	

Table 26. Atomic coordinates ($\times 10^4$) and equivalent isotropic displacement parameters ($\text{\AA}^2 \times 10^3$) for $[\text{Ho}\{1,3\text{-(SiMe}_3)_2\text{C}_3\text{H}_3\}\{\mu\text{-(1-(SiMe}_3)\text{-3-(SiMe}_2\text{CH}_2)\text{C}_3\text{H}_3)\}\}_2$. U_{eq} is defined as one third of the trace of the orthogonalized U_{ij} tensor.

atom	<i>x</i>	<i>y</i>	<i>z</i>	U_{eq}
Si1	8401(6)	6632(7)	1096(5)	47(1)
C1	9464(10)	7253(10)	470(5)	56(2)
C2	8623(10)	5123(8)	832(8)	86(4)
C3	8940(20)	6489(17)	1888(7)	89(5)
Si1'	8336(13)	6532(17)	1175(12)	47(1)
C1'	9410(30)	6860(20)	430(12)	56(2)
C2'	8430(30)	4968(19)	1204(18)	86(4)
C3'	8810(60)	6850(40)	1916(17)	89(5)
Si2	3268(4)	7079(4)	1142(2)	49(1)
C7	3728(9)	6637(9)	256(3)	78(2)
C8	1653(6)	8212(8)	1330(5)	71(2)
C9	3242(13)	5737(8)	1653(5)	103(3)
Si2'	3420(20)	6870(20)	1173(16)	49(1)
C7'	3390(50)	6450(50)	340(20)	78(2)
C8'	1820(30)	7820(50)	1600(30)	71(2)
C9'	3840(70)	5460(40)	1660(30)	103(3)
Ho1	5151(1)	9394(1)	787(1)	31(1)
Si3	7113(1)	11111(1)	1421(1)	59(1)
Si4	2623(1)	11530(1)	1064(1)	37(1)
C4	6671(4)	7534(4)	1258(2)	47(1)
C5	5748(4)	7149(3)	1113(2)	42(1)
C6	4423(4)	7709(4)	1293(2)	46(1)
C10	8459(5)	10689(6)	664(4)	102(2)
C11	6856(6)	12668(5)	1626(3)	88(2)
C12	7519(8)	10161(7)	2130(4)	128(3)
C13	5654(4)	10983(3)	1263(2)	46(1)
C14	4683(4)	10788(4)	1765(2)	48(1)
C15	3503(4)	10779(4)	1701(2)	46(1)
C16	2702(5)	13043(4)	862(2)	58(1)
C17	923(4)	11657(4)	1419(2)	55(1)
C18	3338(3)	10583(3)	304(2)	34(1)
Ho2	722(1)	10317(1)	4193(1)	34(1)
Si5	2810(1)	12642(1)	3717(1)	59(1)
Si6	4073(1)	7655(1)	3712(1)	52(1)
Si7	-843(1)	8783(1)	3986(1)	44(1)
Si8	-1824(1)	13398(1)	3745(1)	53(1)
C19	4315(7)	12100(7)	3998(4)	126(3)

Table 26., continued.

atom	<i>x</i>	<i>y</i>	<i>z</i>	<i>U</i> _{eq}
C20	1603(6)	13714(5)	4336(3)	89(2)
C21	3061(7)	13429(5)	2924(3)	88(2)
C22	2368(4)	11341(4)	3598(2)	48(1)
C23	3090(4)	10185(4)	3731(2)	48(1)
C24	2929(4)	9131(4)	3590(2)	50(1)
C25	3424(6)	6498(4)	3587(3)	79(2)
C26	4379(5)	7551(5)	4546(3)	75(2)
C27	5626(5)	7423(5)	3124(3)	92(2)
C28	-351(6)	7305(4)	3605(2)	67(1)
C29	-2603(5)	9344(5)	4284(3)	69(1)
C30	-92(4)	8719(3)	4699(2)	36(1)
C31	-270(4)	9769(4)	3344(2)	46(1)
C32	-666(4)	10993(4)	3329(2)	48(1)
C33	-1221(4)	11777(3)	3869(2)	44(1)
C34	-3345(7)	13862(5)	3493(4)	112(3)
C35	-659(6)	13844(5)	3081(3)	80(2)
C36	-2087(6)	14203(4)	4512(3)	79(2)

Table 27. Crystal data and structure refinement for $\text{Ho}_2[\mu\text{-}\{1\text{-(SiMe}_3\text{)-3-(SiMe}_2\text{CH}_2\text{)C}_3\text{H}_3\}\}_2[\mu\text{-}\{1,3\text{-(SiMe}_3\text{)}_2\text{C}_3\text{H}_2\}](\text{thf})_2$.

Empirical formula	$\text{C}_{35}\text{H}_{76}\text{Ho}_2\text{O}_2\text{Si}_6$	
Formula weight	1027.36	
Temperature	173(2) K	
Wavelength	0.71073 Å	
Crystal system	Triclinic	
Space group	$P\bar{1}$	
Unit cell dimensions	$a = 10.5760(11)$ Å	$\alpha = 82.540(2)^\circ$
	$b = 11.8757(13)$ Å	$\beta = 87.940(2)^\circ$
	$c = 19.561(2)$ Å	$\gamma = 78.290(2)^\circ$
Volume	2385.2(4) Å ³	
Z	2	
Density (calculated)	1.430 Mg/m ³	
Absorption coefficient	3.469 mm ⁻¹	
$F(000)$	1040	
Crystal color, morphology	Yellow, block	
Crystal size	0.25 × 0.20 × 0.10 mm ³	
Theta range for data collection	1.05 to 27.50°	
Index ranges	$-13 \leq h \leq 13, -15 \leq k \leq 15, -25 \leq l \leq 25$	
Reflections collected	27613	
Independent reflections	10794 [$R(\text{int}) = 0.0349$]	
Observed reflections	8571	
Completeness to $\theta = 27.50^\circ$	98.4%	
Absorption correction	Multi-scan	
Max. and min. transmission	0.7084 and 0.4680	
Refinement method	Full-matrix least-squares on F^2	
Data / restraints / parameters	10794 / 18 / 448	
Goodness-of-fit on F^2	1.015	
Final R indices [$I > 2\sigma(I)$]	$R1 = 0.0411, wR2 = 0.0838$	
R indices (all data)	$R1 = 0.0589, wR2 = 0.0890$	
Largest diff. peak and hole	3.20 and -1.29 $e \text{ \AA}^{-3}$	

Table 28. Atomic coordinates ($\times 10^4$) and equivalent isotropic displacement parameters ($\text{\AA}^2 \times 10^3$) for $\text{Ho}_2[\mu\text{-}\{1\text{-(SiMe}_3\text{)-3-(SiMe}_2\text{CH}_2\text{)C}_3\text{H}_3\}\text{]}_2[\mu\text{-}\{1,3\text{-(SiMe}_3\text{)}_2\text{C}_3\text{H}_2\}\text{]}(\text{thf})_2$. U_{eq} is defined as one third of the trace of the orthogonalized U_{ij} tensor.

atom	<i>x</i>	<i>y</i>	<i>z</i>	U_{eq}
Ho1	9208(1)	8238(1)	8069(1)	23(1)
Ho2	9414(1)	6809(1)	6784(1)	25(1)
Si1	6131(2)	11071(1)	7605(1)	31(1)
Si2	6569(2)	6386(1)	7609(1)	30(1)
Si3	12267(2)	7567(2)	9456(1)	38(1)
Si4	10640(2)	9958(1)	7149(1)	30(1)
Si6	10957(2)	4640(1)	7650(1)	30(1)
O2	8224(4)	7588(3)	5771(2)	39(1)
C1	6897(7)	12219(5)	7878(4)	59(2)
C2	4824(6)	10865(6)	8254(3)	48(2)
C3	5377(6)	11656(6)	6745(3)	47(2)
C4	7249(5)	9684(4)	7535(3)	28(1)
C5	6816(5)	8613(4)	7613(3)	27(1)
C6	7534(5)	7536(4)	7461(3)	26(1)
C7	7040(6)	5356(5)	6946(3)	41(1)
C8	6731(7)	5481(6)	8475(3)	51(2)
C9	4790(6)	6987(6)	7493(4)	49(2)
C10	11336(7)	8053(8)	10230(3)	66(2)
C11	13883(6)	7938(8)	9525(4)	63(2)
C12	12519(9)	5965(6)	9496(4)	74(3)
C13	11424(5)	8321(4)	8668(3)	29(1)
C14	10679(5)	9437(5)	8631(3)	31(1)
C15	10092(5)	10117(4)	8045(3)	32(1)
C16	10333(6)	8572(5)	6895(3)	32(1)
C17	9728(6)	11221(5)	6567(3)	45(2)
C18	12394(6)	10013(6)	7055(4)	47(2)
Si5	12570(9)	6665(9)	5375(2)	34(1)
C19	12210(20)	8284(12)	5220(9)	61(5)
C20	14364(13)	6200(20)	5522(11)	89(6)
C21	12219(14)	6093(13)	4573(6)	36(2)
Si5'	12298(18)	6948(15)	5366(7)	34(1)
C19'	11730(60)	8550(20)	5170(30)	61(5)
C20'	14100(30)	6650(60)	5460(30)	89(6)
C21'	11880(30)	6270(40)	4620(20)	36(2)
C22	11659(5)	6141(4)	6129(3)	30(1)
C23	11037(5)	5215(5)	6152(3)	34(1)
C24	10480(6)	4675(5)	6726(3)	34(1)
C25	10361(5)	6087(4)	7961(3)	30(1)

Table 28., continued.

atom	<i>x</i>	<i>y</i>	<i>z</i>	<i>U</i> _{eq}
C26	10198(7)	3490(5)	8152(3)	48(2)
C27	12757(6)	4211(6)	7714(3)	46(2)
C32	8507(7)	7224(7)	5091(3)	58(2)
C33	7346(7)	7664(8)	4679(4)	68(2)
C34	6624(9)	8668(7)	5015(4)	73(2)
C35	7082(9)	8499(8)	5720(4)	85(3)
O1	8268(6)	7934(5)	9186(2)	37(1)
C28	7330(9)	8866(7)	9436(4)	51(2)
C29	7163(12)	8510(11)	10172(4)	69(4)
C30	7479(10)	7217(10)	10254(5)	61(3)
C31	8445(8)	6920(6)	9694(3)	40(2)
O1'	8374(8)	8095(6)	9214(3)	37(1)
C28'	7992(8)	9094(6)	9583(3)	51(2)
C29'	7530(60)	8660(30)	10256(14)	69(4)
C30'	7180(50)	7530(30)	10191(18)	61(3)
C31'	7860(30)	7140(20)	9557(14)	40(2)

Table 29. Crystal data and structure refinement for Yb[1,3-(SiMe₃)₂C₃H₃]₂(tpy).

Empirical formula	C ₃₃ H ₄₉ N ₃ Si ₄ Yb	
Formula weight	773.15	
Temperature	293(2) K	
Wavelength	0.71073 Å	
Crystal system	Triclinic	
Space group	<i>P</i> -1	
Unit cell dimensions	<i>a</i> = 10.202(4) Å	$\alpha = 71.618(5)^\circ$
	<i>b</i> = 12.018(4) Å	$\beta = 77.715(5)^\circ$
	<i>c</i> = 17.226(6) Å	$\gamma = 71.934(5)^\circ$
Volume	1889.8(12) Å ³	
<i>Z</i>	2	
Density (calculated)	1.359 Mg/m ³	
Absorption coefficient	2.625 mm ⁻¹	
<i>F</i> (000)	788	
Crystal color	Red-brown	
Theta range for data collection	1.26 to 26.57°	
Index ranges	-12 ≤ <i>h</i> ≤ 12, -15 ≤ <i>k</i> ≤ 15, -21 ≤ <i>l</i> ≤ 20	
Reflections collected	14218	
Independent reflections	7517 [<i>R</i> (int) = 0.0564]	
Observed reflections	5775	
Completeness to theta = 25.00°	97.5%	
Absorption correction	Multi-scan	
Refinement method	Full-matrix least-squares on <i>F</i> ²	
Data / restraints / parameters	7517 / 22 / 358	
Goodness-of-fit on <i>F</i> ²	1.069	
Final <i>R</i> indices [<i>I</i> > 2σ(<i>I</i>)]	<i>R</i> 1 = 0.1065, <i>wR</i> 2 = 0.2859	
<i>R</i> indices (all data)	<i>R</i> 1 = 0.1278, <i>wR</i> 2 = 0.2957	
Largest diff. peak and hole	8.844 and -2.044 e Å ⁻³	

Table 30. Atomic coordinates and equivalent isotropic displacement parameters (\AA^2) for $\text{Yb}[1,3-(\text{SiMe}_3)_2\text{C}_3\text{H}_3]_2(\text{tpy})$. U_{eq} is defined as one third of the trace of the orthogonalized U_{ij} tensor.

atom	<i>x</i>	<i>y</i>	<i>z</i>	U_{eq}
Yb1	0.04087(7)	0.69923(6)	0.24125(4)	0.0245(2)
Si1	0.1601(5)	0.8822(4)	0.3676(3)	0.0323(11)
Si2	0.4086(5)	0.7158(4)	0.0810(3)	0.0309(10)
Si3	-0.3048(5)	0.9727(4)	0.2862(3)	0.0341(11)
Si4	-0.2182(5)	0.4733(4)	0.3017(3)	0.0306(10)
N1	-0.0290(15)	0.7545(13)	0.1075(9)	0.033(3)
N2	0.1283(14)	0.5446(13)	0.1804(9)	0.030(3)
N3	0.1689(14)	0.5229(12)	0.3305(9)	0.029(3)
C1	-0.1105(17)	0.8654(15)	0.0742(11)	0.031(4)
H1	-0.1514	0.9180	0.1074	0.037
C2	-0.1355(19)	0.9035(16)	-0.0061(11)	0.036(4)
H2	-0.1916	0.9807	-0.0268	0.043
C3	-0.075(2)	0.825(2)	-0.0569(11)	0.041(5)
H3	-0.0916	0.8481	-0.1116	0.050
C4	0.0076(19)	0.7129(18)	-0.0235(11)	0.037(4)
H4	0.0505	0.6602	-0.0565	0.044
C5	0.0292(18)	0.6762(17)	0.0593(11)	0.034(4)
C6	0.1105(17)	0.5574(16)	0.0990(10)	0.030(4)
C7	0.1691(19)	0.4675(17)	0.0602(11)	0.035(4)
H7	0.1614	0.4833	0.0047	0.041
C8	0.2402(19)	0.3529(17)	0.1022(13)	0.041(5)
H8	0.2753	0.2903	0.0765	0.050
C9	0.2579(18)	0.3334(15)	0.1848(12)	0.035(4)
H9	0.3051	0.2577	0.2149	0.042
C10	0.2032(18)	0.4300(16)	0.2207(11)	0.034(4)
C11	0.2213(16)	0.4185(14)	0.3056(11)	0.029(4)
C12	0.2882(19)	0.3096(15)	0.3600(12)	0.038(4)
H12	0.3224	0.2383	0.3434	0.046
C13	0.302(2)	0.3098(16)	0.4371(11)	0.040(5)
H13	0.3469	0.2390	0.4733	0.049
C14	0.250(2)	0.4160(17)	0.4603(12)	0.041(4)
H14	0.2579	0.4172	0.5127	0.049
C15	0.1858(17)	0.5191(15)	0.4073(11)	0.033(4)
H15	0.1522	0.5902	0.4242	0.040
C16	0.0009(18)	0.8780(19)	0.4461(11)	0.038(4)
H16A	-0.0208	0.8018	0.4569	0.058
H16B	-0.0760	0.9433	.4251	0.058
H16C	0.0183	0.8867	0.4962	0.058

Table 30., continued.

atom	<i>x</i>	<i>y</i>	<i>z</i>	<i>U</i> _{eq}
C17	0.182(2)	1.0386(17)	0.3390(13)	0.048(5)
H17A	0.1924	1.0570	0.3872	0.072
H17B	0.1010	1.0955	0.3158	0.072
H17C	0.2625	1.0441	.2991	0.072
C18	0.3178(19)	0.7810(19)	0.4120(11)	0.039(4)
H18A	0.3982	0.7938	0.3733	0.058
H18B	0.3153	0.6980	0.4239	0.058
H18C	0.3223	0.7982	0.4620	0.058
C19	0.476(2)	0.5499(19)	0.1132(13)	0.045(5)
H19A	0.4056	0.5125	0.1128	0.067
H19B	0.5013	0.5254	0.1679	0.067
H19C	0.5563	0.5250	0.0757	0.067
C20	0.5520(19)	0.7833(18)	0.0817(13)	0.042(5)
H20A	0.5668	0.7694	0.1376	0.063
H20B	0.5263	0.8692	0.0560	0.063
H20C	0.6361	0.7459	0.0518	0.063
C21	0.361(2)	0.761(2)	-0.0246(12)	0.049(5)
H21A	0.4405	0.7314	-0.0610	0.073
H21B	0.3314	0.8482	-0.0434	0.073
H21C	0.2870	0.7275	-0.0243	0.073
C22	-0.4358(18)	0.9920(15)	0.2170(12)	0.036(4)
H22A	-0.3882	0.9673	0.1683	0.053
H22B	-0.4873	1.0757	0.2017	0.053
H22C	-0.4986	0.9427	0.2459	0.053
C23	-0.401(2)	1.0076(18)	0.3855(13)	0.047(5)
H23A	-0.4690	0.9615	0.4078	0.070
H23B	-0.4472	1.0927	0.3750	0.070
H23C	-0.3367	0.9863	0.4243	0.070
C24	-0.207(2)	1.0903(17)	0.2357(13)	0.042(5)
H24A	-0.1386	1.0817	0.2695	0.063
H24B	-0.2700	1.1697	0.2289	0.063
H24C	-0.1609	1.0799	0.1827	0.063
C25	-0.187(2)	0.468(2)	0.1927(14)	0.052(5)
H25A	-0.2227	0.5478	0.1582	0.078
H25B	-0.2338	0.4133	0.1871	0.078
H25C	-0.0893	0.4403	0.1765	0.078
C26	-0.123(2)	0.3265(17)	0.3675(15)	0.049(5)
H26A	-0.1646	0.2634	0.3703	0.073
H26B	-0.1288	0.3341	0.4220	0.073
H26C	-0.0276	0.3065	0.3440	0.073
C27	-0.4087(18)	0.494(2)	0.3371(13)	0.045(5)
H27A	-0.4588	0.5735	0.3093	0.068
H27B	-0.4258	0.4838	0.3955	0.068

Table 30., continued.

atom	<i>x</i>	<i>y</i>	<i>z</i>	<i>U</i> _{eq}
H27C	-0.4390	0.4339	0.3245	0.068
C28	-0.1614(16)	0.5984(15)	0.3178(9)	0.036(3)
C29	-0.2267(16)	0.7355(14)	0.2879(9)	0.036(3)
H29	-0.2965	0.7621	0.2542	0.044
C30	-0.1895(16)	0.8165(17)	0.3074(10)	0.036(3)
C31	0.2517(17)	0.7808(13)	0.1512(10)	0.030(2)
C32	0.2446(15)	0.7900(12)	0.2416(9)	0.030(2)
H32	0.3220	0.7533	0.2698	0.036
C33	0.1324(15)	0.8478(12)	0.2756(11)	0.030(2)

Table 31. Crystal data and structure refinement for [K{1,3-(SiMe₃)₂C₃H₃}(dme)]_∞.

Empirical formula	C ₂₆ H ₆₂ K ₂ O ₄ Si ₄
Formula weight	629.32
Temperature	173(2) K
Wavelength	0.71073 Å
Crystal system	Monoclinic
Space group	P2 ₁ /c
Unit cell dimensions	$a = 10.7102(10)$ Å $\alpha = 90^\circ$ $b = 20.4087(19)$ Å $\beta = 93.045(2)^\circ$ $c = 18.6521(17)$ Å $\gamma = 90^\circ$
Volume	4071.2(7) Å ³
Z	4
Density (calculated)	1.027 Mg/m ³
Absorption coefficient	0.374 mm ⁻¹
<i>F</i> (000)	1376
Crystal color, morphology	Colorless, block
Crystal size	0.35 × 0.30 × 0.22 mm ³
Theta range for data collection	1.48 to 25.05°
Index ranges	-12 ≤ <i>h</i> ≤ 12, 0 ≤ <i>k</i> ≤ 24, 0 ≤ <i>l</i> ≤ 22
Reflections collected	26915
Independent reflections	7209 [<i>R</i> (int) = 0.0441]
Observed reflections	5562
Completeness to theta = 25.05°	99.9%
Absorption correction	Multi-scan
Max. and min. transmission	0.9222 and 0.8802
Refinement method	Full-matrix least-squares on <i>F</i> ²
Data / restraints / parameters	7209 / 98 / 413
Goodness-of-fit on <i>F</i> ²	1.039
Final <i>R</i> indices [<i>I</i> > 2σ(<i>I</i>)]	<i>R</i> 1 = 0.0394, <i>wR</i> 2 = 0.0952
<i>R</i> indices (all data)	<i>R</i> 1 = 0.0568, <i>wR</i> 2 = 0.1067
Largest diff. peak and hole	0.350 and -0.230 e Å ⁻³

Table 32. Atomic coordinates ($\times 10^4$) and equivalent isotropic displacement parameters ($\text{\AA}^2 \times 10^3$) for $[\text{K}\{1,3\text{-(SiMe}_3\text{)}_2\text{C}_3\text{H}_3\}\text{(dme)}]_\infty$. U_{eq} is defined as one third of the trace of the orthogonalized U_{ij} tensor.

atom	<i>x</i>	<i>y</i>	<i>z</i>	U_{eq}
K1	1111(1)	4090(1)	3016(1)	44(1)
K2	2461(1)	6525(1)	1813(1)	46(1)
C1	4781(3)	2785(2)	4684(2)	96(1)
C2	2234(4)	2585(2)	5315(2)	94(1)
C3	3061(3)	3922(1)	4884(1)	67(1)
Si1	3099(1)	3037(1)	4624(1)	48(1)
C4	2381(2)	2887(1)	3734(1)	41(1)
C5	2937(2)	2984(1)	3084(1)	37(1)
C6	2448(2)	2915(1)	2382(1)	39(1)
Si2	3222(1)	3103(1)	1565(1)	46(1)
C7	3397(3)	2377(1)	971(2)	71(1)
C8	4794(3)	3463(2)	1773(2)	93(1)
C9	2289(4)	3705(2)	990(2)	98(1)
C10	3501(2)	5666(1)	4322(1)	55(1)
C11	4907(2)	6289(1)	3153(1)	52(1)
C12	5315(2)	4854(1)	3455(1)	52(1)
Si3	4096(1)	5511(1)	3410(1)	39(1)
C13	2829(2)	5294(1)	2766(1)	44(1)
C14	1597(2)	5505(1)	2780(1)	40(1)
C15	593(2)	5433(1)	2282(1)	43(1)
Si4	-946(1)	5787(1)	2361(1)	49(1)
C16	-2158(2)	5304(1)	1835(2)	70(1)
C17	-1364(3)	5828(2)	3315(2)	103(1)
C18	-1067(3)	6648(2)	2008(3)	120(2)
C19	-434(6)	4396(5)	4661(3)	148(4)
O1	-730(3)	4163(2)	3969(2)	82(1)
C20	-1656(5)	3690(3)	3940(3)	84(2)
C21	-2094(5)	3527(5)	3164(4)	73(2)
O2	-1050(3)	3336(2)	2805(2)	77(1)
C22	-1428(5)	3128(3)	2104(3)	84(2)
C19'	-1082(15)	3775(7)	4454(5)	138(6)
O1'	-870(5)	3577(3)	3752(3)	81(2)
C20'	-1945(9)	3418(10)	3343(6)	73(2)
C21'	-1603(8)	3171(4)	2609(4)	77(1)
O2'	-976(5)	3648(2)	2250(3)	73(2)
C22'	-858(10)	3485(6)	1519(4)	111(4)
C23	5600(20)	6773(11)	1093(10)	89(4)
O3	4620(20)	6315(10)	1045(8)	69(3)

Table 32., continued.

atom	<i>x</i>	<i>y</i>	<i>z</i>	<i>U</i> _{eq}
C24	4492(6)	5991(4)	393(4)	85(3)
C25	3418(12)	5505(9)	378(12)	85(2)
O4	2334(10)	5743(6)	649(6)	70(2)
C26	1264(18)	5650(20)	188(18)	106(2)
C23'	5446(19)	6627(9)	817(8)	89(4)
O3'	4644(18)	6221(9)	1182(7)	69(3)
C24'	4476(6)	5588(3)	883(4)	85(2)
C25'	3418(11)	5615(8)	292(10)	85(2)
O4'	2295(9)	5912(6)	429(5)	70(2)
C26'	1189(17)	5582(18)	191(16)	106(2)

Table 33. Crystal data and structure refinement for Y[1,3-(SiMe₃)₂C₃H₃]₃.

Empirical formula	C ₂₇ H ₆₃ Si ₆ Y	
Formula weight	645.22	
Temperature	173(2) K	
Wavelength	0.71073 Å	
Crystal system	Orthorhombic	
Space group	<i>Pna</i> 2 ₁	
Unit cell dimensions	<i>a</i> = 20.658(5) Å	$\alpha = 90^\circ$
	<i>b</i> = 10.580(5) Å	$\beta = 90^\circ$
	<i>c</i> = 18.999(3) Å	$\gamma = 90^\circ$
Volume	4152(2) Å ³	
<i>Z</i>	4	
Density (calculated)	1.032 Mg/m ³	
<i>F</i> (000)	1392	
Crystal color, morphology	Yellow, block	
Reflections collected	7322	
Absorption correction	Multi-scan	
Refinement method	Full-matrix least-squares on <i>F</i> ²	
Data / restraints / parameters	7322 / 367 / 265	
Final <i>R</i> indices [<i>I</i> > 2σ(<i>I</i>)]	<i>R</i> 1 = 0.0968	
<i>R</i> indices (all data)	<i>R</i> 1 = 0.2098	

Table 34. Atomic coordinates for $\text{Y}[1,3-(\text{SiMe}_3)_2\text{C}_3\text{H}_3]_3$.

atom	<i>x</i>	<i>y</i>	<i>z</i>
Y1	0.875731	0.400407	0.263087
C1	0.849917	0.530491	0.372141
C2	0.884901	0.615081	0.334020
C3	0.919675	0.626117	0.273226
C4	0.809504	0.440016	0.150164
C5	0.770130	0.359290	0.187643
C6	0.785391	0.249371	0.224763
C7	0.954438	0.266499	0.327845
C8	0.963480	0.227354	0.259173
C9	0.967577	0.290380	0.195852
C1'	0.814771	0.574565	0.326721
C11	0.687710	0.551031	0.400339
C12	0.786377	0.732989	0.447320
C13	0.786567	0.447506	0.498322
C2'	0.778109	0.559207	0.265711
C21	0.058701	0.659953	0.320305
C22	0.043800	0.609504	0.167801
C23	0.002230	0.830961	0.238535
C31	0.705892	0.670024	0.140282
C32	0.843654	0.706786	0.097497
C33	0.750889	0.520876	0.018281
C41	0.742396	0.980884	0.226300
C42	0.742214	0.092173	0.365144
C43	0.657245	0.167632	0.251100
C51	0.060738	0.093963	0.404495
C52	0.920353	0.033127	0.403017
C53	0.982374	0.295991	0.469623
C61	0.046160	0.136105	0.090442
C62	0.908431	0.081365	0.085976
C63	0.964962	0.305336	0.040193
C11'	0.830868	0.671690	0.484901
C12'	0.714024	0.720567	0.398124
C13'	0.750598	0.441139	0.445847
C21'	0.699224	0.645543	0.096410
C22'	0.833919	0.632235	0.040073
C23'	0.745492	0.426873	0.067416
C3'	0.794421	0.531127	0.197768
C31'	0.947744	0.821839	0.216564
C32'	0.009898	0.755112	0.348583
C33'	0.077179	0.702822	0.201034

Table 34., continued.

atom	<i>x</i>	<i>y</i>	<i>z</i>
C4'	0.979002	0.530080	0.251984
C41'	0.052810	0.258295	0.056373
C42'	0.986724	0.041631	0.120121
C43'	0.930852	0.219335	0.029904
C5'	0.984916	0.448239	0.196774
C51'	0.055360	0.194126	0.414646
C52'	0.938618	0.113294	0.486340
C53'	0.985275	0.402289	0.483665
C6'	0.958507	0.341575	0.167061
C61'	0.724111	0.139281	0.188435
C62'	0.689421	0.076966	0.334687
C63'	0.779408	0.945200	0.248877
C7'	0.905586	0.298337	0.378560
C8'	0.868357	0.206100	0.348618
C9'	0.838937	0.174527	0.286486
Si1	0.777395	0.566700	0.424167
Si2	0.004296	0.683471	0.263002
Si3	0.782772	0.584038	0.106168
Si4	0.969925	0.195984	0.409769
Si5	0.727166	0.131978	0.263700
Si6	0.982357	0.217189	0.108301
Si1'	0.775313	0.601684	0.412286
Si2'	0.761968	0.558141	0.109882
Si3'	0.003634	0.695766	0.259641
Si4'	0.977501	0.253114	0.428396
Si5'	0.959580	0.202501	0.113661
Si6'	0.764283	0.097014	0.257404

Table 35. Anisotropic displacement parameters (\AA^2) for $\text{Y}[1,3-(\text{SiMe}_3)_2\text{C}_3\text{H}_3]_3$. The anisotropic displacement factor exponent takes the form: $-2\pi^2[h^2 a^{*2} U_{11} + \dots + 2 h k a^* b^* U_{12}]$.

	U_{11}	U_{22}	U_{33}	U_{23}	U_{13}	U_{12}
Y1	0.1019	0.0842	0.1201	0.0025	0.0024	-0.0051
Si1	0.2452	0.1533	0.1803	0.0038	0.0503	-0.0462
Si2	0.1458	0.1140	0.3341	-0.0360	-0.0058	-0.0095
Si3	0.1422	0.1503	0.1824	0.0082	-0.0671	0.0082
Si4	0.2725	0.1567	0.1521	0.0387	-0.0841	0.0046
Si5	0.1799	0.2212	0.2388	-0.1256	0.0310	0.0240
Si6	0.1404	0.2222	0.2243	0.0586	0.0516	-0.0760
Si1'	0.2452	0.1533	0.1803	0.0038	0.0503	-0.0462
Si2'	0.1422	0.1503	0.1824	0.0082	-0.0671	0.0082
Si3'	0.1458	0.1140	0.3341	-0.0360	-0.0058	-0.0095
Si4'	0.2725	0.1567	0.1521	0.0387	-0.0841	0.0046
Si5'	0.1404	0.2222	0.2243	0.0586	0.0516	-0.0760
Si6'	0.1799	0.2212	0.2388	-0.1256	0.0310	0.0240

Table 36. Crystal data and structure refinement for $V_2[\mu\text{-}\{1,3\text{-(SiMe}_3\text{)}_2\text{C}_3\text{H}_3\}\text{]}_3\text{Cl}$.

Empirical formula	$C_{27}H_{63}Cl_{0.73}Si_6V_2$
Formula weight	683.98
Temperature	173(2) K
Wavelength	0.71073 Å
Crystal system	Monoclinic
Space group	$P2_1/n$
Unit cell dimensions	$a = 10.297(2)$ Å $\alpha = 90^\circ$ $b = 17.766(4)$ Å $\beta = 100.380(4)^\circ$ $c = 22.420(5)$ Å $\gamma = 90^\circ$
Volume	$4034.1(15)$ Å ³
Z	4
Density (calculated)	1.126 Mg/m ³
Absorption coefficient	0.704 mm ⁻¹
$F(000)$	1469
Crystal color, morphology	Brown, plate
Crystal size	$0.28 \times 0.13 \times 0.04$ mm ³
Theta range for data collection	1.47 to 25.05°
Index ranges	$-12 \leq h \leq 12, -21 \leq k \leq 21, -26 \leq l \leq 26$
Reflections collected	38798
Independent reflections	7153 [$R(\text{int}) = 0.1483$]
Observed reflections	3648
Completeness to theta = 25.05°	99.9%
Absorption correction	Semi-empirical from equivalents
Max. and min. transmission	1.000000 and 0.748677
Refinement method	Full-matrix least-squares on F^2
Data / restraints / parameters	7153 / 7 / 338
Goodness-of-fit on F^2	1.025
Final R indices [$I > 2\sigma(I)$]	$R1 = 0.0713, wR2 = 0.1583$
R indices (all data)	$R1 = 0.1627, wR2 = 0.1940$
Largest diff. peak and hole	0.828 and -0.620 e Å ⁻³

Table 37. Atomic coordinates ($\times 10^4$) and equivalent isotropic displacement parameters ($\text{\AA}^2 \times 10^3$) for $V_2[\mu\text{-}\{1,3\text{-(SiMe}_3\text{)}_2\text{C}_3\text{H}_3\}]_3\text{Cl}$. U_{eq} is defined as one third of the trace of the orthogonalized U_{ij} tensor.

atom	x	y	z	U_{eq}
V1	3426(1)	2432(1)	7486(1)	29(1)
V2	2601(1)	2382(1)	6400(1)	38(1)
Si1	5244(2)	917(1)	8104(1)	41(1)
Si2	3549(2)	720(1)	5775(1)	50(1)
Si3	1090(2)	2488(1)	8390(1)	44(1)
Cl1	1676(3)	2353(1)	5321(1)	57(1)
C12	783(6)	2807(3)	6526(3)	37(2)
Si4	-882(3)	2577(2)	6078(2)	50(1)
C16	-1027(13)	1580(6)	5811(5)	73(4)
C17	-2095(9)	2677(6)	6591(5)	72(3)
C18	-1323(11)	3260(5)	5439(4)	67(3)
C12'	783(6)	2807(3)	6526(3)	37(2)
Si4'	-487(9)	2363(5)	5945(4)	50(1)
C16'	-970(40)	1387(12)	6147(15)	73(4)
C17'	200(20)	2237(16)	5232(10)	72(3)
C18'	-1920(20)	3003(14)	5789(12)	67(3)
Si5	5349(2)	3935(1)	8002(1)	44(1)
Si6	3871(2)	3862(1)	5645(1)	48(1)
C1	3828(6)	1322(3)	7567(3)	33(2)
C2	3870(6)	1444(3)	6925(3)	33(1)
C3	2951(6)	1225(3)	6399(3)	37(2)
C4	6838(6)	1263(4)	7929(3)	63(2)
C5	5126(8)	1160(5)	8898(3)	71(2)
C6	5173(7)	-139(3)	8030(3)	61(2)
C7	2137(8)	302(4)	5246(3)	76(3)
C8	4626(8)	-61(4)	6146(3)	84(3)
C9	4561(9)	1320(4)	5363(4)	89(3)
C10	1710(6)	2787(3)	7699(3)	32(1)
C11	1238(6)	2437(3)	7101(3)	35(1)
C13	979(8)	1436(4)	8421(3)	71(2)
C14	-582(6)	2877(4)	8371(3)	53(2)
C15	2206(7)	2857(5)	9072(3)	70(2)
C19	4858(6)	3191(3)	7428(3)	32(1)
C20	3940(6)	3337(3)	6855(3)	37(2)
C21	4047(6)	3124(3)	6240(3)	33(2)
C22	5960(8)	3487(4)	8746(3)	72(2)
C23	3925(7)	4567(4)	8052(4)	81(3)

Table 37., continued.

atom	<i>x</i>	<i>y</i>	<i>z</i>	<i>U</i> _{eq}
C24	6699(7)	4514(4)	7778(4)	73(2)
C25	5280(8)	4528(4)	5872(3)	73(2)
C26	3976(9)	3448(4)	4887(3)	79(3)
C27	2321(7)	4393(4)	5607(3)	70(2)

Appendix B

ATOMIC FRACTIONAL COORDINATES FOR DENSITY FUNCTIONAL THEORY
OPTIMIZED STRUCTURES

Table 38. Atomic coordinates for optimized structure of Yb[1,3-(SiMe₃)₂C₃H₃]₂(tpy) (B3PW91/SDD).

atom	x	y	z
Yb	0.0098	0.0492	0.0027
N	-1.2021	-0.7839	-1.9723
N	-0.1453	-2.3671	-0.0631
C	-2.5386	-0.1567	1.1258
C	-2.1423	1.1918	1.2559
C	-1.0034	1.6875	1.9373
C	-1.7487	0.0629	-2.8806
H	-1.6614	1.1218	-2.6587
C	-2.3903	-0.3724	-4.0407
H	-2.8120	0.3473	-4.7337
C	-2.4624	-1.7580	-4.2810
H	-2.9432	-2.1409	-5.1760
C	-1.9096	-2.6376	-3.3473
H	-1.9669	-3.7049	-3.5237
C	-1.2864	-2.1304	-2.1867
C	-0.7258	-2.9984	-1.1326
C	-0.8090	-4.3992	-1.2008
H	-1.2694	-4.8888	-2.0501
C	-0.3005	-5.1719	-0.1499
H	-0.3583	-6.2550	-0.1844
N	1.0761	-1.0316	1.9366
C	1.7051	-0.3102	2.8985
H	1.7563	0.7615	2.7342
C	2.2637	-0.8835	4.0412
H	2.7565	-0.2601	4.7792
C	2.1595	-2.2783	4.2047
H	2.5696	-2.7654	5.0841
C	1.5240	-3.0309	3.2145
H	1.4456	-4.1051	3.3313
C	0.9929	-2.3885	2.0751
C	0.3535	-3.1229	0.9663
C	0.2831	-4.5262	0.9465
H	0.6846	-5.1150	1.7620
C	2.5393	-0.3994	-1.0915
C	2.2871	0.9851	-1.2062
C	1.2142	1.6050	-1.8921
Si	4.2007	-1.0797	-0.5426
Si	1.2122	3.4060	-2.4260
Si	-4.2661	-0.6548	0.5860

Table 38., continued.

atom	<i>x</i>	<i>y</i>	<i>z</i>
Si	-0.8178	3.4690	2.5044
C	-4.9656	0.5543	-0.7204
H	-5.9830	0.2558	-1.0064
H	-5.0206	1.5782	-0.3285
H	-4.3502	0.5688	-1.6282
C	-5.4592	-0.6216	2.0879
H	-5.4932	0.3821	2.5309
H	-6.4802	-0.9038	1.7947
H	-5.1245	-1.3190	2.8674
C	-4.3324	-2.4362	-0.1073
H	-3.8564	-2.5091	-1.0920
H	-3.8272	-3.1390	0.5687
H	-5.3759	-2.7631	-0.2108
C	-2.1949	4.5710	1.7692
H	-2.0504	5.6155	2.0753
H	-2.2117	4.5451	0.6731
H	-3.1797	4.2488	2.1314
C	-0.9788	3.5187	4.4144
H	-0.8791	4.5439	4.7967
H	-1.9549	3.1276	4.7285
H	-0.2022	2.9053	4.8915
C	0.8874	4.2319	2.0919
H	1.7031	3.6342	2.5222
H	1.0451	4.2872	1.0091
H	0.9686	5.2480	2.5012
C	5.0046	0.0326	0.7893
H	5.9858	-0.3688	1.0762
H	5.1617	1.0535	0.4177
H	4.3865	0.0899	1.6936
C	5.4070	-1.1465	-2.0330
H	5.5414	-0.1462	-2.4643
H	6.3934	-1.5280	-1.7338
H	5.0149	-1.8006	-2.8233
C	4.0782	-2.8681	0.1251
H	3.6060	-2.9039	1.1137
H	3.4940	-3.5018	-0.5556
H	5.0805	-3.3085	0.2145
C	1.3866	3.4793	-4.3342
H	1.3812	4.5171	-4.6949
H	2.3252	3.0089	-4.6537
H	0.5608	2.9480	-4.8272
C	-0.4107	4.3262	-2.0022
H	-1.2796	3.8215	-2.4472

Table 38., continued.

atom	<i>x</i>	<i>y</i>	<i>z</i>
H	-0.5672	4.3743	-0.9188
H	-0.3899	5.3537	-2.3903
C	2.6889	4.3493	-1.6648
H	2.6581	5.4067	-1.9594
H	2.6918	4.3091	-0.5690
H	3.6377	3.9291	-2.0225
H	2.9508	1.6506	-0.6412
H	-2.7383	1.9310	0.7075
H	1.9666	-1.0458	-1.7721
H	0.6923	0.9350	-2.5881
H	-0.5480	0.9575	2.6195
H	-2.0279	-0.8702	1.7885

Table 39. Atomic coordinates for optimized structure of Yb[1-(SiMe₃)C₃H₄]₂(tpy) (B3PW91/SDD).

atom	x	y	z
Yb	0.0000	0.0003	-1.1099
N	0.7076	2.1347	-0.2149
N	0.0000	0.0003	1.2560
C	2.5200	-1.0330	-1.0164
C	2.4304	-0.2755	-2.2125
C	1.5370	-0.4740	-3.2726
C	1.0565	3.1718	-1.0183
H	1.0180	2.9836	-2.0881
C	1.4466	4.4176	-0.5285
H	1.7169	5.2154	-1.2118
C	1.4767	4.6011	0.8695
H	1.7718	5.5555	1.2950
C	1.1237	3.5387	1.7044
H	1.1468	3.6755	2.7792
C	0.7404	2.2996	1.1460
C	0.3640	1.1292	1.9548
C	0.3730	1.1491	3.3580
H	0.6636	2.0419	3.8991
C	-0.0002	0.0004	4.0701
H	-0.0003	0.0005	5.1551
N	-0.7072	-2.1343	-0.2148
C	-1.0559	-3.1714	-1.0182
H	-1.0174	-2.9833	-2.0880
C	-1.4458	-4.4173	-0.5283
H	-1.7160	-5.2152	-1.2116
C	-1.4761	-4.6007	0.8697
H	-1.7710	-5.5551	1.2952
C	-1.1233	-3.5382	1.7045
H	-1.1465	-3.6749	2.7793
C	-0.7402	-2.2991	1.1461
C	-0.3640	-1.1286	1.9549
C	-0.3732	-1.1483	3.3580
H	-0.6640	-2.0411	3.8991
C	-2.5203	1.0324	-1.0163
C	-2.4305	0.2751	-2.2125
C	-1.5371	0.4740	-3.2725
Si	-3.9265	0.8644	0.2127
Si	3.9260	-0.8653	0.2128
C	4.4419	0.9637	0.4301

Table 39., continued.

atom	<i>x</i>	<i>y</i>	<i>z</i>
H	5.2841	1.0422	1.1306
H	4.7630	1.4035	-0.5235
H	3.6154	1.5689	0.8217
C	5.4794	-1.8231	-0.3803
H	5.8270	-1.4338	-1.3461
H	6.3034	-1.7376	0.3420
H	5.2522	-2.8892	-0.5131
C	3.4394	-1.5939	1.9102
H	2.6306	-1.0183	2.3750
H	3.0987	-2.6327	1.8038
H	4.2985	-1.5920	2.5944
C	-4.4416	-0.9649	0.4302
H	-5.2842	-1.0435	1.1302
H	-4.7620	-1.4050	-0.5235
H	-3.6151	-1.5696	0.8224
C	-5.4801	1.8215	-0.3808
H	-5.8274	1.4317	-1.3465
H	-6.3041	1.7358	0.3415
H	-5.2532	2.8876	-0.5139
C	-3.4403	1.5933	1.9101
H	-2.6310	1.0184	2.3749
H	-3.1004	2.6324	1.8036
H	-4.2994	1.5908	2.5943
H	-3.0327	-0.6395	-2.2608
H	3.0328	0.6390	-2.2605
H	-2.0196	2.0112	-1.0318
H	-1.0341	1.4348	-3.4034
H	1.0338	-1.4347	-3.4038
H	2.0192	-2.0118	-1.0322
H	1.5414	0.1761	-4.1425
H	-1.5412	-0.1758	-4.1425

Table 40. Atomic coordinates for optimized structure of Yb(C₅Me₅)₂(tpy) (B3PW91/SDD).

atom	x	y	z
Yb	0.0000	0.0000	0.4102
N	1.5100	-1.6761	-0.6059
N	0.0000	0.0000	-2.0644
C	2.5655	0.6752	1.4517
C	1.6392	1.1194	2.4452
C	0.8917	2.2174	1.9010
C	1.3516	2.4409	0.5616
C	2.3715	1.4722	0.2769
C	3.7481	-0.2194	1.7174
H	4.5996	0.3699	2.0944
H	4.0992	-0.7351	0.8152
H	3.5361	-0.9805	2.4805
C	1.6550	0.7065	3.8946
H	2.4976	1.1739	4.4295
H	1.7628	-0.3790	4.0236
H	0.7387	1.0078	4.4128
C	0.0000	3.1266	2.7119
H	0.5790	3.6641	3.4786
H	-0.7954	2.5862	3.2469
H	-0.4761	3.8914	2.0873
C	1.0189	3.6112	-0.3269
H	1.8002	4.3853	-0.2693
H	0.0738	4.0904	-0.0462
H	0.9386	3.3228	-1.3843
C	3.2315	1.4450	-0.9600
H	4.1007	2.1156	-0.8644
H	2.6780	1.7680	-1.8515
H	3.6257	0.4409	-1.1631
C	2.2267	-2.5182	0.1767
H	2.1167	-2.3801	1.2434
C	3.0668	-3.5112	-0.3302
H	3.6153	-4.1560	0.3482
C	3.1806	-3.6418	-1.7268
H	3.8243	-4.3985	-2.1650
C	2.4453	-2.7805	-2.5437
H	2.5208	-2.8750	-3.6204
C	1.6092	-1.8033	-1.9610
C	0.7880	-0.8766	-2.7625
C	0.8071	-0.8946	-4.1687

Table 40., continued.

atom	<i>x</i>	<i>y</i>	<i>z</i>
H	1.4378	-1.5907	-4.7073
C	0.0000	0.0000	-4.8799
H	0.0000	0.0000	-5.9653
N	-1.5100	1.6761	-0.6059
C	-2.2267	2.5182	0.1767
H	-2.1167	2.3801	1.2434
C	-3.0668	3.5112	-0.3302
H	-3.6153	4.1560	0.3482
C	-3.1806	3.6418	-1.7268
H	-3.8243	4.3985	-2.1650
C	-2.4453	2.7805	-2.5437
H	-2.5208	2.8750	-3.6204
C	-1.6092	1.8033	-1.9610
C	-0.7880	0.8766	-2.7625
C	-0.8071	0.8946	-4.1687
H	-1.4378	1.5907	-4.7073
C	-2.5655	-0.6752	1.4517
C	-1.6392	-1.1194	2.4452
C	-0.8917	-2.2174	1.9010
C	-1.6550	-0.7065	3.8946
H	-2.4976	-1.1739	4.4295
H	-1.7628	0.3790	4.0236
H	-0.7387	-1.0078	4.4128
C	-1.3516	-2.4409	0.5616
C	-2.3715	-1.4722	0.2769
C	-3.7481	0.2194	1.7174
H	-4.5996	-0.3699	2.0944
H	-4.0992	0.7351	0.8152
H	-3.5361	0.9805	2.4805
C	-1.0189	-3.6112	-0.3269
H	-1.8002	-4.3853	-0.2693
H	-0.0738	-4.0904	-0.0462
H	-0.9386	-3.3228	-1.3843
C	-3.2315	-1.4450	-0.9600
H	-4.1007	-2.1156	-0.8644
H	-2.6780	-1.7680	-1.8515
H	-3.6257	-0.4409	-1.1631
C	0.0000	-3.1266	2.7119
H	-0.5790	-3.6641	3.4786
H	0.7954	-2.5862	3.2469
H	0.4761	-3.8914	2.0873

Table 41. Atomic coordinates for optimized structure of $Y(C_5H_5)_2(OC_6H_5)$ (C,H,O: B3PW91/6-311G(d,p); Y: B3PW91/DGDZVP).

atom	x	y	z
O	0.0000	0.0000	-1.1343
C	-1.7152	0.4652	2.9330
C	-1.8605	-0.9032	2.6140
C	-2.4301	-0.9914	1.3160
C	-2.6349	0.3199	0.8363
C	-2.1807	1.2221	1.8293
C	2.1807	-1.2221	1.8293
C	2.6349	-0.3199	0.8363
C	2.4301	0.9914	1.3160
C	1.8605	0.9032	2.6140
C	1.7152	-0.4652	2.9330
C	0.0000	0.0000	-2.4636
C	-0.0021	-1.2057	-3.1826
C	-0.0021	-1.1992	-4.5716
C	0.0000	0.0000	-5.2785
C	0.0021	1.1992	-4.5716
C	0.0021	1.2057	-3.1826
H	0.0000	0.0000	-6.3629
Y	0.0000	0.0000	0.9471
H	2.6884	1.9033	0.7928
H	0.0043	2.1443	-5.1066
H	0.0040	2.1401	-2.6303
H	-0.0040	-2.1401	-2.6303
H	-0.0043	-2.1443	-5.1066
H	1.3343	-0.8645	3.8628
H	1.6226	1.7367	3.2617
H	3.0503	-0.5864	-0.1257
H	-1.3343	0.8645	3.8628
H	-1.6226	-1.7367	3.2617
H	-2.6884	-1.9033	0.7928
H	-3.0503	0.5864	-0.1257
H	-2.2310	2.3027	1.7757
H	2.2310	-2.3027	1.7757

Table 42. Atomic coordinates for optimized structure of $Y(C_5H_5)_2(OC_6H_3(t-Bu)_2)$
(C,H,O: B3PW91/6-311G(d,p); Y: B3PW91/DGDZVP).

atom	<i>x</i>	<i>y</i>	<i>z</i>
O	-0.4664	-0.1043	-0.2104
C	3.4496	0.2394	1.9340
C	2.9215	-1.0653	2.0695
C	1.5779	-0.9491	2.5093
C	1.2740	0.4221	2.6356
C	2.4293	1.1588	2.2715
C	2.6641	-1.5315	-1.8904
C	1.8626	-0.5898	-2.5807
C	2.4568	0.6801	-2.4253
C	3.6353	0.5257	-1.6483
C	3.7675	-0.8430	-1.3301
C	-1.7771	0.0724	-0.0940
C	-2.6436	-1.0543	0.0008
C	-4.0077	-0.8196	0.1815
C	-4.5418	0.4556	0.2464
C	-3.6923	1.5398	0.1147
C	-2.3151	1.3922	-0.0584
C	-2.2296	-2.5450	-0.0759
C	-1.5246	2.7137	-0.2297
H	-5.6070	0.6024	0.3887
C	-2.6055	-3.2391	1.2491
H	-3.6757	-3.1758	1.4587
H	-2.3343	-4.3001	1.2128
H	-2.0765	-2.7807	2.0900
C	-3.0018	-3.2130	-1.2341
H	-2.7484	-4.2771	-1.2935
H	-4.0841	-3.1366	-1.1116
H	-2.7426	-2.7475	-2.1896
C	-0.7441	-2.8461	-0.3290
H	-0.3851	-2.3862	-1.2499
H	-0.1163	-2.5178	0.5029
H	-0.6235	-3.9316	-0.4203
C	-1.7791	3.6310	0.9842
H	-1.2348	4.5750	0.8690
H	-2.8363	3.8737	1.1046
H	-1.4426	3.1537	1.9093
C	0.0040	2.6102	-0.3714
H	0.4587	2.2270	0.5528
H	0.2876	2.0159	-1.2433

Table 42., continued.

atom	<i>x</i>	<i>y</i>	<i>z</i>
H	0.4134	3.6156	-0.5161
C	-2.0225	3.4163	-1.5106
H	-3.0945	3.6194	-1.4700
H	-1.5049	4.3718	-1.6525
H	-1.8377	2.7921	-2.3899
H	-4.6809	-1.6651	0.2756
H	-4.1201	2.5363	0.1461
Y	1.6058	-0.0160	0.0163
H	0.9076	-1.7682	2.7326
H	3.4613	-1.9900	1.9136
H	4.4592	0.4907	1.6396
H	0.3277	0.8327	2.9599
H	2.5319	2.2363	2.2995
H	4.5754	-1.2904	-0.7679
H	2.4901	-2.5988	-1.8414
H	4.3333	1.3108	-1.3889
H	2.1031	1.6049	-2.8618
H	0.9535	-0.8040	-3.1252

Table 43. Atomic coordinates for optimized structure of $Y[N(\text{SiMe}_3)_2]_3$ (C,H,N,Si: B3PW91/6-311G(d,p); Y: B3PW91/DGDZVP).

atom	x	y	z
Y	0.0000	0.0000	0.3998
N	-0.9965	1.9546	-0.0373
Si	-0.4591	3.1367	1.1121
C	0.6236	2.1912	2.3738
C	0.6028	4.5144	0.3896
C	-1.8428	3.9390	2.1142
N	2.1910	-0.1143	-0.0373
N	-1.1944	-1.8403	-0.0373
Si	2.9460	-1.1708	1.1121
Si	-2.4869	-1.9660	1.1121
Si	-2.2138	2.2552	-1.2502
Si	3.0600	0.7896	-1.2502
Si	-0.8461	-3.0448	-1.2502
C	1.5858	-1.6357	2.3738
C	3.6082	-2.7793	0.3896
C	4.3327	-0.3736	2.1142
C	-2.2094	-0.5555	2.3738
C	-4.2110	-1.7352	0.3896
C	-2.4899	-3.5654	2.1142
C	-2.1996	0.8513	-2.5105
C	-3.9524	2.3614	-0.5131
C	-1.9273	3.8660	-2.1976
C	1.8370	1.4793	-2.5105
C	4.0212	2.2422	-0.5131
C	4.3117	-0.2639	-2.1976
C	0.3626	-2.3306	-2.5105
C	-0.0688	-4.6036	-0.5131
C	-2.3844	-3.6021	-2.1976
H	1.5028	1.6949	1.9382
H	1.0333	2.9134	3.0875
H	0.0546	1.4783	2.9868
H	1.4308	4.1156	-0.2018
H	0.0162	5.1638	-0.2662
H	1.0255	5.1413	1.1823
H	-2.4918	3.1923	2.5812
H	-2.4727	4.5815	1.4914
H	-1.4251	4.5667	2.9090
H	0.7164	-2.1489	1.9382
H	2.0064	-2.3516	3.0875

Table 43., continued.

atom	<i>x</i>	<i>y</i>	<i>z</i>
H	1.2530	-0.7864	2.9868
H	2.8489	-3.2969	-0.2018
H	4.4639	-2.5960	-0.2662
H	3.9397	-3.4588	1.1823
H	4.0105	0.5618	2.5812
H	5.2041	-0.1493	1.4914
H	4.6674	-1.0492	2.9090
H	-2.2192	0.4540	1.9382
H	-3.0398	-0.5618	3.0875
H	-1.3075	-0.6919	2.9868
H	-4.2796	-0.8187	-0.2018
H	-4.4801	-2.5679	-0.2662
H	-4.9652	-1.6825	1.1823
H	-1.5187	-3.7542	2.5812
H	-2.7313	-4.4322	1.4914
H	-3.2423	-3.5175	2.9090
H	-3.0266	0.9713	-3.2185
H	-1.2725	0.8479	-3.0924
H	-2.3118	-0.1295	-2.0374
H	-4.7024	2.4379	-1.3081
H	-4.1967	1.4811	0.0883
H	-4.0662	3.2389	0.1299
H	-2.6674	3.9618	-2.9998
H	-0.9346	3.8984	-2.6561
H	-2.0304	4.7476	-1.5572
H	2.3544	2.1354	-3.2185
H	1.3706	0.6781	-3.0924
H	1.0438	2.0669	-2.0374
H	4.4625	2.8535	-1.3081
H	3.3810	2.8938	0.0883
H	4.8381	1.9020	0.1299
H	4.7647	0.3292	-2.9998
H	3.8435	-1.1398	-2.6561
H	5.1268	-0.6154	-1.5572
H	0.6721	-3.1067	-3.2185
H	-0.0981	-1.5260	-3.0924
H	1.2681	-1.9374	-2.0374
H	0.2399	-5.2913	-1.3081
H	0.8156	-4.3750	0.0883
H	-0.7719	-5.1409	0.1299
H	-2.0973	-4.2909	-2.9998
H	-2.9088	-2.7586	-2.6561
H	-3.0963	-4.1322	-1.5572

Table 44. Atomic coordinates for optimized structure of Y(thd)₃ (C,H,O: B3PW91/6-311G(d,p); Y: B3PW91/DGDZVP).

atom	x	y	z
Y	0.0139	0.0011	-0.0169
O	1.9043	0.2824	-1.2131
O	1.6723	-0.9268	1.2381
O	-0.6621	-1.8255	-1.1741
O	-1.6337	-0.9284	1.2371
C	3.1415	0.0047	-1.0877
C	3.6778	-0.6546	0.0237
C	2.9236	-1.0850	1.1340
C	4.0263	0.4574	-2.2593
C	3.6427	-1.7853	2.3012
C	-1.5289	-2.7420	-1.0321
C	-2.4023	-1.9338	1.1514
C	-1.6320	-3.7875	-2.1576
C	-2.3887	-2.8342	0.0735
C	-3.3972	-2.1564	2.3055
C	4.3491	-3.0514	1.7852
C	4.6802	-0.8223	2.9066
C	3.4837	-0.2124	-3.5340
C	5.5060	0.1051	-2.0927
C	-0.5155	-3.5679	-3.1819
C	-1.5112	-5.2073	-1.5787
C	-2.9967	-3.6253	-2.8528
C	-3.2263	-1.0639	3.3642
C	-3.1340	-3.5295	2.9488
C	-4.8342	-2.1078	1.7569
O	-1.2154	1.4496	-1.2293
C	-1.5940	2.6629	-1.1357
C	-2.4622	3.1583	-2.3020
C	-1.6445	2.9817	-3.5937
C	-2.8978	4.6200	-2.1754
C	-3.7100	2.2593	-2.3614
C	-1.2600	3.4973	-0.0636
C	-0.4686	3.1038	1.0347
O	0.0246	1.9460	1.1674
C	-0.1777	4.1231	2.1509
C	0.7293	3.4948	3.2121
C	0.5214	5.3575	1.5548
C	-1.5065	4.5439	2.8049
C	2.6313	-2.1784	3.3810

Table 44., continued.

atom	x	y	z
C	3.8786	1.9844	-2.3833
H	4.7396	-0.8453	0.0396
H	-3.0909	-3.6556	0.0965
H	4.8333	-3.5693	2.6195
H	3.6345	-3.7426	1.3287
H	5.1169	-2.8214	1.0427
H	4.2035	0.0961	3.2612
H	5.1721	-1.2989	3.7607
H	5.4532	-0.5447	2.1859
H	2.4305	0.0331	-3.6787
H	4.0480	0.1319	-4.4064
H	3.5774	-1.3014	-3.4779
H	6.0649	0.4591	-2.9643
H	5.9415	0.5803	-1.2089
H	5.6627	-0.9751	-2.0191
H	-0.5988	-4.3115	-3.9808
H	-0.5725	-2.5728	-3.6266
H	0.4707	-3.6651	-2.7221
H	-0.5659	-5.3360	-1.0437
H	-2.3242	-5.4442	-0.8884
H	-1.5410	-5.9403	-2.3914
H	-3.8271	-3.8077	-2.1661
H	-3.1112	-2.6172	-3.2612
H	-3.0788	-4.3370	-3.6808
H	-3.4073	-0.0723	2.9445
H	-3.9361	-1.2305	4.1803
H	-2.2158	-1.0657	3.7777
H	-3.8107	-3.6771	3.7969
H	-3.2942	-4.3502	2.2454
H	-2.1076	-3.5996	3.3203
H	-5.0378	-1.1483	1.2725
H	-5.0231	-2.8997	1.0281
H	-5.5488	-2.2297	2.5775
H	-2.2505	3.2613	-4.4612
H	-0.7522	3.6154	-3.5852
H	-1.3263	1.9443	-3.7084
H	-2.0416	5.3004	-2.1505
H	-3.5089	4.8933	-3.0410
H	-3.5028	4.7904	-1.2800
H	-4.3200	2.3714	-1.4595
H	-4.3269	2.5320	-3.2235
H	-3.4238	1.2103	-2.4532
H	-1.6295	4.5109	-0.0736

Table 44., continued.

atom	<i>x</i>	<i>y</i>	<i>z</i>
H	1.6819	3.1770	2.7828
H	0.9319	4.2258	4.0010
H	0.2643	2.6165	3.6639
H	0.7626	6.0665	2.3533
H	1.4553	5.0794	1.0577
H	-0.1065	5.8752	0.8260
H	-1.3116	5.2473	3.6210
H	-2.1772	5.0319	2.0936
H	-2.0291	3.6786	3.2227
H	2.1073	-1.3042	3.7725
H	1.8773	-2.8641	2.9886
H	3.1509	-2.6717	4.2083
H	4.2667	2.4911	-1.4940
H	4.4400	2.3455	-3.2508
H	2.8300	2.2602	-2.5056

Table 45. Atomic coordinates for optimized structure of $V_2[\mu-(C_3H_5)]_3Cl$ (B3PW91/DGDZVP2).

atom	x	y	z
V	1.0827	0.0447	0.0842
V	-1.3978	0.2202	-0.1270
Cl	3.0345	-0.9767	-0.4252
C	-0.3405	0.6551	1.8285
C	-2.7665	-1.4255	-0.9366
C	0.9233	-0.0171	2.1020
C	-1.6666	-2.0233	-0.3613
C	0.0432	1.5802	-1.2637
C	1.2800	1.9617	-0.5886
C	-1.2794	2.1005	-0.9194
C	-0.3068	-1.6556	-0.7197
C	-1.6609	0.0520	1.8839
H	1.2034	2.7480	0.1630
H	-0.1275	-1.5938	-1.7978
H	-1.8230	-2.6283	0.5293
H	-2.6778	-0.9309	-1.9104
H	-1.3181	2.9465	-0.2334
H	0.1587	1.2033	-2.2829
H	-0.3108	1.7422	1.8862
H	-1.7659	-0.9290	2.3458
H	0.8831	-1.0385	2.4860
H	0.4427	-2.2915	-0.2412
H	-3.7744	-1.6400	-0.5974
H	-1.9815	2.1897	-1.7550
H	-2.4803	0.7386	2.1279
H	1.7082	0.5902	2.5563
H	2.1694	2.0371	-1.2144

Table 46. Atomic coordinates for optimized structure of $V_2[\mu\text{-}\{1,3\text{-(SiH}_3\text{)}_2\text{C}_3\text{H}_3\}\text{]}_3\text{Cl}$ (B3PW91/DGDZVP2).

atom	x	y	z
V	-1.3755	0.0705	0.0854
V	1.0625	-0.2744	0.0880
Cl	-3.2816	0.6179	1.1783
C	0.1034	1.5677	-0.8177
C	0.9094	-2.1223	-0.6689
C	-1.2116	1.4489	-1.4411
C	-0.3547	-1.5642	-1.1520
C	1.3416	-0.0726	2.1946
C	-0.1108	0.0103	2.0152
C	2.2683	0.8879	1.8040
C	-1.6947	-1.8069	-0.6270
C	1.3557	1.0810	-1.4077
H	-0.4731	1.0380	2.1516
H	-1.7414	-2.4675	0.2460
H	-0.3222	-1.2120	-2.1850
H	0.8200	-2.7426	0.2358
H	1.8954	1.8882	1.5794
H	1.7356	-1.0365	2.5347
H	0.2073	2.3783	-0.0892
H	1.1908	0.5439	-2.3498
H	-1.1961	0.9453	-2.4115
Si	-2.3939	2.9018	-1.3682
Si	2.8424	2.2077	-1.5195
Si	-1.0537	-1.1863	3.1552
Si	4.1033	0.6651	2.0916
Si	-3.1358	-2.0232	-1.8042
Si	2.2331	-2.6876	-1.8675
H	-4.4242	-1.9427	-1.0725
H	-3.0893	-0.9708	-2.8574
H	-3.7940	2.4778	-1.6195
H	-2.0250	3.9075	-2.4113
H	-2.2827	3.5667	-0.0415
H	-3.0599	-3.3459	-2.4929
H	2.7152	3.1348	-2.6814
H	2.9676	3.0386	-0.2899
H	4.9025	1.0141	0.8896
H	4.5590	1.5235	3.2197
H	-0.0381	-2.1302	3.7123
H	4.3377	-0.7646	2.4388

Table 46., continued.

atom	x	y	z
H	4.0942	1.4242	-1.7040
H	-2.0939	-2.0091	2.4936
H	-1.6670	-0.4189	4.2683
H	2.1090	-4.1430	-2.1554
H	2.0919	-1.9261	-3.1382
H	3.5946	-2.4498	-1.3099

Table 47. Atomic coordinates for optimized structure of $V_2[\mu\text{-}\{1,3\text{-(SiMe}_3\text{)}_2\text{C}_3\text{H}_3\}]_3\text{Cl}$ (B3PW91/DGDZVP2).

atom	<i>x</i>	<i>y</i>	<i>z</i>
C	1.1733	2.3526	-0.2963
C	2.3990	3.0750	-3.0692
C	1.8457	5.1980	-0.9192
C	4.1794	3.3147	-0.5307
C	-1.8947	-1.2955	-1.0458
C	-0.5561	-1.8437	-0.7990
C	0.5948	-1.8575	-1.6621
C	-3.2061	-3.5173	0.7066
C	-4.9433	-1.2392	-0.4232
C	-3.7772	-3.3410	-2.3081
C	3.0142	-3.1587	-3.1107
C	0.3587	-4.6438	-2.8797
C	2.0772	-4.2942	-0.3858
C	-1.3506	1.9956	-0.4102
C	0.0415	1.6904	-0.8948
C	-2.8060	1.7771	-3.1771
C	-2.0799	4.5098	-2.0292
C	-4.2790	2.8605	-0.6815
C	-1.0712	-0.3354	2.1175
C	0.3456	-0.0829	1.7877
C	1.3991	-1.0669	1.5666
C	-3.7633	0.7579	3.2110
C	-1.1504	2.2775	3.8005
C	-1.6918	-0.4473	5.1135
C	2.7588	-1.4539	4.2779
C	4.4064	-1.9302	1.7537
C	3.5789	0.9258	2.5297
Cl	3.1693	-0.0342	-1.3569
H	1.4077	3.2537	-3.4983
H	2.6962	2.0462	-3.2860
H	3.1004	3.7447	-3.5784
H	1.8423	5.4380	0.1493
H	0.8385	5.3725	-1.3071
H	2.5242	5.9021	-1.4143
H	4.1989	3.5517	0.5374
H	4.8110	4.0490	-1.0432
H	4.6118	2.3232	-0.6771
H	1.0318	2.6139	0.7565
H	-1.9531	-0.7502	-2.0002

Table 47., continued.

atom	x	y	z
H	-0.5205	-2.5712	0.0165
H	0.4572	-1.2740	-2.5855
H	-3.0557	-2.9909	1.6537
H	-2.3587	-4.1917	0.5524
H	-4.1011	-4.1387	0.8172
H	-4.8396	-0.6634	0.5013
H	-5.8495	-1.8479	-0.3349
H	-5.1024	-0.5345	-1.2455
H	-3.9600	-2.6851	-3.1653
H	-4.6609	-3.9752	-2.1787
H	-2.9297	-3.9856	-2.5565
H	3.7533	-2.5096	-2.6364
H	2.7025	-2.6810	-4.0452
H	3.4924	-4.1109	-3.3660
H	-0.4874	-4.9204	-2.2424
H	0.8802	-5.5659	-3.1598
H	-0.0412	-4.1956	-3.7951
H	2.8003	-3.6795	0.1539
H	2.5502	-5.2562	-0.6105
H	1.2307	-4.4943	0.2794
H	-1.3344	2.5451	0.5452
H	0.1132	1.5495	-1.9789
H	-1.8392	1.5805	-3.6512
H	-3.4043	2.3539	-3.8904
H	-3.3118	0.8199	-3.0243
H	-1.1616	4.5016	-2.6234
H	-1.8992	5.1157	-1.1362
H	-2.8563	5.0066	-2.6211
H	-4.1990	3.4646	0.2281
H	-4.6509	1.8714	-0.4009
H	-5.0321	3.3308	-1.3226
H	-1.3270	-1.4061	2.1117
H	0.6928	0.9057	2.0956
H	1.0302	-2.0985	1.5917
H	-4.2373	-0.2151	3.0459
H	-3.9577	1.3823	2.3335
H	-4.2623	1.2237	4.0675
H	-1.2334	2.9166	2.9161
H	-0.0929	2.2100	4.0723
H	-1.6673	2.7878	4.6201
H	-2.1438	-1.4388	5.0084
H	-2.1669	0.0475	5.9676
H	-0.6331	-0.5876	5.3495

Table 47., continued.

atom	<i>x</i>	<i>y</i>	<i>z</i>
H	2.0103	-0.8379	4.7865
H	3.6899	-1.3917	4.8522
H	2.4159	-2.4934	4.3119
H	4.1936	-2.9992	1.8515
H	5.3469	-1.7343	2.2803
H	4.5528	-1.6968	0.6959
H	2.8566	1.5693	3.0425
H	3.7248	1.3048	1.5155
H	4.5316	1.0146	3.0628
Si	-3.4436	-2.3374	-0.7452
Si	1.5381	-3.4585	-1.9863
Si	-2.6240	2.7602	-1.5773
Si	2.4320	3.4177	-1.2184
Si	-1.9146	0.5719	3.5411
Si	3.0317	-0.8772	2.4929
V	-1.2173	0.1293	0.1853
V	1.1048	-0.2916	-0.3537

REFERENCES

- (1) Wilke, G.; Bogdanovic, B. *Angew. Chem.* **1961**, 73, 756.
- (2) Wilke, G.; Bogdanovic, B.; Hardt, P.; Heimbach, P.; Keim, W.; Kroner, M.; Oberkirch, W.; Tanaka, K.; Walter, D. *Angew. Chem., Int. Ed. Engl.* **1966**, 5, 151-164.
- (3) Wilke, G.; Bogdanovic, B.; Hardt, P.; Heimbach, P.; Keim, W.; Kroner, M.; Oberkirch, W.; Tanaka, K.; Walter, D.; Zimmermann, H. *Angew. Chem., Int. Ed. Engl.* **1966**, 5, 151-266.
- (4) Grosselin, J. M.; Dixneuf, P. H. *J. Organomet. Chem.* **1986**, 314, C76-C80.
- (5) Gabor, B.; Holle, S.; Jolly, P. W.; Mynott, R. *J. Organomet. Chem.* **1994**, 466, 201-9.
- (6) Fraenkel, G.; Chow, A.; Winchester, W. R. *J. Am. Chem. Soc.* **1990**, 112, 1382-1386.
- (7) Harvey, M. J.; Hanusa, T. P.; Young, V. G., Jr. *Angew. Chem. Int. Ed.* **1999**, 38, 217-219.
- (8) Quisenberry, K. T. Ph.D. Dissertation, Vanderbilt University, 2005.
- (9) Gren, C. K.; Hanusa, T. P.; Brennessel, W. W. *Polyhedron* **2006**, 25, 286-292.
- (10) Boche, G.; Fraenkel, G.; Cabral, J.; Harms, K.; Van Eikema Hommes, N. J. R.; Lohrenz, J.; Marsch, M.; Schleyer, P. v. R. *J. Am. Chem. Soc.* **1992**, 114, 1562-1565.
- (11) Carlson, C. N. Ph.D. Dissertation, Vanderbilt University, 2004.
- (12) Quisenberry, K. T.; Smith, J. D.; Voehler, M.; Stec, D. F.; Hanusa, T. P.; Brennessel, W. W. *J. Am. Chem. Soc.* **2005**, 127, 4376-4387.
- (13) Smith, J. D.; Hanusa, T. P.; Young, V. G., Jr. *J. Am. Chem. Soc.* **2001**, 123, 6455-6456.
- (14) Smith, J. D.; Quisenberry, K. T.; Hanusa, T. P.; Brennessel, W. W. *Acta Crystallogr., Sect. C.* **2004**, 60, m507-m508.
- (15) Carlson, C. N.; Smith, J. D.; Hanusa, T. P.; Brennessel, W. W.; Young, V. G., Jr. *J. Organomet. Chem.* **2003**, 683, 191-199.

- (16) Schormann, M.; Garratt, S.; Bochmann, M. *Organometallics* **2005**, 24, 1718-1724.
- (17) Layfield, R. A.; Humphrey, S. M. *Angew. Chem.* **2004**, 43, 3067-3069.
- (18) Kuehl, C. J.; Simpson, C. K.; John, K. D.; Sattelberger, A. P.; Carlson, C. N.; Hanusa, T. P. *J. Organomet. Chem.* **2003**, 683, 149-154.
- (19) Simpson, C. K.; White, R. E.; Carlson, C. N.; Wroblewski, D. A.; Kuehl, C. J.; Croce, T. A.; Steele, I. M.; Scott, B. L.; Hanusa, T. P.; Sattelberger, A. P.; John, K. D. *Organometallics* **2005**, 24, 3685-3691.
- (20) Woodman, T. J.; Schormann, M.; Hughes, D. L.; Bochmann, M. *Organometallics* **2004**, 23, 2972-2979.
- (21) Woodman, T. J.; Schormann, M.; Bochmann, M. *Isr. J. Chem.* **2003**, 42, 283-293.
- (22) Ihara, E.; Koyama, K.; Yasuda, H.; Kanehisa, N.; Kai, Y. *J. Organomet. Chem.* **1999**, 574, 40-49.
- (23) Carlson, C. N.; Hanusa, T. P.; Brennessel, W. W. *J. Am. Chem. Soc.* **2004**, 126, 10550-10551.
- (24) Williams, R. A.; Hanusa, T. P.; Huffman, J. C. *Organometallics* **1990**, 9, 1128-1134.
- (25) Schultz, M.; Burns, C. J.; Schwartz, D. J.; Andersen, R. A. *Organometallics* **2000**, 19, 781-789.
- (26) Schultz, M.; Boncella, J. M.; Berg, D. J.; Tilley, T. D.; Andersen, R. A. *Organometallics* **2002**, 21, 460-472.
- (27) Veauthier, J. M.; Schelter, E. J.; Kuehl, C. J.; Clark, A. E.; Scott, B. L.; Morris, D. E.; Martin, R. L.; Thompson, J. D.; Kiplinger, J. L.; John, K. D. *Inorg. Chem.* **2005**, 44, 5911-5920.
- (28) Harder, S. *Angew. Chem., Int. Ed.* **2004**, 43, 2714-2718.
- (29) Pregosin, P. S. *Transition Metal Nuclear Magnetic Resonance*; Elsevier Science Publishing Company Inc.: New York, **1991**.
- (30) Shannon, R. D. *Acta Crystallogr., Sect. A.* **1976**, 32, 751-767.
- (31) Zachariasen, W. H. *Acta Cryst.* **1948**, 1, 265-268.

- (32) Forrester, J. D.; Zalkin, A.; Templeton, D. H.; Wallmann, J. C. *Inorg. Chem.* **1964**, 3, 185-188.
- (33) Templeton, D. H.; Carter, G. F. *J. Phys. Chem.* **1954**, 58, 940-944.
- (34) Morosin, B. *J. Chem. Phys.* **1968**, 49, 3007-3012.
- (35) Schumann, H.; Meese-Marktscheffel, J. A.; Esser, L. *Chem. Rev.* **1995**, 95, 865-986.
- (36) Woodman, T. J.; Schormann, M.; Hughes, D. L.; Bochmann, M. *Organometallics* **2003**, 22, 3028-3030.
- (37) Evans, D. F. *J. Chem. Soc.* **1959**, 2003-2005.
- (38) Grant, D. H. *J. Chem. Educ.* **1995**, 72, 39-40.
- (39) O'Hare, D.; Green, J. C.; Marder, T.; Collins, S.; Stringer, G.; Kakkar, A. K.; Kaltsoyannis, N.; Kuhn, A.; Lewis, R.; Mehnert, C.; Scott, P.; Kurmoo, M.; Pugh, S. *Organometallics* **1992**, 11, 48-55.
- (40) Sur, S. K. *J. Magn. Reson.* **1989**, 82, 169-173.
- (41) Schwarzenbach, G.; Flaschka, H. *Complexometric Titrations*; 2nd ed.; Methuen: London, **1969**.
- (42) Perrin, D. D.; Armarego, W. L. F. *Purification of Laboratory Chemicals*; 3rd ed.; Pergamon: Oxford, **1988**.
- (43) SHELXTL, V6.14; Bruker Analytical X-ray Systems: Madison, WI, 2000.
- (44) SMART, V5.054; Bruker Analytical X-ray Systems: Madison, WI, 2001.
- (45) Blessing, R. H. *Acta Crystallogr.* **1995**, A51, 33-38.
- (46) SAINT+, V6.45; Bruker Analytical X-ray Systems: Madison, WI, 2003.
- (47) Evans, W. J.; Lee, D. S.; Rego, D. B.; Perotti, J. M.; Kozimor, S. A.; Moore, E. K.; Ziller, J. W. *J. Am. Chem. Soc.* **2004**, 126, 14574-14582.
- (48) Gehrhus, B.; Hitchcock, P. B.; Zhang, L. *Angew. Chem., Int. Ed.* **2004**, 43, 1124-1126.
- (49) Nakata, N.; Izumi, R.; Ya, V.; Ichinohe, M.; Sekiguchi, A. *J. Am. Chem. Soc.* **2004**, 126, 5058-5059.

- (50) Athimoolam, A.; Gambaroota, S.; Korobkov, I. *Organometallics* **2005**, 24, 1996-1999.
- (51) Pu, L.; Phillips, A. D.; Richards, A. F.; Stender, M.; Simons, R. S.; Olmstead, M. M.; Power, P. P. *J. Am. Chem. Soc.* **2003**, 125, 11626-11636.
- (52) Sockwell, S. C.; Hanusa, T. P. *Inorg. Chem.* **1990**, 29, 76-80.
- (53) Raymond, K. N.; Eigenbrot, C. W. *Acc. Chem. Res.* **1980**, 13, 276-283.
- (54) Atwood, J. L.; Hunter, W. E.; Wayda, A. L.; Evans, W. J. *Inorg. Chem.* **1981**, 1981, 4115-4119.
- (55) Williams, R. A.; Tesh, K. F.; Hanusa, T. P. *J. Am. Chem. Soc.* **1991**, 113, 4843-4851.
- (56) Harvey, M. J.; Hanusa, T. P.; Young, V., G., Jr. *J. Organomet. Chem.* **2001**, 626, 43-48.
- (57) Corradi, M. M.; Frankland, A. D.; Hitchcock, P. B.; Lappert, M. F.; Lawless, G. A. *Chem. Commun.* **1996**, 2323-2324.
- (58) Schumann, H.; Mueller, J.; Bruncks, N.; Lauke, H.; Pickardt, J.; Schwarz, H.; Eckart, K. *Organometallics* **1984**, 3, 69-74.
- (59) Kornienko, A.; Freedman, D.; Emge, T. J.; Brennan, J. G. *Inorg. Chem.* **2001**, 40, 140-145.
- (60) Kobayashi, S. *Synlett* **1994**, 689-701.
- (61) Horáček, M.; Hiller, J.; Thewalt, U.; Polásek, M.; Mach, K. *Organometallics* **1997**, 16, 4185-4191.
- (62) Poole, J. A.; Lobkovsky, E.; Chirik, P. J. *J. Am. Chem. Soc.* **2003**, 125, 2241-2251.
- (63) Morss, L. R. *Chem. Rev.* **1976**, 76, 827-841.
- (64) Meyer, G.; Wickleder, M. S. In *Handbook on the Physics and Chemistry of Rare Earths*; Gschneider, K. A., Jr., Eyring, L., Eds.; Elsevier Science B. V.: Amsterdam, **2000**; Vol. 28, p 53-129.
- (65) Choukroun, R.; Wolff, F.; Lorber, C.; Donnadiou, B. *Organometallics* **2003**, 22, 2245-2248.

- (66) Skinner, M. E. G.; Toupance, T.; Cowhig, D. A.; Tyrrell, B. R.; Mountford, P. *Organometallics* **2005**, 24, 5586-5603.
- (67) Eisenstadt, A.; Efraty, A. *Organometallics* **1982**, 1, 1100-1101.
- (68) Frisch, M. J.; Trucks, G. W.; Schlegel, H. B.; Scuseria, G. E.; Robb, M. A.; Cheeseman, J. R.; J. A. Montgomery, J.; Vreven, T.; Kudin, K. N.; Burant, J. C.; Millam, J. M.; Iyengar, S. S.; Tomasi, J.; Barone, V.; Mennucci, B.; Cossi, M.; Scalmani, G.; Rega, N.; Petersson, G. A.; Nakatsuji, H.; Hada, M.; Ehara, M.; Toyota, K.; Fukuda, R.; Hasegawa, J.; Ishida, M.; Nakajima, T.; Honda, Y.; Kitao, O.; Nakai, H.; Klene, M.; Li, X.; Knox, J. E.; Hratchian, H. P.; Cross, J. B.; Adamo, C.; Jaramillo, J.; Gomperts, R.; Stratmann, R. E.; Yazyev, O.; Austin, A. J.; Cammi, R.; Pomelli, C.; Ochterski, J. W.; Ayala, P. Y.; Morokuma, K.; Voth, G. A.; Salvador, P.; Dannenberg, J. J.; Zakrzewski, V. G.; Dapprich, S.; Daniels, A. D.; Strain, M. C.; Farkas, O.; Malick, D. K.; Rabuck, A. D.; Raghavachari, K.; Foresman, J. B.; Ortiz, J. V.; Cui, Q.; Baboul, A. G.; Clifford, S.; Cioslowski, J.; Stefanov, B. B.; Liu, G.; Liashenko, A.; Piskorz, P.; Komaromi, I.; Martin, R. L.; Fox, D. J.; Keith, T.; Al-Laham, M. A.; Peng, C. Y.; Nanayakkara, A.; Challacombe, M.; Gill, P. M. W.; Johnson, B.; Chen, W.; Wong, M. W.; Gonzalez, C.; Pople, J. A. GAUSSIAN 03W, revision C.02, Gaussian, Inc.: Wallingford, CT, 2004.
- (69) Elschenbrioch, C. *Organometallics*; Wiley-VCH: Weinheim, **2005**.
- (70) Aoki, T.; Furusaki, A.; Tomie, Y.; Ono, K.; Tanaka, K. *Bull. Chem. Soc. Jpn.* **1969**, 42, 545-547.
- (71) Kuehl, C. J.; Da Re, R. E.; Scott, B. L.; Morris, D. E.; John, K. D. *Chem. Commun.* **2003**, 2336-2337.
- (72) Da Re, R. E.; Kuehl, C. J.; Brown, M. G.; Rocha, R. C.; Bauer, E. D.; John, K. D.; Morris, D. E.; Shreve, A. P.; Sarrao, J. L. *Inorg. Chem.* **2003**, 42, 5551-5559.
- (73) Veauthier, J. M.; Carlson, C. N.; Collis, G. E.; Kiplinger, J. L.; John, K. D. *Synthesis* **2005**, 2683-2686.
- (74) SHELXTL, version 5.1; Bruker Analytical X-ray Systems: Madison, WI, 1997.
- (75) SMART, version 4.210; Bruker Analytical X-ray Systems: Madison, WI, 1996.
- (76) SAINT, version 4.05; Bruker Analytical X-ray Systems: Madison, WI, 1996.
- (77) Sheldrick, G. M. SADABS, University of Göttingen: Germany, 1996.
- (78) Becke, A. D. *Phys. Rev. A* **1988**, 38, 3098-3100.

- (79) Lee, C.; Yang, W.; Parr, R. G. *Phys. Rev. B* **1988**, 37, 785-789.
- (80) John, K. D.; Salazar, K. V.; Scott, B. L.; Baker, R. T.; Sattelberger, A. P. *Organometallics* **2001**, 20, 296-304.
- (81) Ionova, G.; Rabbe, C.; Guillaumont, R.; Ionov, S.; Madic, C.; Krupa, J.-C.; Guillaneux, D. *New J. Chem.* **2002**, 26, 234-242.
- (82) Rabbe, C.; Mikhalko, V.; Dognon, J. P. *Theor. Chem. Acc.* **2000**, 104, 280-283.
- (83) Dilman, A. D.; Mayr, H. *Eur. J. Org. Chem.* **2005**, 1760-1764.
- (84) Coerver, H. J.; Curran, C. *J. Am. Chem. Soc.* **1958**, 80, 3522-3523.
- (85) Kubota, M.; Schulze, S. R. *Inorg. Chem.* **1964**, 3, 853-856.
- (86) Hendrickson, D. N.; Pierpont, C. G. In *Topics in Current Chemistry*; Springer-Verlag: Berlin, **2004**.
- (87) Schulz, D. A. In *Magnetism: Molecules to Materials II: Molecule-Based Materials*; Wiley-VCH: Weinheim, **2002**.
- (88) Maiwald, S.; Weißenborn, H.; Sommer, C.; Müller, G.; Taube, R. *J. Organomet. Chem.* **2001**, 640, 1-9.
- (89) Taube, R.; Windisch, H.; Maiwald, S.; Hemling, H.; Schumann, H. *J. Organomet. Chem.* **1996**, 513, 49-61.
- (90) Woodman, T. J.; Schormann, M.; Bochmann, M. *Organometallics* **2003**, 22, 2938-2943.
- (91) Peat, I. R.; Reynolds, W. F. *Tetrahedron Lett.* **1972**, 1359-1362.
- (92) Ober, C. K. *J. Chem. Educ.* **1989**, 66, 645-647.
- (93) McCord, E. F.; Anton, W. L.; Wilczek, L.; Ittel, S. D.; Nelson, L. T. J.; Raffell, K. D.; Hansen, J. E.; Berge, C. *Macromol. Symp.* **1994**, 86, 47-64.
- (94) Harvey, M. J. Ph.D. Dissertation, Vanderbilt University, 2000.
- (95) Pangborn, A. B.; Giardello, M. A.; Grubbs, R. H.; Rosen, R. K.; Timmers, F. J. *Organometallics* **1996**, 15, 1518-1520.
- (96) Dinnebier, R. E.; Behrens, U.; Olbrich, F. *Organometallics* **1997**, 16, 3855-3858.

- (97) Jutzi, P.; Leffers, W.; Hampel, B.; Pohl, S.; Saak, W. *Angew. Chem.* **1987**, 99, 563-4.
- (98) Harvey, M. J.; Hanusa, T. P.; Pink, M. *J. Chem. Soc., Dalton Trans.* **2001**, 1128-1130.
- (99) Parry, A. In *Reactivity, Mechanism and Structure in Polymer Chemistry*; Jenkins, A. D., Ledwith, A., Eds.; John Wiley & Sons: London, **1974**, p 350-382.
- (100) Chen, E. Y.-X. *J. Polym. Sci., Part A* **2004**, 42, 3395-3403.
- (101) Li, Y.; Deng, H.; Brittain, W.; Chisholm, M. S. *Polym. Bull. (Berlin)* **1999**, 42, 635-639.
- (102) Knjazhanski, S. Y.; Elizalde, L.; Cadenas, G.; Bulychev, B. M. *J. Polym. Sci., Part A* **1998**, 36, 1599-1606.
- (103) Harder, S.; Feil, F.; Knoll, K. *Angew. Chem. Int. Ed.* **2001**, 40, 4261-4264.
- (104) Zhou, S.-L.; Wang, S.-W.; Yang, G.-S.; Liu, X.-Y.; Sheng, E.-H.; Zhang, K.-H.; Cheng, L.; Huang, Z.-X. *Polyhedron* **2003**, 22, 1019-1024.
- (105) Boffa, L. S.; Novak, B. M. *Transition Metal Catalysis in Macromolecular Design*; Oxford University Press: Washington, DC, **2000**.
- (106) Odian, G. *Principles of Polymerization*; 3rd ed.; John Wiley & Sons, Inc.: New York, **1991**.
- (107) Yasuda, H.; Ihara, E. *Macromol. Chem. Phys.* **1995**, 196, 2417-2441.
- (108) Braun, D.; Herner, M.; Johnson, U.; Kern, W. *Makromol. Chem.* **1962**, 51, 15-38.
- (109) Bandrup, J.; Immergut, E. H.; Grulke, E. A. *Polymer Handbook*; 4th ed.; John Wiley: New York, **1998**.
- (110) Gudat, D. *Annual Reports on NMR Spectroscopy* **2003**, 51, 59-103.
- (111) Gaemers, S.; Groenevelt, J.; Elsevier, C. J. *Eur. J. Inorg. Chem.* **2001**, 829-835.
- (112) Gaemers, S.; Van Slageren, J.; O'Connor, C. M.; Vos, J. G.; Hage, R.; Elsevier, C. J. *Organometallics* **1999**, 18, 5238-5244.
- (113) Ogoma, Y.; Kobayashi, H.; Fujii, T.; Kondo, Y.; Hachimori, A.; Shimizu, T.; Hatano, M. *Int. J. Bio. Macromol.* **1992**, 14, 279-286.
- (114) Rehder, D. *Chimia* **1986**, 40, 186-199.

- (115) von Philipsborn, W. *Chem. Soc. Rev.* **1999**, 28, 95-105.
- (116) Mason, J. *Polyhedron* **1989**, 8, 1657-1668.
- (117) Adam, M.; Behrens, U.; Fischer, R. D. *Acta Crystallogr., Sect. C: Cryst. Struct. Commun.* **1991**, C47, 968-971.
- (118) Arduengo, A. J., III; Tamm, M.; McLain, S. J.; Calabrese, J. C.; Davidson, F.; Marshall, W. J. *J. Am. Chem. Soc.* **1994**, 116, 7927-7928.
- (119) Karsch, H. H.; Graf, V.; Reisky, M.; Witt, E. *Eur. J. Inorg. Chem.* **1998**, 1403-1406.
- (120) Broussier, R.; Delmas, G.; Perron, P.; Gautheron, B.; Petersen, J. L. *J. Organomet. Chem.* **1996**, 511, 185-192.
- (121) Schumann, H.; Keitsch, M. R.; Muhle, S. H. *Z. Anorg. Allg. Chem.* **2002**, 628, 1311-1318.
- (122) Schaverien, C. J. *J. Mol. Catal.* **1994**, 90, 177-184.
- (123) Voth, P.; Arndt, S.; Spaniol, T. P.; Okuda, J.; Ackerman, L. J.; Green, M. L. H. *Organometallics* **2003**, 22, 65-76.
- (124) Avent, A. G.; Caro, C. F.; Hitchcock, P. B.; Lappert, M. F.; Li, Z.; Wei, X.-H. *Dalton Trans.* **2004**, 1567-1577.
- (125) Evans, W. J.; Brady, J. C.; Ziller, J. W. *J. Am. Chem. Soc.* **2001**, 123, 7711-7712.
- (126) Woodman, T. J.; Schormann, M.; Bochmann, M. *Isr. J. Chem.* **2002**, 42, 283-293.
- (127) Arndt, S.; Spaniol, T. P.; Okuda, J. *Organometallics* **2003**, 22, 775-781.
- (128) Evans, W. J.; Meadows, J. H.; Wayda, A. L.; Hunter, W. E.; Atwood, J. L. *J. Am. Chem. Soc.* **1982**, 104, 2008-2014.
- (129) Evans, W. J.; Meadows, J. H.; Hanusa, T. P. *J. Am. Chem. Soc.* **1984**, 106, 4454-4460.
- (130) Schaverien, C. J.; Frijns, J. H. G.; Heeres, H. J.; Van den Hende, J. R.; Teuben, J. H.; Spek, A. L. *Journal of the Chemical Society, Chemical Communications* **1991**, 642-644.
- (131) Schaverien, C. J. *Organometallics* **1994**, 13, 69-82.

- (132) Evans, W. J.; Sollberger, M. S.; Shreeve, J. L.; Olofson, J. M.; Hain, J. H. J.; Ziller, J. W. *Inorg. Chem.* **1992**, 31, 2492-2501.
- (133) Hubert-Pfalzgraf, L. G.; Daniele, S.; Bennaceur, A.; Daran, J.-C.; Vaissermann, J. *Polyhedron* **1997**, 16, 1223-1234.
- (134) Mehrotra, R. C.; Singh, A.; Tripathi, U. M. *Chem. Rev.* **1991**, 91, 1287-1303.
- (135) Westerhausen, M.; Hartmann, M.; Schwarz, W. *Inorg. Chim. Acta* **1998**, 269, 91-100.
- (136) Westerhausen, M.; Hartmann, M.; Pfitzner, A.; Schwarz, W. *Z. Anorg. Allg. Chem.* **1995**, 621, 837-850.
- (137) Purdy, A. P.; Berry, A. D.; George, C. F. *Inorg. Chem.* **1997**, 36, 3370-3375.
- (138) Edelmann, F. T.; Freckmann, D. M. M.; Schumann, H. *Chem. Rev.* **2002**, 102, 1851-1896.
- (139) Piers, W. E.; Emslie, D. J. H. *Coord. Chem. Rev.* **2002**, 233-234, 131-155.
- (140) O'Keefe, B. J.; Hillmyer, M. A.; Tolman, W. B. *J. Chem. Soc., Dalton Trans.* **2001**, 2215-2224.
- (141) Ovitt, T. M.; Coates, G. W. *J. Am. Chem. Soc.* **1999**, 121, 4072-4073.
- (142) Ovitt, T. M.; Coates, G. W. *J. Am. Chem. Soc.* **2002**, 124, 1316-1326.
- (143) Tan, C.-S.; Hsu, T.-J. *Macromolecules* **1997**, 30, 3147-3150.
- (144) Arndt, S.; Spaniol, T. P.; Okuda, J. *Angew. Chem., Int. Ed.* **2003**, 42, 5075-5079.
- (145) Berry, A. D.; Gaskill, D. K.; Holm, R. T.; Cukauskas, E. J.; Kaplan, R.; Henry, R. L. *Appl. Phys. Lett.* **1988**, 52, 1743-1745.
- (146) Pinkerton, A. A.; Earl, W. L. *J. Chem. Soc., Dalton Trans.* **1979**, 1347-1349.
- (147) Ishikawa, M.; Iino, T.; Kaizu, Y. *J. Phys. Chem.* **2002**, 106, 9543-9550.
- (148) Corneillie, T. M.; Whetstone, P. A.; Fisher, A. J.; Meares, C. F. *J. Am. Chem. Soc.* **2003**, 125, 3436-3437.
- (149) Kronenbitter, J.; Schwenk, A. *J. Magn. Reson.* **1977**, 25, 147-165.
- (150) Adam, R. M.; Fazakerley, G. V.; Reid, D. G. *J. Magn. Reson.* **1979**, 33, 655-657.

- (151) Levy, G. C.; Rinaldi, P. L.; Bailey, J. T. *J. Magn. Reson.* **1980**, 40, 167-173.
- (152) Bruno, J.; Herr, B. R.; Horrocks, W. D., Jr. *Inorg. Chem.* **1993**, 32, 756-762.
- (153) Wu, J.; Boyle, T. J.; Shreeve, J. L.; Ziller, J. W.; Evans, W. J. *Inorg. Chem.* **1993**, 32, 1130-1134.
- (154) Smith, M. E. In *Annual Reports on NMR Spectroscopy*; Academic Press Ltd.: London, **2001**; Vol. 43, p 121-175.
- (155) Plioger, P. G.; John, K. D.; Keizer, T. S.; McCleskey, T. M.; Burrell, A. K.; Martin, R. L. *J. Am. Chem. Soc.* **2004**, 126, 14651-14658.
- (156) Shapiro, P. J. *Coord. Chem. Rev.* **1999**, 189, 1-17.
- (157) Coan, P. S.; Hubert-Pfalzgraf, L. G.; Caulton, K. G. *Inorg. Chem.* **1992**, 31, 1262-1267.
- (158) Bradley, D. C.; Chudzynska, H.; Hursthouse, M. B.; Motevalli, M. *Polyhedron* **1991**, 10, 1049-1059.
- (159) Bühl, M.; Parrinello *Chem.-Eur. J.* **2001**, 7, 4487-4494.
- (160) Bühl, M. *Theor. Chem. Acc.* **2002**, 107, 336-342.
- (161) Schreckenbach, G. *J. Chem. Phys.* **1999**, 110, 11936-11949.
- (162) Godbout, N.; Havlin, R.; Salzmann, R.; Debrunner, P. G.; Oldfield, E. *J. Phys. Chem. A* **1998**, 102, 2342-2350.
- (163) Bühl, M.; Gaemers, S.; Elsevier, C. J. *Chem—Eur. J.* **2000**, 6, 3272-3280.
- (164) Orian, L.; Bisello, A.; Santi, S.; Ceccon, A.; Saielli, G. *Chem.-Eur. J.* **2004**, 10, 4029-4040.
- (165) Autschbach, J.; Le Guennic, B. *Chem.-Eur. J.* **2004**, 10, 2581-2589.
- (166) Kaupp, M.; Bühl, M.; Malkin, V. G. *Calculation of NMR and EPR Parameters: Theory and Applications*; John Wiley: Weinheim, **2004**.
- (167) Wilson, E. K. *Chem. Eng. News* **1998**, 76, 25.
- (168) Barfield, M.; Fagerness, P. *J. Am. Chem. Soc.* **1997**, 119, 8699-8711.
- (169) Dash, A. K.; Razavi, A.; Mortreux, A.; Lehmann, C. W.; Carpentier, J.-F. *Organometallics* **2002**, 21, 3238-3249.

- (170) SAINT, V6.2; Bruker Analytical X-Ray Systems: Madison, WI, 2001.
- (171) Becke, A. D. *J. Chem. Phys.* **1993**, 98, 5648-5652.
- (172) Perdew, J. P.; Wang, Y. *Phys. Rev. B* **1992**, 45, 13244-13249.
- (173) Smith, J. D.; Hanusa, T. P. *Organometallics* **2001**, 20, 3056-3062.
- (174) Ziegler, T. *Chem. Rev.* **1991**, 91, 651-667.
- (175) White, R. E.; Hanusa, T. P. *Organometallics* **2006**, submitted.
- (176) Ahlrichs, R.; May, K. *Phys. Chem. Chem. Phys.* **2000**, 2, 943-945.
- (177) Handy, N. C.; Cohen, A. J. *Mol. Phys.* **2001**, 99, 403-412.
- (178) Hamprecht, F. A.; Cohen, A. J.; Tozer, D. J.; Handy, N. C. *J. Chem. Phys.* **1998**, 109, 6264-6271.
- (179) Adamo, C.; Barone, V. *J. Chem. Phys.* **1998**, 108, 664-675.
- (180) Perdew, J. P.; Burke, K.; Ernzerhof, M. *Phys. Chem. Lett.* **1996**, 77, 3865-3868.
- (181) Evans, W. J.; Meadows, J. H.; Kostka, A., G.; Closs, G. L. *Organometallics* **1985**, 4, 324-326.
- (182) Marciniak, B.; Maciejewski, H. *Coord. Chem. Rev.* **2001**, 223, 301-335.
- (183) Cabaço, M. I.; Marques, M. A.; de Barros Marques, M. I.; Bushnell-Wye, G.; Costa, M. M.; de Almeida, M. J.; Andrade, L. C. *J. Phys.: Condens. Matter* **1995**, 7, 7409-7418.
- (184) Lindquist-Reis, P.; Lambale, K.; Pattaneik, S.; Persson, I.; Sandstroem, M. *J. Phys. Chem. B* **2000**, 104, 402-408.
- (185) Sandström, M.; Persson, I.; Jalilehvand, F.; Lindquist-Reis, P.; Spangberg, D.; Hermansson, K. *J. Synchrotron Rad.* **2001**, 8, 657-659.
- (186) Rogers, R. D.; Kurihara, L. K. *Inorg. Chim. Acta* **1987**, 129, 277-272.
- (187) Reger, D. L.; Lindeman, J. A.; Lebioda, L. *Inorg. Chem.* **1988**, 27, 1890-1896.
- (188) Arndt, S.; Okuda, J. *Adv. Synth. Catal.* **2005**, 347, 339-354.
- (189) Schaverien, C. *Adv. Organomet. Chem.* **1994**, 36, 283-362.

- (190) Helgaker, T.; Jaszunski, M.; Ruud, K. *Chem. Rev.* **1999**, 99, 293-352.
- (191) den Haan, K. H.; de Boar, J. L.; Teuben, J. L.; Spek, A. L.; Kojic'-Prodic', B.; Hays, G. R.; Huis, R. *Organometallics* **1986**, 5, 1726-1733.
- (192) Kutzelnigg, W.; U., F.; Schindler, M. In *NMR Basic Principles and Progress*; Diehl, P., Fluck, E., Günther, H., Kosfeld, R., Seelig, J., Eds.; Springer-Verlag: Berlin, **1991**; Vol. 23, p 165.
- (193) Forsyth, D. A.; Sebag, A. B. *J. Am. Chem. Soc.* **1997**, 119, 9483-9494.
- (194) Hultsch, K. C.; Voth, P.; Beckerle, K.; Spaniol, T. P.; Okuda, J. *Organometallics* **2000**, 19, 228-243.
- (195) Gleizes, A.; Sans-Lenain, S.; Medus, D.; Hovnanian, N.; Miele, P.; Foulon, J.-D. *Inorganica Chimica Acta* **1993**, 209, 47-53.
- (196) Evans, W. J.; Peterson, T. T.; Rausch, M. D.; Hunter, W. E.; Zhang, H.; Atwood, J. L. *Organometallics* **1985**, 4, 554-559.
- (197) Personal communication from K. C. Jayaratne.
- (198) Overby, J. S.; Jayaratne, K. C.; Schoell, N. J.; Hanusa, T. P. *Organometallics* **1999**, 18, 1663-1668.
- (199) Krishnan, R.; Binkley, J. S.; Seeger, R.; Pople, J. A. *J. Chem. Phys.* **1980**, 72, 650-654.
- (200) Jonas, K.; Wiskamp, V. *J. Am. Chem. Soc.* **1983**, 105, 5480-5481.
- (201) Cotton, F. A.; Frenz, B. A.; Kruczynski, L. *J. Am. Chem. Soc.* **1973**, 95, 951-952.
- (202) Kowaleski, R. M.; Basolo, F.; Trogler, W. C.; Gedridge, R. W.; Newbound, T. D.; Ernst, R. D. *J. Am. Chem. Soc.* **1987**, 109, 4860-4869.
- (203) Köhler, F. H.; Mölle, R.; Strauss, W.; Weber, B.; Gedridge, R. W.; Basta, R.; Trakarnpruk, W.; Tomaszewski, R.; Arif, A. M.; Ernst, R. D. *Organometallics* **2003**, 22, 1923-1930.
- (204) Gamboratta, S.; Floriani, C.; Chiesi-Villa, A.; Guastini, C. *Inorg. Chem.* **1984**, 23, 1739-1748.
- (205) Henc, B.; Jolly, P. W.; Salz, R.; Stobbe, S.; Wilke, G.; Benn, R.; Mynott, R.; Seevogel, K.; Goddard, R.; Krueger, C. *J. Organomet. Chem.* **1980**, 191, 449-475.